Faculty of Engineering and Technology

Department of Mechanical Engineering

Experimental and Numerical Evaluation of a Solar Dryer for Drying **Banana** *(Musa spp)*

A dissertation submitted in partial fulfillment of the requirement for the Master of Science Degree in Mechanical Engineering

By

Philemon Xavery Mutabilwa

ID Nº. 201705256

Supervisor: Dr. K. N. Nwaigwe

October, 2019

DECLARATION

By submitting this thesis I, **PHILEMON XAVERY MUTABILWA,** do hereby declare that the contents in this thesis are my original work and have not been previously in part or entirely submitted to any University for obtaining any award of a degree or any other qualification.

Signature …….. Date ……..

CERTIFICATION

The undersigned certify that he has read and hereby recommend for acceptance by the Department of Mechanical Engineering, the thesis entitled Experimental and Numerical Evaluation of a Solar Dryer for Drying Banana as part of the work recommended in fulfillment of the requirement for the Master of Science Degree in Mechanical Engineering at the University of Botswana.

Approved by: Supervisor

Signature …… Date ……

ABSTRACT

A forced convection indirect type solar dryer having a double pass flat collector that can be used for drying bananas was designed, constructed and tested experimentally and numerically evaluated. The study mainly tried to address the problem associated with losses of bananas due to the average distance from neighboring countries to the market and the failure of market to consume the product within its shelf life. Hence, preservation method of bananas through solar drying technology was evaluated in this study so that to extend their shelf life.

The descriptions of the design methodology, development and operation of the newly constructed solar dryer are reported. The physical properties of banana fruits and relevant environmental factors of Botswana were considered in the development of the dryer. The dryer comprises of solar panel, flexible pipe, solar collector and drying chamber. The solar collector is made up of two glasses of 5 mm thickness and 1.6mm black painted aluminum absorber plate, all are enclosed in a casing made from plywood. The drying chamber is made from plywood with 20mm thickness. The dryer features a unique arrangement as the drying chamber is underneath the solar collector and the solar collector itself can be adjusted to an angle of 0^0 up to 35^0 at an interval of 5^0. The drying chamber is incorporated with a fan that sucks hot air from the collector on to the product for drying.

To investigate its performance, the solar collector was tested and achieved an optimal peak outlet temperature of 345K with a maximum efficiency of 72.5%, whereas the maximum useful heat gained by the solar collector from the solar radiation was 828.21W. The minimum and maximum ambient temperature, relative humidity and solar insolation recorded were 306.8K and 313K, 13.6% and 44.5% and 529 W/m^2 and 983W/m^2 respectively. Approximately 3.69kg of banana pulps sliced to a thickness of 3 to 5mm with moisture content of up to 82% dried within 8-13hrs to the final moisture content of >20%.

The geometry of the developed solar dryer was modeled using CFD software and 3D CFD simulations for the solar collector and drying chamber were performed using ANSYS 18.2. The fluid flow was characterized by RNG k-ε turbulent viscous model and Discrete Transfer Radiation Model (DTRM) to allow radiation within the flow domain. A total number of 3,816,337 elements with nodes of 746,255 were generated in order to enhance smooth convergence of the simulation. The CFD results were compared with experimental results, and a good correlation was established between the two approaches particularly on airflow and the maximum temperatures of both the absorber plate and top glass. During the experiment, the maximum temperature of the absorber plate was 374K while that of CFD results was 384K. The maximum temperature reached on the top glass of the collector from the experimental result was 330K, while for CFD the result was approximately 325K-331K.

DEDICATION

This research work is dedicated to my family members especially my wife, DORCAS who at all times has been praying for my success and rendering unconditional support to me during the whole period of my study: “you are the way and light of my life above the smile of my life”. To my boys, NIVAN & NEVIS, and to my lovely Twin sister, PHILIMINA, and to my Mother whom I will remain grateful to forever, may the almighty God be with you, bless and protect you all.

ACKNOWLEDGEMENTS

I am highly grateful to my sponsor, The Association of Commonwealth Universities (ACU) under the umbrella of the Commonwealth Scholarships in Low & Middle Income Countries for the award to pursue Masters in Mechanical Engineering at the University of Botswana. It was a dream come true to be sponsored by ACU.

I am also pleased to thank the Office of Research and Development (ORD) at the University of Botswana through its Internal Research Funding. It was through this funding that the fabrication of the dryer was made possible. Dissemination and publications together with entire ethics and IP issues in my work were managed by ORD.

I would like to thank my Supervisor Dr. Kevin Nwaigwe from the Department of Mechanical Engineering. He was always present anytime to assist me whenever I needed help, whether on a working day or during the weekend. I appreciate his advises, new knowledge and solutions that helped improve both the organization and contents of this work. Through regular discussions with him the **complexity** of my work diminished day after day.

I would also like to thank Dr. Jaap Hoffmann from the Faculty of Engineering of the University of Stellenbosch for his assistance during my training at Stellenbosch University. His guidance in performing ANSYS simulations in my research was helpful and I really appreciate it.

I would like to acknowledge the Head of Mechanical Department Prof. Jerekias Gandure together with the entire staff members for the academic support and input to this work. It was helpful to share ideas with them during presentations, this further enabled me to acquire more insightful comments that helped to move my work forward.

Finally, I would like to thank fellow graduate (PhD/Masters) students and my classmates who at some point helped me during difficult times. Their views were fruitful to this work. They include M. Lame, R. Ndeda, J. Goreit, P. Muiruri, M. Kalanja and B. Ebangu.

TABLE OF CONTENTS

LIST OF FIGURES

LIST OF TABLES

LIST OF NOTATIONS

Nomenclatures	U_∞ = Momentum Flux
A_{g_t} = Area of top glass (m^2)	V_w = Wind velocity (m/s)
A_{g_b} = Area of bottom glass (m^2)	W = Width of the solar colector (m)
A_{ab} = Surface area of solar absorber (m^2)	W_b = Weight of banana to be dried
C_p = Specific heat capacity (J/kg. K)	**Dimensionless variables**
h_g = Enthalpy of water as a liquid (kJ/kg)	Nu = Nusselt number
h_f = Enthalpy of water as a vapor (kJ/kg)	Re = Reynolds number
h_{cp} = Convective heat transfer (glass & plate W/m^2K)	**List of Greek symbols**
H = Depth chansels of solar collector (m)	ε = Emmisivity
h_c = Convective heat transfer coefficient (W/m^2K)	ω = Coefficient
h_r = Radiative heat transfer coefficient (W/m^2K)	ζ = Coefficient
I = Incident solar radiation (W/m^2)	α = Absorbancy
k = Thermal conductivity (W/m. K)	τ = Transmittance
k_P = Thermal conductivity of Plywood (W/m. K)	σ = Stefan − Boltzmann constant ($Wm^{-2}K^{-4}$)
L_v = Latent heat of vaporization (kJ/kg)	λ = Thermal conductivity
L_c = Length of solar collector (m)	**Sub − scripts**
L_i = Inside length of banana (m)	a = Ambient
L_o = Inside length of banana (m)	ab = Absorber plate
l_c = Characteristic length of solar collector (m)	ad = After drying
M_b = Mass of banana fruits to be dried (kg)	b = Banana
M_i = Initial moisture contents (%)	bd = Before drying
M_f = Final moisture contents (%)	bo = bottom
M_{bd} = Mass of sample before drying (kg)	c = Collector
M_{ad} = Mass of sample after drying (kg)	co = Convective
m_w = mass of water vapour to be evaporated (kg)	c1 = Upper Channel
N_{batch} = Batch of banana fruits to be dried (kg)	c2 = Bottom Channel
N_t = Banana fruits to be dryed (kg)	d = drying
N_g = Number of transparent glasses	f = final
Δp = Pressure drop (N/m^2 or Pa)	g = glass
Q_a = Heat to effects the initial moisture contents (kJ)	g_t = top glass
Q_a = Heat required to evaporate the moisture contents (kJ)	g_b = bottom glass
Q = Total useful energy	L = Loss
Q_u = Useful heat gained by the collector (W)	r = radiatice
α_g = Absorbance of the glass	u = usefull
α_p = Absorbance of the plate	
δ_g = Thickness of the glass (m)	**List of abbreviations**
δ_p = Thickness of the absorber plate (m)	AP's = Agricultural products
δ_P = Thickness of the Plywood (m)	PHL = Post Harvest Losses
δ_b = Thickness of a banana slice (m)	DRC = Drying chamber
S_d = Sunshine hours per day (hrs)	DTRM = Discrete Transfer Radiation Model

T_{max} = Maximum drying temperature(K)	FVM = Finite Volume Method
T_d = Allowable drying temperature(K)	FEM = Finite Element Method
T_{air} or T_a = Ambient temperature(K)	FDM = Finite Difference Method
T_{c1} = Temperature of the Top channel(K)	N − S − E = Navier Stocks Equation
T_{c2} = Temperature of the Bottom channel(K)	RANS − Reynolds Averaged Navier Stokes
T_{g_t} = Temperature of the top glass(K)	IP = Interactual Properties
T_{g_b} = Temperature of the bottom glass(K)	ORD = Office of Research & Development
T_∞ = Temperature flux (K)	ACU = Association of Commonwealth Universities
T_W = Temperature of the absorber plate (K)	SUN = Stellenbosch University
U_t = Heat loss from the top glass (W/m^2K)	IC = Internal Combustion
U_L = Overall heat loss coefficient (W/m^2K)	CAD = Computer Aided Design
U_b = Heat loss from the bottom of collector (W/m^2K)	

CHAPTER ONE: INTRODUCTION

1.1. Background

Many developing countries depend more on agricultural sector to drive and sustain their economic growth. A report from Food Agricultural Organization (FAO) shows that about 2.5 billion people out of 3 billion worldwide who live in rural area depend on the agricultural sector (FAO, 2013). A recent population projection report (2011-2016) on Botswana show that in 2011 the population was 2,024,904 persons; this means that by 2019 Botswana will have a total population of approximately 2.31 million, due to the population increasing rate of approximately 36,063 persons every year (Statistics, 2015)

Botswana has about 258,520 square kilometers of agricultural land, which represents 45.6% percent of the total land area. Botswana's agricultural sector employs about 29.9% of its total labor force and accounts for 3% of the country's GDP (Yearbook, 2013). Livestock production in Botswana dominates the whole of the agricultural sector while crop production is very low due to the agro-ecological conditions which are unsuitable for cropping. Botswana, therefore, relies on net importation of agricultural products like maize, wheat, potatoes, and fruits such as bananas from neighboring countries like South Africa and Mozambique, amounting to millions of Pula annually. This is affirmed by the statistics (2016) which show that the majority (64%) of banana fruits exported from South Africa to members of Southern African Customs Union (SACU) were absorbed by Botswana as shown on Figure 1.1 (Marketing", 2017). In addition to that, and according to the United Nations COMTRADE database (2017) on international trade, Botswana imported Banana fruits and plantains from Mozambique amounting to USD 81.32 thousands, equivalent to P870, 286.60 as shown on Figure 1.2 (Economics, 2018).

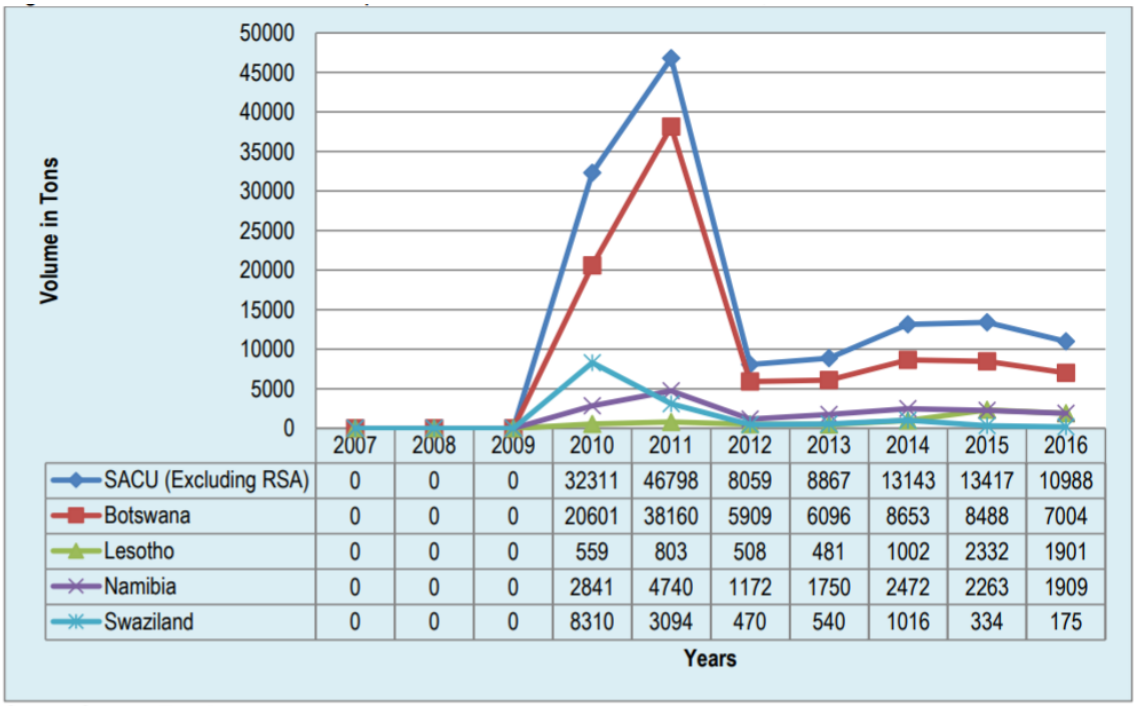

	2007	2008	2009	2010	2011	2012	2013	2014	2015	2016
SACU (Excluding RSA)	0	0	0	32311	46798	8059	8867	13143	13417	10988
Botswana	0	0	0	20601	38160	5909	6096	8653	8488	7004
Lesotho	0	0	0	559	803	508	481	1002	2332	1901
Namibia	0	0	0	2841	4740	1172	1750	2472	2263	1909
Swaziland	0	0	0	8310	3094	470	540	1016	334	175

Source: Quantec Easydata

Figure 1. 1 Volume of Banana exported from South Africa to members of SACU (Marketing", 2017).

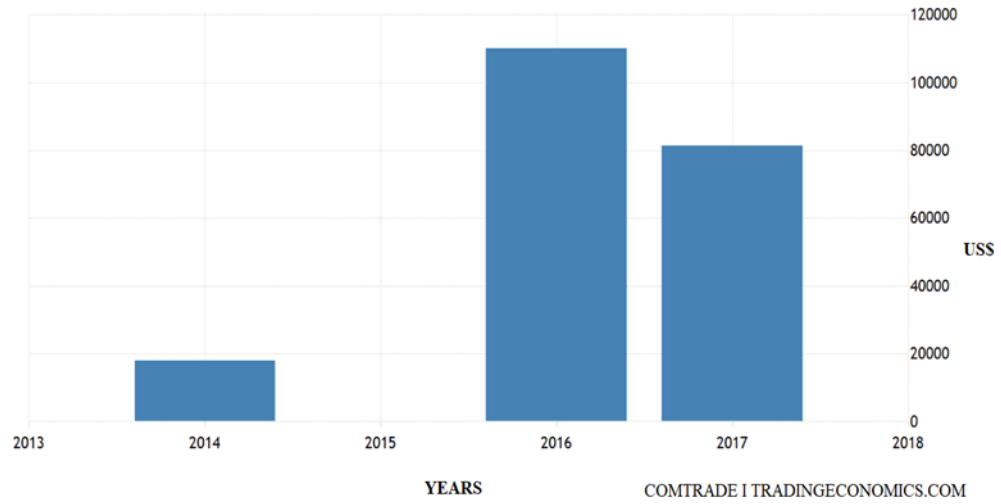

Figure 1. 2 Value of Banana and Plantains imported into Botswana in 2014, 2016 & 2017 (Economics, 2018).

The agricultural sector is one of the important industries for the production of food for consumption. A number of challenges arise during the production and marketing chain of fruits and vegetables, and these contribute enormously to losses of agricultural products. Challenges arise due to climate change, agricultural policy, conservation issues, financial and technological

restrictions. For purposes of this work, the technological challenge of preserving agricultural products like banana fruits in Botswana is of great interest.

1.2. Motivation

Drying is the process of removing some amount of water present in agricultural products like banana fruits. The water is removed to stop microorganism activities (Sanghi et al., 2018). Drying processes of agricultural products are complex and energy intensive processes due to their non-linearity phenomena and high moisture content. Drying time for agricultural products sometimes is unpredictable due to the continuous change of drying conditions (Corzo et al., 2008, Fayose and Huan, 2016, Nwakuba et al., 2017). It is with regard to this that design of solar dryers for drying agricultural products must be properly looked into in order to meet drying requirements. Any improvement of design and drying parameters of a solar dryer is an area of great interest. During the design of solar dryers, the collector area and its configurations, airflow recirculation, dryer dimensions and volume of drying chamber must be evaluated properly (Janjai et al., 2009).

Forced convective solar dyers normally employ flow of air within a number of channels in the system. Many studies on the use of forced convective solar dryer to dry fruits have been reported in literature (Mahmood et al., 2015, El-Sebaii et al., 2011, Durusoju et al., Labed et al., 2012, Sopian et al., 2009, Gupta et al., 2013, Fudholi et al., 2013, Ramani et al., 2010, Sopian et al., 1999). Despite their succession, the dryers require design and numerical look through. With regard to the design, most of the dryers have been designed in such a way that the solar collector is positioned stationery at an angle prescribed by the geographical location of a place; this phenomena limits tilting of additional angle that may be preferable by users for a reason or research purpose.

Numerical simulation through the use of computational fluid dynamic (CFD) approach is another way that can be used to monitor and predict the internal environmental conditions of a

solar dryer for better design and performance. CFD simulation of the convective drying process of banana solar dryer can be more attractive for better design and performance of banana solar dryers. According to (Norton et al., 2010), the numerical simulation of a drying system as a design tool for making possible parametric study, optimization and geometry adjustment of a system for a better design solution was considered. Application of CFD tools in studying the drying domain helps to simulate the streamlines, contours and volume rendering of steady & unsteady turbulence flow regime of hot air within a drying system. This enhances the effectiveness in removing the amount of moisture content of fruits in the dryer. The CFD tools make use of the turbulence and radiation model simultaneously to solve numerical transfer equations for a finite number of elements and allow participation of radiation within the flow domain of the solar system.

In (Smitabhindu et al., 2008), the optimization of a solar assisted drying system through a mathematical model and simulation using finite different method was studied. Validation of simulation with experimental results showed good agreement of results. The authors concluded by making recommendations on the use of developed simulation model in optimization of similar solar drying system. In the reference (Amer et al., 2010) designed and constructed a hybrid solar dryer for drying banana fruits; the system was able to dry banana fruits from initial moisture content of 82% to 18% for approximate 8-10hrs. Though the paper did not address the simulation part of it, the authors recommended that the dryer was able to be used together with an auxiliary heat source in the event weather conditions change. In (Esquivel et al., 2018) the author optimized the drying process of coffee fruits using experimental and numerical approach on a greenhouse solar dryer. The environmental conditions of the forced convection greenhouse solar dryer were examined. The reason for the authors to use CFD tools was to study the internal behavior of the dryer, since forced convection dryers are accompanied with turbulent flow. A turbulence and buoyancy model was energized to account for turbulences and density during simulation. Radiation model was also activated to solve for radioactive transfer and

participation of radiation in a drying system. All numerical models were developed using the ANSYS tool. In the reference (Alonso-Torres et al., 2013) published a paper on 'CFD modeling and validation of roasting coffee beans' comparing experimental findings of bean temperature and humidity loss from another study. Since the paper did not discuss the use of solar dryer, heat and mass transfer equations were solved through finite volume methods using ANSYS fluent program. Findings indicated that the numerical model predicted the real roasting process and were consistent with experimental results from another paper, therefore making it possible to observe the process in a real time. Other papers which discussed the use of computational fluid dynamics in solar drying process are (Sanghi et al., 2018, Norton et al., 2010, Ingle et al., 2013, Amraoui and Aliane, 2017, Cârlescu et al., 2017).

Visibility of the drying parameters through CFD approach plays most decisive role in determining the effects and influences of drying parameters like temperature, airflow within the solar collector and the drying chamber. In recent reviews in line with the above mentioned references, researchers have published studies on convective solar dryers for drying agricultural products particularly banana fruits through experimental, analytical and/or numerical orientations. However, the visualization of volume flow propagation of drying parameters, influenced by the convective airflow within both double pass solar collector and drying chamber of banana solar dryer through application of CFD approach have not been evaluated to the extent. Among the few papers published on the use of ANSYS Fluent tool in describing the internal behavior of the drying process of agricultural products, no systematic simulation have been done using the ANSYS tool to evaluate the physical phenomena of both the double pass solar collector and the drying chamber of a convective drying process of banana fruits simultaneously. The lack of data on numerical simulation of solar drying processes through computational fluid dynamic tools necessitate the design of suitable dryers constructed under local technology and weather conditions of Botswana.

This research therefore, seeks to design, develop, conduct experiments and evaluate numerically the fluid dynamic behaviors within both the double pass solar collector and the dying chamber of a banana solar dryer. The work will involve development of a numerical model based on implementation and use of ANSYS Fluent tools in order to correlate drying parameters to the experimental tests. Using the CFD approach, the solar load model will be - employed to calculate the effects of solar radiation of Gaborone that enters the computational domain of a solar collector. The study will also try to answer the question of consistency of the CFD model with the geometry of the solar dryer for the purpose of generating ideas that can boost efficiency of the drying process.

1.3. Banana products and their roles in nutrition

Banana *"Musa spp"* is a staple food commodity with a lot of economic significance for food security and commercial use. Banana fruit contains calories, carbohydrates and minerals together with vitamins and natural sugar. It also contains very little fat, is free from cholesterol and has high fiber content (Omolola et al., 2015, da Silva et al., 2013, Ahmad et al., 2007). Bananas fruits are perishable in nature, therefore upon being harvested and/or arriving at the market they should be consumed within few days, otherwise they will spoil. Due to this perishable nature of banana products researchers in different countries are investigating alternative ways of reducing post-harvest losses which account for an average of 30-40% of production (Baini and Langrish, 2007, Karim and Hawlader, 2005). Among the approaches for reducing post-harvest losses is preservation through drying.

Dried banana have a lots of advantages and use. Apart from being preserved for future use, dried banana products can be consumed as banana flakes or milled into banana flour which can be used to make banana cake, bread, biscuits, spaghetti or baby food, hence generate income for small scale vendors. For the purpose of maintaining flavor and taste, banana fruit can be treated prior to drying through dipping into reagents like lemon juice in order to keep its taste,

flavor and meet preferences of users, hence increasing or adding its market value (Chauhan and Jethva, 2016).

Since the agricultural sector in Botswana is dominated by livestock farming, this study will also evaluate drying of bananas to be milled and used as feeding materials for animals like cattle and poultry. This will help in minimizing wastage of banana fruits as they will therefore be used in another form (Jariwala and Syed). For further research banana by-products like peels can also be studies to determine whether they can be dried and used as animal feed in Botswana, this will help to preserve banana peels that would otherwise become waste.

1.4. Problem Statement

Agricultural fruits like bananas are highly perishable and therefore the post-harvest losses are also high. Botswana relies on importation of bananas from neighboring countries amounting to millions of Pula annually, in 2016 majority (64%) of bananas exported from South Africa to members of Southern African Customs Union (SACU) were absorbed by Botswana and 36% were traded to the other counties (Marketing", 2017). Although bananas are highly needed as nutritious and economically significant fruits, they experience losses during marketing. One of the reasons of high losses of bananas in Botswana is overstaying which is caused by two main factors, one is the long time in transit due to the average distance from neighboring countries to the market and the failure of market to consume the product within its shelf life. These two reasons usually accelerates ripening and spoilage of banana fruits, hence causing great economical and income losses to the importers and small-scale vendors. In a country like Botswana which sometimes experiences high temperatures for a period of time, the losses of bananas is likely to be inevitable, this is due to the fact that bananas can be stored for 1 to 1.5 weeks at a temperature of 286K to 289K according to references (Scheepens et al., 2011, Ahmad et al., 2007). Similarly, there is insufficiency in number of research studies on the use of computational fluid dynamic in studying drying process of banana fruits, which should

describe the internal behaviors within the double pass solar collector and drying chamber using ANSYS fluent numerical simulation.

1.5. Objectives

The principal objective of this study is to investigate the performance of a developed solar dryer for drying of banana, using experimental and numerical approach under natural weather conditions of Gaborone, Botswana. In order to achieve this objective, the specific objectives include:

a) To design and construct a solar dryer using locally available materials, for experimental studies.
b) To perform experiments using the developed solar dryer towards studying the drying kinetics of banana fruits.
c) To develop numerical solutions for drying of banana using ANSYS workbench
d) To validate the numerical models using experimental data obtained from the developed solar dryer.

1.6. Justification of the study

This research is conducted to solve the problem generated by the rapid perishability of banana fruits caused by overstaying and spoilage of banana during the market-value chain. This study will promote the use of drying technology in reducing the amount of Pula invested on importation of banana fruits in Botswana. Apart from that, this study aims to increase the shelf life of bananas and turn them into successful multi-use dried products, hence boost food security in the society. Dried banana can be benefited from as flakes or milled baking flour for human use and domestic animal feeding. Botswana receives abundant solar energy, this research will therefore provide insight into what happens in the solar drying process of banana fruits. It will make use of available solar energy to benefit the society by developing the drying industry in

Botswana, hence, enhance socio-economic benefits and foster the use of solar energy (Ketlogetswe and Mothudi, 2009).

1.7. Scope of the study

This research will review different literatures on similar studies. From the review the solar dryer will be designed and fabricated taking into account availability of local materials. Experiments will be conducted using the developed solar dryer. Thin layer modeling of sliced banana as an input to the dryer will be discussed to describe the equation of heat of vaporization of water or drying rate in banana products. The data obtained from experiments will be analyzed and numerical modeling will be done using ANSYS software and validated against experimental results.

CHAPTER TWO: LITERATURE REVIEW

2.1. Overview of solar energy

Solar energy is the energy released by the sun though solar radiations. The sun is capable of producing a high amount of energy enough to sustain the energy requirement in the world. Solar energy also drives important natural cycles such as wind and rainfall formation, and plant photosynthesis all around the world. Despite this, the big challenge in solar energy is how to harvest enough energy from the sun with efficient and cost effective equipment (Mackay, 2015).

For the purpose of extracting solar energy to be used in engineering equipment, it is important to have enough details like geographical information on availability and intensity of solar energy for a particular location. This will help to determine the solar isolation, solar constant together with other design parameters and configurations of a solar collector that will be used to harness solar energy (Hegde et al., 2015)

2.1.1. Solar constant (solar power density)

The solar constant, sometimes called the solar power density, is the energy from the sun radiated per unit time on a unit surface area. At earth's orbit or at a distance of one astronomical unit this value is about 1360 W/m^2 (Da Rosa, 2012). The value is not really constant, it normally varies a little throughout the year and when the earth is nearest to the sun, normally in January, this value is at its highest.

The earth's atmosphere contains different components like water vapor, dust and the ozone layer which affect the total solar radiation that reaches the earth surface from the sun (Brenndorfer et al., 1987). Figure 2.1 illustrates concepts of determination of solar constant and schematic geometry of the sun-earth relationship as described in the reference (Duffie and Beckman, 1980). The summation of all diffuse and direct components as the sun rays travel from the sun to the earth form a total solar energy received on the earth's surface.

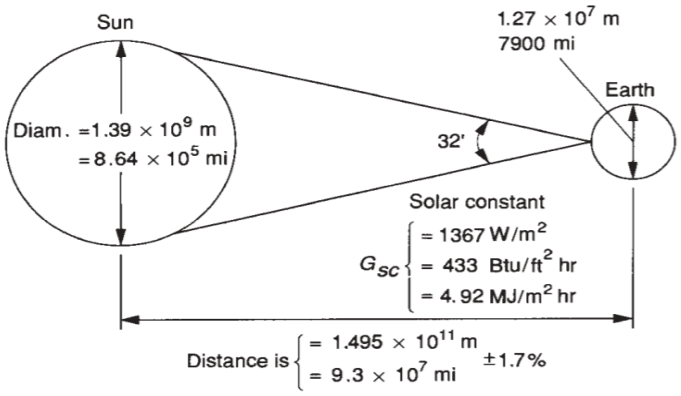

Figure 2. 1 Sun-earth relationship

2.1.2. Solar irradiation in Botswana

Botswana is a land locked country which lies roughly between latitude 18^0 - 27^0S and longitude 20^0 - 29^0E. Gaborone, in particular the University of Botswana, lies between latitude -24.67^0S and longitude 25.92^0E (Luhanga, 1995, Nijegorodov and Monowe, 2011).

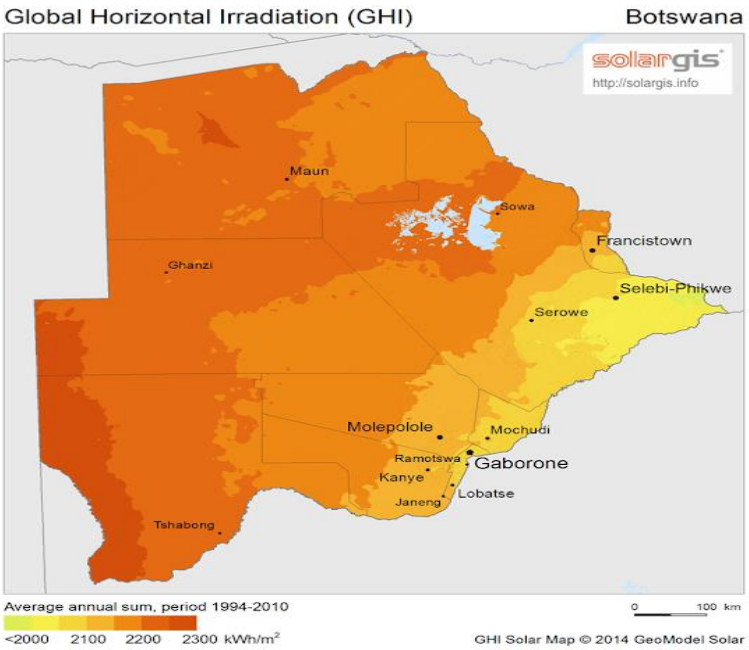

Figure 2. 2 Global horizontal irradiation in Botswana. Solar GIS maps, 2014.

From Figure 2.2 above, it can be depicted that a large area of Botswana land is subjected to high solar irradiation which has the potential for harnessing solar energy to be used for drying processes. According to the World Energy Council report, Botswana receives a high rate of solar isolation of approximately 280-330 days of sun per year with daily average sunshine

ranging from 9.9 hours during the summer to 8.2 hours in winter. The average total solar radiation is approximately between 10MJ/m^2 to 21MJ/m^2 in different consecutive days as reported in (Ketlogetswe and Mothudi, 2009, Andringa, 2017). As evidenced in this report, Botswana receives enough amount of isolation which has sufficient potential for solar drying.

2.2. Solar collectors

Solar collector is a unit used for extracting solar energy. In (Struckmann, 2008, Ekechukwu and Norton, 1999b) the authors focused on define solar collector in terms of its function, stating that it absorbs the incoming solar radiations, converts them into heat at the absorbing surface and transfers heat to a flowing fluid such as water and air. Da Rosa (Da Rosa, 2012) in his book explained four methods of collecting energy from sun for the purpose of producing either electricity or heat; these methods are flat collectors (non-concentrating), evacuated tubes, concentrators, solar ponds and appropriate architecture. Flat and concentrating collectors are basically types of solar collector designs. The author indicated that concentrating types are equipped with a focusing reflector and normally have a specific shape for the purpose of increasing the intensity of solar radiation. Da Rosa (Da Rosa, 2012) characterized concentrating collectors in terms of their concentration ratio which is the ratio of the aperture area and the receiver area, or the ratio of the power density at the absorber surface to that at the aperture. In (Brenndorfer et al., 1987), the authors stated that for drying agricultural crops, flat plate collector types can be designed and attain enough drying temperature.

2.2.1. Covered & bare flat plate solar collectors

Flat plate collectors are simply defined by their absorbing surface, which receive solar energy and exchange it to heat. A typical flat collector consists of an insulated metal box, clear plastic/glass cover (grazing), and a dark-colored absorber. According to (Struckmann, 2008) such flat collector can generate and heat fluid at a temperature of up to 80^0 C. Ekechukwu et al., (Ekechukwu and Norton, 1999a) mentioned two classes of flat plate collectors as shown on Figure 2.3; covered flat plate and the bare flat plate. Selection of the type of flat plate collector

to be used for a specific purpose depends on advantages and disadvantages of a particular type. Bare flat plate flat collectors are simple in construction and they typically operate more efficiently at low temperature areas. Their main disadvantage is high thermal losses due to the absorbing plate surface being exposed out to ambient air, hence low efficiency. Covered flat plate type operates at high efficiency than bare type; the glass cover helps to protect the absorber plate from damage, cooling and also minimizes heat loss that may occur by convection. The limitation of the covered plate collector is the cost of maintenance and construction and it is recommended for temperatures between 283K- 308K above ambient.

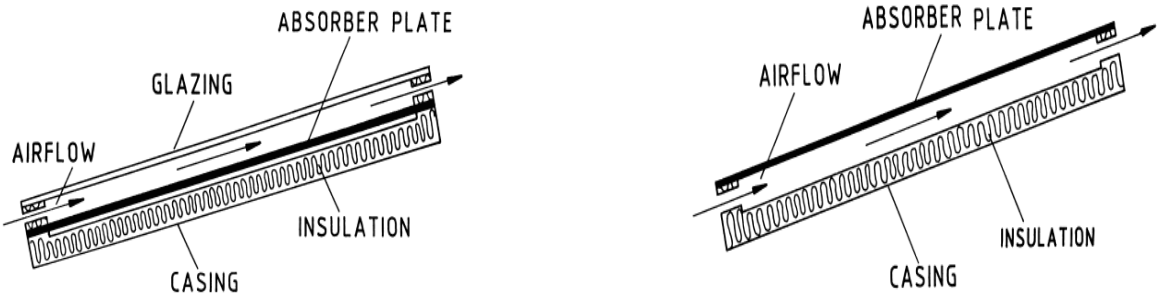

(a) Covered - plate (b) Bare - plate

Figure 2. 3 Typical types of flat plate collectors. Source:(Ekechukwu and Norton, 1999a)

2.2.2. Single and double pass flat plate collectors

Flat plate collectors can also be classified as single-pass or double-pass flat solar collector. Each class has its advantages and shortcomings. Different researchers (Mahmood et al., 2015, Durusoju et al., Sopian et al., 2009, Gupta et al., 2013, Fudholi et al., 2013, El-Khawajah et al., 2011) constructed and performed investigation of single and double pass solar collector systems, both systems were designed the same way as collector with absorber plate and fins painted black. Experimental results of (Mahmood et al., 2015) showed that the maximum efficiency attained by single pass and double pass were 55% and 62.5% respectively. The same improvement was obtained for other parameters like temperature. This scenario leads to the

conclusion that solar collectors designed according to the configurations of air pass may result in significant improvement of outlet air temperature and thermal efficiency solar dryers

Solar dryer, sometimes called drying chamber, is one of the units of a complete solar drying system. Its main function is to hold products to be dried and allow fluid flow to pass through the products either by natural and/or by convection model. According to (Brenndorfer et al., 1987), solar dryers have been classified into three classes, according to the mode of flow of air, the exposure of product to radiation and air inlet temperature and air heating mode. The same classification have been reported and supported in the references (Ekechukwu and Norton, 1999b, Sharma et al., 2009, Belessiotis and Delyannis, 2011).

2.2.3. Active and passive solar dryers

Active and passive are classes of solar dryer classified according to mode of airflow. Sometimes they are classified as natural and forced convection (Ekechukwu and Norton, 1999b). Active or forced convection solar dryers depend on pressure differences produced by a blower or a fan which forces stream of air pass through the product inside dryer. It is applicable in drying large amounts of product with high moisture content due to its high efficiency. The only challenge with active convection is its complexity and high cost due to application of a fan which sometimes demands more power to drive (Ekechukwu and Norton, 1999b). Passive or natural convection depend directly on solar energy. When fluid-like air is heated within the solar collector it becomes denser that ambient air, hence creates a wind force or buoyancy force which drives air through materials within the dryer.

2.2.4. Indirect, direct and mixed solar dryers

Both direct and indirect solar drying methods rely on energy from the sun. Indirect solar drying method involves the application of a designed equipment for drying, which enhances solar radiation, resulting in higher drying temperatures and improved products. This is not the case for direct solar drying methods.

Indirect solar drying methods have been developed in order to overcome shortfalls encountered by the direct solar drying methods. Under this method, crops are dried in a controlled volume which gives superior quality and promotes achievement of the desired final moisture content of the dried product. Drying of products under controlled conditions make the process of transfer of heat and mass more easy, therefore prevents the growth and reactions of microorganisms especially for perishable goods like tomatoes, onions, and banana (Maskan et al., 2002).

Open sun drying is a direct solar drying method commonly used for drying agricultural crops since ancient time. Crops are exposed directly to solar radiation by spreading them on the ground or on the roof and left for number of days to dry. This method leads to high crop losses due to uneven moisture removal, insects and rodents feeding on the crops, dust and dirt contamination, long time for drying, and many other challenges (Tomar et al., 2017, Maisnam et al., 2017).

Mixed solar dryers are those which employ the use of solar energy as one source together with other different heat/energy sources like electricity, biogas, (LPG) (Nwakuba et al., 2017). One of the biggest advantages of this type of dryer is that when one source is not available/functioning the dryer can be switched to the secondary source and drying continues. The only disadvantage is that the cost of employing two sources is higher than one source and sometimes dryers of such type tend to be more expensive due to the application of two-way switching mechanisms.

2.3. Design components of a solar systems

Solar systems are mainly composed of three main units or components. These components include a solar collector, drying chamber and the chimney. The complete structure of a solar dryer is held on a frame although in other cases a dryer can be constructed without frame, in this case the drying chamber can be used to hold all other components.

2.3.1. Solar heat collector

In (Jercan, 2006, Duffie and Beckman, 1974), the authors defined a solar collector in term of its function, stating it is used to convert direct diffuse components of sun radiation into thermal energy which is then transferred to the adjacent flowing fluid. Solar collectors, particularly the flat type are easy to be constructed and require less maintenance than concentrator type and can generate temperatures of up to 353K (Struckmann, 2008). Solar collectors consist of mainly four parts namely: absorber plate; grazing or cover plates; airflow passage and a structure or cabinet that accommodates all other components. The cover, sometimes called glassing, is the first receiver of the solar radiation, is a transparent cover that allows radiation to pass through (Saxena and Goel, 2013). Absorber plate, as the name suggests is made up of material that absorbs heat. For the purpose of increasing its absorptivity it is sometimes painted black (Amrutkar et al., 2012).

2.3.1.1. Design of solar heat collector

Increasing the amount of solar energy absorbed by solar collector depends on the performance of the absorber plate, which on the other hand is influenced by the level of solar isolation, transmittance of the cover materials, incidence angle of solar radiation on surface of absorber and absorbance of the absorber surface (Ekechukwu and Norton, 1999a). On the other hand collector design configurations through application of absorber fins on the air passage and the number of airflow channels can also increase heat energy absorbed by moving fluids along the channel (Daliran and Ajabshirchi, 2018).

2.3.1.2. Sizing and tilt angle of flat plate collector

Struckmann and Sodha (Sodha, 1987, Struckmann, 2008) used the formula shown on Equation [2.1] to obtain the effective area of a solar collector. In their descriptions the authors proposed that the area of a collector (A_c) can also be taken as the area of the absorbing plate and glazing cover as well. Q is taken to be total heat energy required to remove some amount of moisture content, I_T is used to describe the solar isolation of an area and η_c is the collector efficiency.

$$A_c = \frac{Q}{I_T \eta_c} \quad \text{..... [2.1]}$$

Since the area of solar collector (A_c) is the function of length and width, Forson et al., (Forson et al., 2007) highlighted that during the design of a solar collector the length to width ratio of a flat plate collector should be between 1 and 2 inclusively.

Jacobson et al., (Jacobson and Jadhav, 2018) presented a paper "World estimates of optimal tilt angles and ratios of sunlight incident upon tilted and tracked PV panels relative to horizontal panels" For the purpose of design the latitude of the location where the solar collector is to be positioned is normally taken as a tilt angle of the collector. Hoverer the flat plate collector can be orientated at an angle of 10^0 more of the latitude angle and should face either north or south depend on the location as recommended by (Bolaji and Olalusi, 2008, Leon et al., 2002, Adegoke and Bolaji, 2000). On the other hand Da Rosa (Da Rosa, 2012) proposed that the optimum collector angle can be determined using Equation [2.2a].

$$\beta = \phi + \delta \quad \text{.....[2.2a]}$$

$$\delta = 23.45\, Sin\left(360\, \frac{284+n}{365}\right) \quad \text{.....[2.2b]}$$

Whereby:

The variable β is the collector slope, ϕ is the latitude at which evaluation is conducted, δ is the angle of declination obtained using Equation [2.2b] and n is the day number.

2.3.1.3. Air channel or passage

Rangababu et al., (Rangababu et al., 2015) said that the air channel or the gap between the glass and absorber plate in a solar collector is one of the important part to be taking into consideration during design, it plays an important role in achieving actual performance of a system. In the referance (Scanlin, 1997), author suggested that the air velocity of a dryer should be between 0.5m/s to 5.08m/s,. The author also argues on the depth of the air channel to be between

1/15 to 1/20th the lengths of a collector to ensure aerodynamic flow of air along the collector. References (Irtwange and Adebayo, 2009, Sayigh, 1979) presented the range of the value of the air gap of a solar collector. They suggested that the air gab between absorber plate and cover plate should be in a range of 0.04m and 0.08m.

2.3.2. Drying chamber

Different sizes and structure of drying chamber can be designed depend on the physical size of the dryer which is the direct measure of the drying capacity or sometimes called batch drying capacity or loading density. This is the quantity of products (in kg of fresh products) dried in a single batch loading density of the product to be dried (Leon et al., 2002). Basically, aperture area of collector, the size of the dryer, type of product to be dried or loaded and its moisture contents serve in determining the drying capacity. For tray type cabinet solar dryers, the loading density depends on the product to be loaded and its moisture contents, the airflow rate and conditions of drying air based on the following rules, Firstly: Solar collector area should be equals to 0.75xtotal try area, Secondly: The average dryer loading should be equal to 4kg of fresh products per meter square of tray area, Thirdly: Airflow rate should be equal to $0.75m^3/m$ for every square meter of tray (Leon et al., 2002).

Basically drying chamber are like box-type in view and most of them are tray-type for allowing easy loading and offloading of product to be dried. Drying chamber are equipped with a rear door for easy accessing of products to be dried. Since drying chambers are tunnels within which heat is stored normally are sealed and well insulated to avoid heat leakage or heat losses. Materials like plywood, polyethylene forms, asbestos etc. are used to construct drying chambers, these materials are normally bad heat conductor and therefore do not allow heat lost to the surroundings.

2.3.3. Chimney or exhaust

In (Ekechukwu and Norton, 1996) the performance of a solar chimney was measured, the authors said that if the temperature of the air inside the chimney is greater to than of ambient in

a sense that the air density inside the chimney is less than the outside air, the air will flow through chimney to outside. It is good idea to construct a solar dryer having a means to release air outside, this means the air absorb moisture from a product and released to the ambient so that to allow another fresh and hot air to come in. This is obvious to all most all solar dryers.

2.4. Material for constructing solar dryer

In (Hossain and Bala, 2007, Bala et al., 2003) the materials for constructing solar dryers were suggested, the author said that the solar dryer can be constructed using simple and available local materials. Different designs used various materials for constructing solar dryer, the major factor used during materials selection and design is the availability of materials within the area. In addition to that choosing of proper materials in terms of cost, suitability to use in a particular unit, products to be dried (quality) and capability to resist environmental conditions are also factors considered in most of the designs.

Materials like glass or plastic with transmittance of close to 1 are highly recommended to be used as glazing covers, since they transmit insolation to the absorber plate much easier than those with 0 or close to 0 transmissivity. In order to enhance absorbance rate of solar energy from the sun to the absorbing plate special coating material is normally suggested. Ekechukwu et al., (Ekechukwu and Norton, 1999a) suggested that absorbance materials are required to be poor or low emissivity but good conductivity of heat and temperature stability properties. The authors recommended to use galvanized iron (GI) with black coating to increase absorption rates. Table 2.1 shows properties of some coating materials as described in (Ekechukwu and Norton, 1999a).

Table 2. 1 Properties of some coating materials.

Coating	Substrate	Absorptivity	Emissivity	Maximum temp.	Durability
Black nickel	Iron, copper, zinc/aluminium	0.85–0.96	0.05–0.15	288°C	medium
Black chrome	Nickel/aluminium copper, iron	0.82–0.96	0.04–0.15	427°C	Very good
Black copper	Copper	0.85–0.95	0.10–0.15	316°C	—
Copper oxide	Copper, iron, aluminium	0.87–0.90	0.08–0.16	—	—
Anodic aluminium	Aluminium	0.90–0.96	0.10–0.23	—	—
Metal carbide	Copper, glass	0.82–0.93	0.02–0.05	—	—
PbS paint	ANY	0.90	0.30	—	—
Selective paint (coralur)	Most	0.93	0.30	—	—
Black paint	Any	0.95–0.97	0.95–0.97	—	—

2.5. Thermal and physical properties of banana fruits

Physical and thermal properties of drying products are subjects of interest during designing of solar dryers, as they play a very important role in designing of drying equipment (Soltani et al., 2011). Physical properties like weight, dimensions, surface area, and volume together with thermal properties like moisture contents, latent heat of vaporization and specific heat are of great important in drying process, through these properties one may be able to calculate drying time and even energy required to effect moisture loss of products to be dried (Nwakuba et al., 2016).

2.5.1. Physical properties of banana fruits

In references (Wasala et al., 2012, Soltani et al., 2011) authors explained the method of determining some physical properties of banana fruits. The properties of interest measured by authors include weight, lengths, surface area and volume for both peeled and unpeeled banana fruits together with banana peels. The dimensions shown of Figure 2.4 were used in (Soltani et al., 2011) to find physical properties of banana fruit which was assumed to have a shape of ellipsoidal.

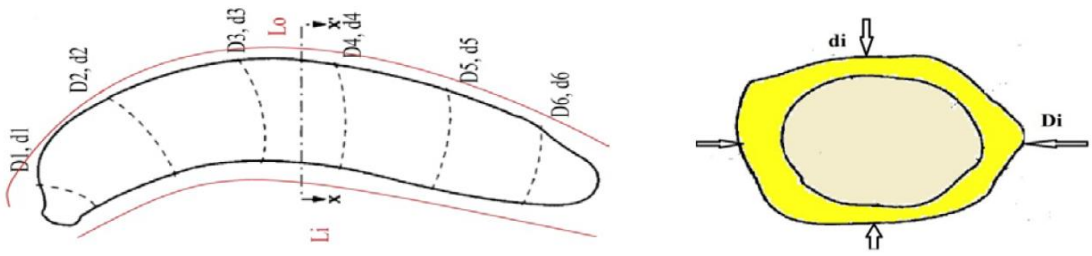

Figure 2. 4 Longitudinal section and diametrical cut axis of banana fruit.

From the Figure 2.4 above and according to (Soltani et al., 2011) and (Wasala et al., 2012) the average geometric mean diameters (D_{ave} and d_{ave}) of a banana fruit can be obtained using Equation [2.3a and 2.3b]. The geometric mean diameter (D_g) of a single banana fruit can be calculated using Equation [2.3c]. The average values of internal and external lengths of banana fruit is calculated using Equation [2.3d] in order to obtain the length (L_b) of the banana fruit. The authors suggested to use a flexible ruler in measuring the external and internal lengths, digital caliper and digital mass balance for measuring the diameter of sample of banana fruit as well as the weight respectively.

$$D_{ave} = \frac{D_3 + D_4}{2} \quad \text{[2.3a]}$$

$$d_{ave} = \frac{d_3 + d_4}{2} \quad \text{[2.3b]}$$

$$D_g = (L_{ave} * D_{ave} * d_{ave})^{0.333} \quad \text{[2.3c]}$$

$$L_b = \frac{(L_0 + L_i)}{2} \quad \text{[2.3d]}$$

2.5.2. Total heat energy required for drying food products

In the following references (Youcef-Ali et al., 2001, Bolaji, 2005), the authors came out with a formula to find the total energy required to dry food products. The formula proposed is the basic energy balance as shown in Equation [2.4].

$$m_w * L_v = m_a * c_p * (T_1 - T_2) \quad \text{[2.4]}$$

Whereby:

m_w = mass of water vapour to be evaporated (kg)

L_v = Latent heat of vaporization (kJ/kg)

m_a = mass of drying air (kg)

T_{in} and T_{out} = Initial and final Temperatures (K)

Mercer (Mercer, 2007) proposed that the heat energy required to dry the food product is the summation of two energies, in this regard two Equations [2.5a] and [2.6] are to be added together for calculating heat energy required to remove amount of water from agricultural fruits. The formula consist two stages.

The first stage is to find the heat energy that will increase the temperature of the wet materials to the level at which the amount of moisture contents can be removed, this is shown by the Equation [2.5a] below:

$$Q_a = M_b * C_p * \Delta T \quad \text{..... [2.5a]}$$

The value of specific heat capacity (C_p) of fruits to be dried is calculated using chemical composition of the fruits itself, therefore Equation [2.5b] as stated by (Mercer, 2007) with the chemical composition of fruits given by (Kasa and G/Yohanis, 2017) can serve on finding the specific heat capacity of fruits to be dried.

$$C_p = 1.424m_c + 1.549m_p + 1.675m_f + 0.837m_a + 4.187m_{fw} + 2.0505m_i \text{..... [2.5b]}$$

Whereby;

m_c is the mass fraction of carbohydrate

m_p is mass fraction of protein

$m_{f\,is}$ mass fraction of fat

m_{ash} is mass fraction of ash

m_{fw} is mass fraction of water

m_i is mass fraction of ice (for fruits stored in freezers)

The second stage is to calculate the heat required to evaporate the moisture contents of the products after being warmed up, this can be calculated using the equation below:

$$Q_b = m_w * (h_g - h_f) \text{ ……..…… [2.6]}$$

From the steam table the value of the enthalpy of water as a liquid h_g and the enthalpy of water as a vapor h_f can be obtained as long as the drying temperature is known.

2.6. Drying principles

Drying, as described by various researchers, is the process of remove moisture contents from a substance (Belessiotis and Delyannis, 2011), in a context of food material, drying refers to a simultaneous process of heat and mass transfer whereby heat is transferred from a moving fluid into materials to be dried, at the same time the moisture is transferred from the core of the material to its outside surfaces and being vaporized by the moving fluid. During this process the moisture contents within the products will continue to be moved until the vapor pressure within the products equalize with that of the nearby atmosphere surrounding the products. This is what is referred to as **equilibrium moisture content** and the relative humidity at this point is referred to as **equilibrium relative humidity.**

Bradley (Bradley, 2010) explained a way of calculating initial moisture contents. The author used one of the standard method of moisture content determination of different agricultural product by oven drying method using the formula shown in Equation [2.7]. Normally the weight of water is the difference between weight of material before and after drying.

$$MC = \left[\frac{\text{Initial weight} - \text{Oven dry weight}}{\text{Initial weight}}\right] x100\% \text{ ……..…. [2.7]}$$

2.7. Performance evaluation of solar dryer

Enough testings' of solar dryer system and quality evaluation of end products are important factors in assessing the technical performance of a dryer and quality of end products. These factors normally create a basis for comparison with other solar dryers and selection of suitable dryer design for the given particular conditions. Leon et al., (Leon et al., 2002) suggested a comprehensive evaluation procedure of solar dryer performance given test conditions and methodology for the purpose of developing standard analysis. The authors reviewed parameters

that provide basis and can easily be differentiated with other solar dryers. The performance parameters reported are dryer efficiency, drying rate, maximum drying temperature and costs. Evaluation parameter like solar collector sizing & dimensions, relative humidity and airflow rate were also discussed by the author.

2.7.1. Collector useful energy

Struckmann (Struckmann, 2008) on his project report "Analysis of a flat plate solar collector" applied Equation [2.8] to obtain the heat or amount of solar radiation received by the collector

$$Q_i = I\left({}^{W}/_{m^2}\right) A(m^2) \ldots\ldots\ldots\ldots\ldots\ldots\ldots\ldots\ldots\ldots\ldots\ldots \quad [2.8]$$

In the Figure 2.5, the author (Struckmann, 2008) depicted that when solar radiations hit the glass cover, 10% of solar input reflected back to the sky, 5% being absorbed by the glass while the remains pass through glass and absorbed by the absorber plate. Out of 85% only 45% of heat can be usefully collected and 40% is lost. Therefore the total amount of energy in watt (W) received by collector is given by Equation [2.9]

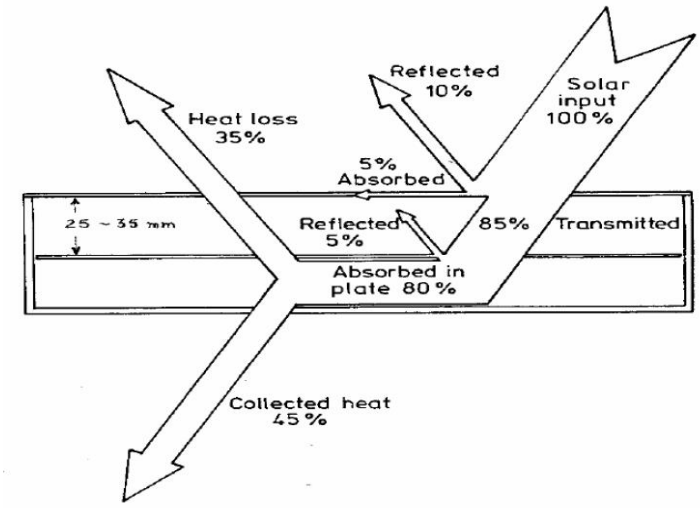

Figure 2. 5 Heat dissipation on a flat plat collector

$$Q_i = I({}^{W}/_{m^2}) * (\alpha\tau) * A\,(m^2) \ldots\ldots\ldots\ldots\ldots\ldots\ldots\ldots\ldots\ldots\ldots\ldots\ldots \quad [2.9]$$

Collector normally loses heat as it become hotter than the environment surrounding it. The loosing rate depend on the heat transfer coefficient of the overall collector (U_L) and the

temperature of the collector (Struckmann, 2008). Hence the heat loss (Q_{loss}) is given in equation [2.10]

$$Q_{loss} = U_L A(T_c - T_a) \quad \text{[2.10]}$$

Whereby;

T_c is a collector average temperature and

T_a is ambient temperature

α is the absorption coefficient of absorber plate

τ is the transmission coefficient of glazing cover/glass

The amount of useful energy generated by collector (Equation 2.11) can be obtained by taking the amount of energy received by collector less the heat lost to the surrounding by the collector. On the other hand, the useful amount extracted by the collector is the same as the amount of energy taken away by the stream of a moving fluid. Mathematically;

$$Q_u = F_R * A[I\alpha\tau - U_L(T_i - T_a)] \quad \text{[2.11]}$$

$\mathbf{F_R}$ is the collector heat removal factor

2.7.2. Collector efficiency

Dhanushkodi et al., (Dhanushkodi et al., 2014) expressed collector efficiency as a useful parameter for evaluating the thermal performance and overall effectiveness of the drying system. The performance of a flat plate collector is expressed in terms of overall efficiency of a collector (η_c) as shown in Equation [2.12a&b]. The overall efficiency of collector is given by the ratio of useful energy gain at any time period (Q_u) to the incident solar energy over the same period.

$$\eta = F_R\alpha\tau - F_R U_L\left(\frac{T_i - T_a}{I}\right) \quad \text{[2.12a]}$$

$$\eta = mC_p\frac{T_o - T_i}{IA_c} \quad \text{[2.12b]}$$

From Equations [2.12a] above the performance of the flat plate solar collector can be determined by measuring only three parameters during experiment, these are inlet temperature

of the fluid (T_i), ambient temperature (T_a) and solar radiation intensity of the location where experiment is conducted (I), other parameter left as constants.

2.7.3. Moisture contents

Moisture contents of a product to be dried is one of the important factor used to evaluate the effective performance of a solar dryer. Different studies have defined moisture contents in terms of the total weight of product to be dried or sometimes the solid weight within the product. In (Fudholi et al., 2013) and (Mercer, 2007) the papers defined moisture contents in two basis terms, dry basis and wet basis. Dry basis (X) is defined as the ratio of weight of water contents (m_w) to the weight of dry solid material (m_d) as shown on Equation [2.13]. Wet basis (W) is expressed as the weight of moisture per unit of wet materials as shown on equation [2.14]. In agricultural products it's recommended to express the moisture contents in wet basis.

$$X = \frac{m_w}{m_d} \text{ (kg of water per kg of dry solid material)} \quad \text{[2.13]}$$

$$W = \frac{m_w}{m_w + m_d} \text{ (kg per kg of a mixture)} \quad \text{[2.14]}$$

2.7.4. Drying rate

According to (Da Silva et al., 2014) and (Dhanushkodi et al., 2014) drying rate Equation [2.15] is defined as the rate of moisture removal from a product. It is the function of time which in turn is a function of moisture contents. Most of agricultural products are hygroscopic in nature i.e. moisture contents are trapped in closed capillaries, therefore during drying the large portion of energy is utilized to transform liquid water into vapor form as discussed in section 2.6.2. In (Belessiotis and Delyannis, 2011) stated that, the water inside material can be in a free unbound forms or bound forms and they are related directly to drying rate which on the other hand depends on relative humidity, velocity of drying air together with moisture contents and temperature of the product to be dried.

$$\text{Drying rate (DR)} = \frac{M_{bd} - M_{ad}}{t_d} \quad \text{[2.15]}$$

Whereby:

M_{bd} = mass of sample before drying

M_{ad} = mass of sample after drying

t_d = drying period

2.8. Pressure drop across the dryer

In the designing of a drying system it is important to take into account the pressure drop that might occur during drying process. For a convection drying system that employs fan as a means of driving air across a system, regardless of their sizes, it is important to ensure that an evenly circulation of air within the system is achieved for the better drying process. Under this phenomena determination of the pressure drop within the solar collector and within drying chamber is inevitable. There are various ways that can be used to calculate the pressure drop across the heater, according to (Ho et al., 2018) and (Shewen, 1981) the authors described and recommend Equations [2.16a-e] below to be used for calculation of the pressure drop across the rectangular cross-section of a solar air collector.

$$\Delta p = \rho f_s \Phi^2 \left[\frac{L_c}{H}\right]^3 \ N/m^2 \text{ or Pa} \quad \text{[2.16a]}$$

Whereby:

Δp = Change in Pressure

f_s = friction factor = $0.1335 Re^{-0.317}$ [2.16b]

$\Phi = \frac{m}{\rho_a L_c w}$ (volumetric flow rate per unit area of solar collector)…… [2.16c]

L_C =Length of the solar collector,

w = Width of the solar collector

H = Height of the air gap of the collector channel

$$R_e = \text{is the Reynolds Number} = \frac{w l_c \rho_a}{\mu_a} \quad \text{..... [2.16d]}$$

$$l_c = \frac{4wH}{2(w+H)} \quad \text{..... [2.16e]}$$

2.8.1. Criteria for selection of fan

In order to develop a forced convection system, there is a need to know the total air flow within the system that will be derived by a fan, type of a fan and the power of the solar panel to use in the system. Other parameters are like: Operating airflow or volumetric flow rate, the total pressure in the drying chamber and solar collector, inlet diameter and the operating temperature. The fan should be able to withstand temperature and overcome pressure drop in the system.

2.9. Quality of end products

Leon et al., (Leon et al., 2002) mentioned product evaluation through quality of end product as another criteria of interest to be evaluated. Drying process normally tends to modify simultaneously food properties, it is obvious that change in product properties like size, shape, color and aroma or test during drying process is inevitable and can influence consumer's demand perception (Kumar et al., 2014), therefore optimal control of quality attributes and assessment of quality of dried product are the most important keys to establish a basis comparison among drying systems. However (Kader, 2004) said that it is difficult and more challenging to measure the qualitative losses of product than quantitative although better preservation process can be applied to maintain quantitative level and reduces qualitative losses.

Pretreatment of fruits prior to drying is one of the technique reported by the researchers. This techniques is usually used to maintain the quality of dried product. It minimizes the changes that could occur during drying operation and keeps products from turning brown, darkens, stops metabolism of cut tissues and makes product more delicious and healthy (Abano and Sam-Amoah, 2011, Osunde, 2017, Tunde-Akintunde and Ogunlakin, 2011). Lemon juice and honey dip, chilling, ascorbic acid solution, sucrose, blanching, salt solution are some of the

pretreatment reagents normally applied. In (Osunde, 2017) the effects of pretreatment in quality of dried product was examined, the paper came with results which clearly show that pretreatment applied to the samples prior to drying were having significant effects on higher retention of quality and vitamins compared to untreated samples.

2.10. Thin layer modeling in drying process

Drying of agricultural product is the energy and time demand operation, although it increases the shelf life of product but decreasing large volume of water particularly those with high moisture contents. In (Onwude et al., 2016) the authors defined thin layer drying model as the method for describing and determining drying kinetics of agriculture products. The paper describes water removal and heat penetration through mass and heat transfer theories during which material is fully subjected under drying conditions of hot air. In order to enhance drying rate under thin layer drying modeling, products are normally sliced into a specific thickness prior to drying, to make possible for the thin layer model to easy predict drying rate. In the following references (Akpinar, 2006, Aregbesola et al., 2015, Da Silva et al., 2014, Kadam et al., 2011, Onwude et al., 2016, Purkayastha et al., 2013, Alam, 2014, Fadhel et al., 2011) researchers have applied thin layer modeling in drying of various products.

The thin layer drying model of agricultural products is normally described through drying models. According to (Onwude et al., 2016) there are 22 thin layer models already designed specifically for fruits and vegetables. The models contain empirical or diffusion equations for the latent heat of vaporization of water in product during drying as a function of temperature and moisture contents. Through the use of relevant statistical parameters, a suitable drying model is normally selected based on the raw data obtained from experiments expressing drying curve of a product. The best equation of model which expressing drying curve of samples is normally selected using the coefficient of determination R^2. The Chi square χ^2, root mean square (RMS), mean bias error (MBE) and t-value are used to determine the consistency of the fits. "The higher the value of R^2 in a particular model the better the model is in predicting the drying

kinetic of a product" (Onwude et al., 2016), on the other hand the lower the value of Chi square or RMS the better the model (Kucuk et al., 2014).

.

2.11. Numerical Modeling

One of the objectives of this study is to develop a numerical model that will evaluate the performance of banana solar dryer so as to aid design and prediction of drying parameters without repeating the experiment studies. Heat transfer and fluid flow problems in a computational fluid dynamic tools (CFD) can be solved using selected numerical discretization methods. Currently there are different numerical discretization methods to be used aiming to solve complex differential equations governing the heat transfer and flow phenomena, which cannot be solved analytically. These methods include the Finite Element Method (FEM), Finite Volume Method (FVM) and Finite Difference Method (FDM) (Anandharamakrishnan, 2013, Mostaghimi). Under Finite element method the fluid flow problem to be computed is discretized into finite number of sub-domains in which the function is set to account for the variation, the total variation of variables for each sub-domains is now be used to generalize the whole domain field. This chapter therefore intends to present the meaning of computational fluid dynamic and its application areas, governing equations used to solve fluid flow and heat transfer problems, advantages of CFD approach, CFD processes, ANSYS Fluent as a CFD tools together with reviews of CFD studies particularly in solar energy drying process.

2.11.1. Computational fluid dynamic (CFD)

Computational fluid dynamic is a study of predicting the fluid flow, heat and mass transfer together with other related phenomena through application of mathematical of partial differential and numerical equations which represent laws that governing the whole process (Ashgriz and Mostaghimi, 2002). It helps and enables scientists to perform numerical experiments through the application of powerful computer simulations. In most cases of engineering problems it is difficult to solve these equations analytically, therefore CFD makes

possible way to achieve computer based solutions using the governing equations for various engineering tasks (Bhaskaran and Collins, 2002). Due to its cost-effective than physical testing, CFD approach has been used in various industrial fields like design of IC engines, gas turbines combustion chamber, aircraft design and bio-medical engineering, metrological forecasting, environmental hazards etc. However for a complex flow simulations CFD become more challenging accompanying with error-prone and time consuming to achieve desired and converged results (Bhaskaran and Collins, 2002). There are different CFD tools software currently available, these include ANSYS Fluent, Comsol Multiphysics, and TRANSYS etc. According to (Versteeg and Malalasekera, 2007) the authors said, in order to achieve desire solutions using CFD tools, the physics applied to the fluid together with the numerical algorithms need to be well understood before selection of the desire CFD tool to be used for a particular problem

2.11.2. CFD governing equations and theory in drying processes

As far as drying process is concerned the fundamental parameters used to describe the drying process are temperature, velocity and moisture contents of the fluid that flow within the drying system. The flow of air within the drying system can be either compressible or incompressible depending on the assumption to be made. Therefore the drying parameters will be closely governed by the Navier-Stokes equations (N-S-E) which are grounded on the principles of the conservation of Momentum, Mass and Heat transfer. In fact CFD tools are already incorporated with conservation laws of momentum, conservation of mass and conservation of heat. According to (Bhaskaran and Collins, 2002, Anandharamakrishnan, 2013) the governing equations of mass transfer, heat transfer and fluid flow to be solved are continuity equations, momentum equations and energy equations, together with other mathematical equations from thermodynamic. These equation can be written in the form of Cartesian system as shown on Equations [2.17], [2.18] and [2.19] respectively

(a) Continuity equation

In a physical system the continuity Equation [2.17] represents the mass conserved. It is expressed by the law of conservation of mass in differential form.

$$\frac{\partial \rho}{\partial t} + \frac{\partial \rho u}{\partial x} + \frac{\partial \rho v}{\partial y} + \frac{\partial \rho w}{\partial z} = 0 \quad \text{..... [2.17]}$$

(b) Conservation of momentum

Basically these are the Navier-stokes equations for each velocity component based on the Newton second law of motion to a fluid element or particle (Bird, 2002). The law itself states that the rate of momentum change of fluid element of the system remain equal to the sum of body and surface forces acting on an element. The body forces include forces like gravitational forces and the surfaces forces include viscous and pressure forces.

Y-momentum: $\rho\left(\frac{\partial v}{\partial t} + u\frac{\partial v}{\partial x} + v\frac{\partial v}{\partial y} + w\frac{\partial v}{\partial z}\right) = \rho g_y - \frac{\partial P}{dy} + \mu\left[\frac{\partial^2 v}{\partial x^2} + \frac{\partial^2 v}{\partial y^2} + \frac{\partial^2 v}{\partial z^2}\right]$

X-momentum: $\rho\left(\frac{\partial u}{\partial t} + u\frac{\partial u}{\partial x} + v\frac{\partial u}{\partial y} + w\frac{\partial u}{\partial z}\right) = \rho g_x - \frac{\partial P}{dx} + \mu\left[\frac{\partial^2 u}{\partial x^2} + \frac{\partial^2 u}{\partial y^2} + \frac{\partial^2 u}{\partial z^2}\right]$

Z-momentum: $\rho\left(\frac{\partial w}{\partial t} + u\frac{\partial w}{\partial x} + v\frac{\partial w}{\partial y} + w\frac{\partial w}{\partial z}\right) = \rho g_z - \frac{\partial P}{dz} + \mu\left[\frac{\partial^2 w}{\partial x^2} + \frac{\partial^2 w}{\partial y^2} + \frac{\partial^2 w}{\partial z^2}\right]$ ..... [2.18]

(c) Conservation of energy

The equation of conservation of energy is basically the first law of thermodynamics which states that "the rate of change of kinetic and internal energy equals to the sum of the rate of heat addition to and work done on a fluid" as stated by (Bird, 2002) and shown on Equation 2.19a. In CFD Fluent this energy equation is solved in a form as shown in Equation 2.19b.

$$\begin{Bmatrix} \text{Rate of change} \\ \text{of Kinetic and} \\ \text{internal Energy} \end{Bmatrix} = \begin{Bmatrix} \text{Sum of rate} \\ \text{ofKinetic} \\ \text{and Internal} \\ \text{energy by} \\ \text{convective} \end{Bmatrix} + \begin{Bmatrix} \text{Sum of rate of} \\ \text{Heat by} \\ \text{Conduction} \end{Bmatrix} + \begin{Bmatrix} \text{Rate of workdone} \\ \text{on a fluid by} \\ \text{mechanism} \end{Bmatrix} +$$

$$\begin{Bmatrix} \text{Rate of workdone} \\ \text{on a fluid by} \\ \text{esternal forces} \end{Bmatrix} \ldots\ldots\ldots\ldots\ldots\ldots\ldots\ldots\ldots\ldots \text{[2.19a]}$$

$$\rho \frac{DE}{Dt} = -div(pu) + \left[\frac{\partial(u\tau_{xx})}{\partial x} + \frac{\partial(u\tau_{yy})}{\partial y} + \frac{\partial(u\tau_{zx})}{\partial z} + \frac{\partial(v\tau_{xy})}{\partial x} + \frac{\partial(v\tau_{yy})}{\partial y} + \frac{\partial(v\tau_{zy})}{\partial z} + \frac{\partial(w\tau_{zy})}{\partial z} + \right.$$

$$\left. \frac{\partial(w\tau_{xz})}{\partial x} + \frac{\partial(w\tau_{yz})}{\partial y} + \frac{\partial(u\tau_{zz})}{\partial z}\right] + div\,(k\ grad\ T) + S_E \quad \ldots\ldots\ldots\ldots\ldots\ldots \text{[2.19b]}$$

Whereby:

u, v, and w are velocities terms

g_x, g_y, and g_z are components of gravitational force

τ is the normal stress on the x, y, and z faces

$\frac{\partial u}{\partial x}, \frac{\partial v}{\partial y}$ and $\frac{\partial w}{\partial z}$ are convective terms or inertia forces

$\frac{\partial P}{dx}, \frac{\partial P}{dy}$ and $\frac{\partial P}{dz}$ are pressure forces

k is the heat flux

T is the temperature

S_E is the heat source term

2.11.3. Advantages of using CFD

It is obvious that the experimental results normally show a real system behavior and are more convenient, but on the other hand knowing the system performance and behavior during and even design stages is also convenient particularly in term of cost and time. In (Versteeg and Malalasekera, 2007) different advantages of Computational Fluid Dynamic (CFD) application have been described. Through CFD approach, it is easy to evaluate dangerous or hazardous systems than experimental approach, systems that involve high u.v radiations, high heat, air pollution and transport of contaminants. Hence it increases safety and reduces risks that may

occur due to the physical contacts. The CFD approach provides a concrete detailed report than experimental results, uncontrollable and large systems that are difficult to control physically can be evaluated using CFD tools. CFD makes parametric studies of a system within less time, CFD opens a room for any optimizations of parameters and system performances (Norton et al., 2010). This is achieved due to the application of animations and colors effects which visualize the internal behaviors of a system and make easy interpolation of physical phenomena within a computational domain.

2.11.4. The CFD Processes

In order to execute CFD problems, one must have a knowledge to express the problem to be executed mathematically and in a way that CFD tool will help to express the knowledge and execute the problem in a scientific and algorithmic manner. Through application of computer system installed with CFD program, the calculations and interpretation of results will be done based on inputs assigned. According to (Muiruri and Motsamai, 2018) three stages are achieved in order to perform CFD analysis as shown in Figure 2.6

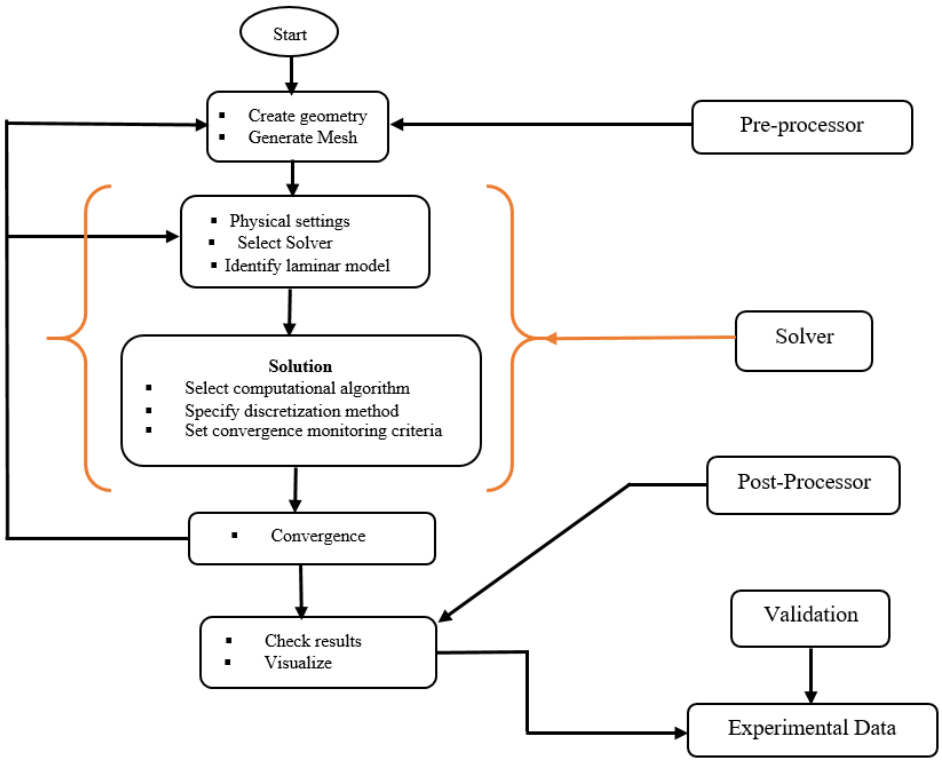

Figure 2. 6 The CFD flow scheme

(a) Pre-processing

This is the first stage whereby the problem is described in term of flow domain or geometry before being solved numerically. Therefore all activities done before solving fall under this stage. The following are sub-stages to be accomplished under this stage: Importing or modelling of flow domain (Geometry) to be executed. Under this stage modeling can be done with the CFD tool itself of with the help of other CAD programs that are compatible with CFD workbench to be used. Normally a geometry designed from other CAD program need to be saved with a specific file type for it to imported and retrieved in a CFD workbench. Meshing: This is another important sub-stage, it is process of dividing the geometry or flow domain into small volumes know as cells or elements, these elements can take a shape of either triangular, tetrahedral etc.

(b) Processing or Solver

This is the core stage of CFD tool whereby a computer is used to run and solve mathematical equations of computational fluid flow. It is a very time consuming stage especially for a complex geometry, this is due to thousands and millions of elements (meshes) being solved using the governing equations and boundary conditions for each individual element involved. Under this stage, the choice of suitable type of fluent to be used in a problem, the conservation equations, the turbulence models and governing boundary conditions of the fluid motion is of great importance. Under this stage the setup of the solver can be made to run the simulation repeatedly or under different frequencies or number of iterations or time steps depending on the complexity of the problem or capacity and capability of the computer until the whole process converge (Xia and Sun, 2002, Fluent, 2015).

(c) Post-Processing

This is the stage whereby generation and visualization of CFD results are done. Visualization of results can be of a different form depending on parameters intended to be evaluated. Different fluid parameters like velocity, temperatures, forces etc. can be viewed. Under this stage the

parameters of interests of the computational fluid domain of the system simulated can be examined through the use streamlines, contour, graphs, plane, volume rendering or animations depending on the parameters chosen to describe the problem (Fluent, 2015, ANSYS, 2011).

2.11.5. Modeling of viscous turbulences in CFD Processing

In a context of forced convective drying process that involve turbulence flow of hot air in the system, the complexity and application of Navier-Stoke Equations depends mainly on the turbulences of the fluid flow. Basically there are two types of fluid flow. A fluid flow can be either Turbulent or Laminar fluid flow depending on either high or low Reynolds number. According to (Sun, 2007) the fluid flow at low Reynolds number can be solved by using equation of conservation but the fluid flow with elevated Reynolds number (turbulent flow) the time-averaged flow field approach need to be applied. In computational fluid dynamic there are different turbulence models to be taken into account in order to arrive in a well-converged solution. As said above, these turbulence models depend on the complexity of the level of solving fluid flow in engineering problems. Not every model can be used in any fluid flow simulation. Attention therefore should be taken to which appropriate turbulent model to be used in simulation. According to (Ferguson, 2005), there are a number of turbulences models to be used, but the most popular turbulence models that are commonly used are Standard k-ε Model, Realizable k-ε, Renormalization Group (RNG) k-ε and Reynolds Stress Model (RSM). These model are more popular due to their accurate in convergences (Malalasekera, 1995).

2.11.6. Modeling of solar load in CFD processing

Normally CFD programs like ANSYS Fluent incorporated with a solar load model are special for the simulation and trucking of sun's radiation effects. The solar radiations transmitted through transparent surface (glass) are being absorbed within a computational domain of a system. For the given latitude and longitude position of a place, date and even time of a day, a solar load model within ANSYS Fluent is able to develop and track sun location using solar calculator (Mathew et al., 2016). According to (ANSYS, 2017), in order to use solar load model

one must have the inputs like geographical position of a place (longitude, latitude and time zone), solar irradiation methods, and grid orientation either north or east, date or time together with sunshine factor. Having these inputs the solar load model can compute solar irradiation diffused by both surfaces.

2.11.7. The CFD modeling in drying processes

The application of computational fluid dynamic tools in drying process of agricultural product is of great important, it help to develop and analyze drying parameters of a particular product. The CFD tool act as a virtual sensor for examining flux concentration and flow distributions within a computational domain. Through CFD application, parametric studies and geometric change of drying equipment can be done during design stage, hence build-up confidences in achieving better design solution and quality of food products (Evans, 1994),(Norton et al., 2010). The CFD tool makes possible prediction of temperature distributions and airflow simulation within a dryer. ANSYS, MATLAB, COMSOL are some of the well-known advanced CFD tools currently used to describe the drying process.

2.11.8. Review of CFD in drying process. A case study of ANSYS Fluent

A recent advances and approaches study on application of CFD programs in simulating food drying processes was done by Narjes et al., (Malekjani and Jafari, 2018). The authors discussed the fundamentals, advantages and shortcoming of computational fluids dynamics (CFD) underlying the drying processes. In discussing the turbulent models used in CFD tools particularly the Reynolds Averaged Navier Stokes (RANS) Model, the authors tabulated and compared advantages and disadvantages of different turbulent models incorporated within the CFD tools. The authors cited that the most vital parameters of interest during drying of food products is the quality of end products associated with crack formation, moisture contents, case hardening etc. Other parameters can be improved through the proper modeling technique. Through CFD application of the hydrodynamic of fluids flow, mass and heat transfer within computational fluid domain can be predicted. The key findings of this paper was that, the

utilization of CFD method in food industry help to develop and enhance new and current dryers for the better improvement of food quality.

In 2018 Esquivel et al., (Esquivel et al., 2018) optimized drying process of coffee fruits using experimental and numerical approach on a greenhouse solar dryer. The environmental condition of the forced convection greenhouse solar dryer were examined. The reason for the authors to use CFD tools was to study the internal behavior of dryer. Since forced convection dryers are accompanied with turbulent flow, a turbulence and buoyancy model were energized to account for turbulences and density during simulation treatment respectively. Radiation model was also activated to solve for radioactive transfer and participation of radiation in a drying system. All numerical models were developed using ANSYS tool which have the potential to analysis the internal surrounding of the greenhouse dryer.

In (Sanghi et al., 2018) the natural convection drying process of corn was simulated with a computational fluid dynamic tools. ANSYS tool was used in this study and different parameters were studied during simulation and compared to the experimental results. The author introduced governing equations of Navier stokes, continuity and heat equations to account for transport phenomena within the system. Refinement of the fluid domain was done and Meshing of the fluid domain contains 89,096 cells/element and 23, 170 nodes, the actual range of the grid quality was set in such a way that the skewness of less than 0.95 and the orthogonal high than 0.15 were maintained. This is an acceptable range as described by (ANSYS, 2017). The flow within collector was assumed to have turbulence flow regime, therefore the Renormalization Group (RNG) k-ω turbulence model was selected during CFD setup in order to account for the unsteady flow. The Numerical model developed by using ANSYS workbench was validated with the experimental results which were previously obtained.

In 2017 Orbegoso et al., (Orbegoso et al., 2017) used computational fluid dynamic model to characterize numerically the thermal behavior of one-step and three step solar air heating

collector configurations in drying cocoa beans. The collector were compared under different operating conditions to see which one would demonstrate the best results of thermal efficiency and outlet air temperature, among the three configurations of solar collectors. The CFD model was developed using ANSYS 14.0 workbench to analyze both radiative and convective phenomena. The setup under CFD approach was accomplished through the use of *k-ω* RANS turbulence model which was suggested by (D.C, 2008) . The author employed sophisticated radiation model called the discrete ordinate model (DOM) to account for the contribution and participation of thermal radiation energy in solar air heater. The geometry/computational domain of the solar air heater was generated in ANSYS program, it was categorized into four subdomains, and each subdomain was discretized into number of hexahedral elements. For the glass and absorber plate the size of the elements was set to 0.32mm whereby the aspect ratio of the element was between 1.40 and 6.69 which is the recommended value. The total number of elements of the computational domain accounted to 490,000. The model validated against experimental data. It was found that the CFD model simulation for the three step solar air heating collector was the best, almost 67% thermally efficiently than on-step solar heating collector, exposed under the same solar irradiation effects.

In the year 2015 Chauhan et al., (Chauhan et al., 2015) presented a review which focused on the use of software in drying systems and explained how software can be employed to develop model and predict performance of solar drying systems. The authors stated that with the help of computational fluid dynamic (CFD) programs like ANSYS and FLUENT, Comsol, Multphysics MATLAB and TRNSYS a researcher, academician and scientists may appropriate simulate and predict temperature & airflow distribution patterns, moisture evaporation and development of mathematical model to describe drying rate and kinetics of the dryer and crop to be dried. By identifying the importance of the application of software in drying process the authors gave out a useful conclusion that understanding performance of solar drying systems at

design stage through supportive use of software's make possible optimization of design parameters, save time and capital investment before fabrication.

In 2014 Romero et al., (Romero et al., 2014) Presented results describing simulation and validation of an indirect solar dryer for drying vanilla products using CFD fluent program. In order to solve the physical phenomena of solar dryer the authors used ANSYS fluent solar load model to check for the effects of sun's rays or radiations within a computational domain. The simulation took into account the three dimensional, transient and laminar flow in an hourly range of 9hrs during daytime. Experimental data of a solar dryer like temperature distribution inside a cabinet of designed solar collector were compared with simulations results obtained. The authors offered a conclusions that due to the weather conditions it was difficult to make estimation of the convection heat transfer coefficient for the experimental data while simulation showed the value to be constant. However, similar behavior was expected to occur if the experimental data were to be adjusted to a six degree polynomial equations. In references (Sanghi et al., 2018, Norton et al., 2010, Ingle et al., 2013, Amraoui and Aliane, 2017) the authors wrote papers on the use of CFD tools in various in drying.

In 2013 (Bhagoria, 2013) presented a paper on heat transfer in a roughened solar collector through application CFD approach. ANSYS Fluent 12.1 was used to simulate the fluid flow. The geometry of the flow regime was meshed with 0.24mm cell size with fine and non-uniform quadrilateral mesh for the aim of resolving sub-layer on the plate, 161,568 total number of mesh elements were obtained during meshing. It was stated that this number was picked in between 103,231 and 197,977 as shown on table 2.3 in order to account for Nusselt number and friction factor, since the value above that range brings less than 1% variations. For the purpose of governing the flow phenomena the energy equation and incompressible N-S equations were used. The authors further decided to use (RMG) k-ε turbulent model during fluent setup to account for turbulent flow of the flow regime.

Grid independence test.

Size of element (mm)	Number of elements	Nusselt number (*Nu*)	% difference	Friction factor (*f*)	% difference
0.3	103231	79.88	–	0.0218	–
0.28	118781	82.83	3.69	0.0227	4.15
0.26	136910	83.59	0.92	0.0229	1.07
0.24	161568	83.88	0.35	0.0231	0.94
0.22	197977	84.97	0.11	0.0232	0.57

Figure 2. 7 Grid Independence test (Bhagoria, 2013)

In the same year of 2013 Alonso-Torres et al., (Alonso-Torres et al., 2013) Published a paper on "CFD modeling and validation of roasting coffee beans". The paper compared experimental findings of bean temperature and humidity loss from another paper. Although the paper did not discuss the use of solar dryer, heat and mass transfer equations were solved through finite volume methods (FVM) using ANSYS fluent 13.0 program. Refined unstructured mesh were used with 167,507 elements having tetrahedral shapes to simulate the model, the author defended that the unstructured meshing provide advantage to the software by reducing set-up time and allows good refinement of the mesh. The paper did not describe the modeled equations used but User define Function (UDF). UDF was used to program equations and were added to the ANSYS Fluent. Findings from this paper indicated that the numerical model predicted the real roasting process and shows good consistence with experimental results from another paper, therefore making it possible to observe the process in a real time.

CHAPTER THREE: MATERIALS AND METHODS

3.1. Design Considerations

Design of solar dryer was considered taking into account various design parameters, assumptions and criteria of interest based on procedures and mathematical equations described in literature review. Specific design criteria and parameters of interest were determined through successions of engineering design calculations by considering a general design of indirect forced convection solar dryer with a double air pass solar collector.

Under this design section, various factors including environmental conditions of Gaborone, physical & dimensional properties of banana fruits, drying and solar system characteristics as reported in literature review, were served as inputs to deliver preliminary approach towards successful design of expected actual solar dryer. While there are extensive varieties of indirect solar dryer design happening in the literature, design of solar dryer in this study was highly considered to keep the system away from becoming more sophisticated. In other words, to keep the dryer designed with 100% green technology without the use of auxiliary power supply.

3.2. Environmental condition of a location

The environmental condition of Gaborone particular University of Botswana served for design of indirect solar dryer. Gaborone has a climate conditions which satisfy the use of solar energy in drying purpose. The average total solar irradiation (I) was taken to be 21 MJ/m^2 and sunshine hours (t_d) to be 8hrs as stated by (WEC, 2018) and supported by (Nijegorodov et al.) that the mean daily global radiation measured at University of Botswana varies from 31 MJ/m^2 in December to 16 MJ/m^2 in June. The estimates of collector optimal tilt angles (β) of sunlight incident upon tilted flat solar collector relative to horizontal was taken to be 29^0 (Jacobson and Jadhav, 2018).

3.3. Physical and dimensional properties of banana fruit

The physical properties of the banana fruits were used in calculations as the design system required to meet specific weight of banana fruits loaded in it. (Soltani et al., 2011) and (Wasala et al., 2012) presented methods to achieve physical and dimensional properties of banana fruits as described in detail in the literature review section 2.5.1. The same method was adopted to determine the average properties of peeled and unpeeled banana fruits.

During design of drying chamber the average length, weight and diameter of samples of few banana fruits were taken in order to know exactly the amount of banana fruits to be loaded on the trays of the drying chamber. The average weight W_b, length L_b and diameter D_b of few samples of banana fruit were measured using flexible ruler and weight balance. It was observed that 0.221 - 0.271kg, 108-154mm and 22-28mm were the average value obtained for the weight, length and diameter of banana fruits (see Table 3.1). Therefore, let's say a single peeled banana fruit (pulp) having average weight of 0.246kg, length of 131mm and diameter of 26mm can be sliced diametrically to produce 26 slices each of thickness of 5mm, excluding ends/tips of bananas which are normally small in diameters. From Figure 3.1 an estimate of drying area on a tray can be made as follows: When 26 banana slices with 28mm diameter each are spread on a tray in one column, an area of 28mm x (28 x 26) = 20,384mm^2 or 0.02m^2 on a tray will be used to accommodate one piece of banana pulp.

Table 3. 1 Preliminary design properties of Banana

Banana properties	Minimum	Maximum	Average
Weight of banana fruit (unpeeled), kg	0.142	0.319	
Weight of Pulp, kg	0.221	0.271	**0.246**
Weight of Peels, kg	0.0327	0.0738	
Percentage of peel, %	29	35	
Length of banana fruit (unpeeled), m	0.112	0.138	
Length of Pulp, m	0.108	0.154	**0.131**
Diameter of banana fruit (unpeeled), m	0.024.5	0.31.8	
Diameter of Pulp, m	0.024.2	0.28.7	**0.026.45**

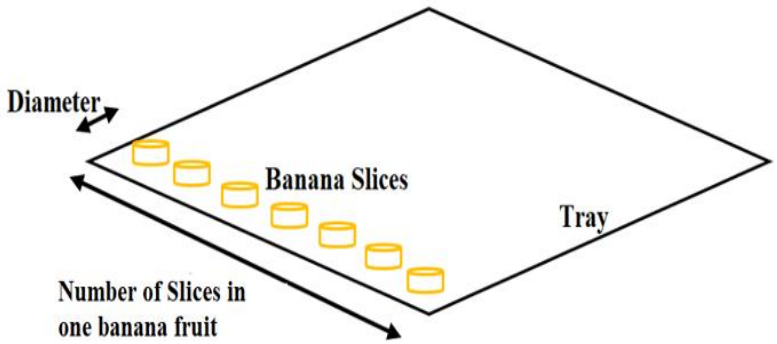

Figure 3. 1 An estimate of drying area on tray.

For the purpose of design and experiment, 15 pieces of peeled banana weighing *(M_b)* approximately 3.69kg to 4kg were taken to be an initial loading capacity of banana fruits to be dried in this study. Figure 3.2 shows one peeled banana and how longitudinal and diametrical measurement were taken in the lab during experiment set up. These measurements served on obtaining the number of slices per one piece of peeled banana.

Figure 3. 2 Longitudinal & diametrical cut axis of peeled & unpeeled banana fruit.

3.4. Design procedures of solar dryer

One of the objective of this study is to design and construct a forced convection-type, solar dryer for use in drying banana fruits under conditions of the Gaborone. To accomplish this task, studies of both the banana properties and the drying system were undertaken in order to develop an adequate solar drying system. Some of the area need to be discussed in this section are physical properties of banana, geographical conditions of Gaborone, energy required to effect the moisture contents, collector and drying chamber sizing and thermal properties of air required to dry banana. Some of these design procedures were comprised of integral steps,

procedures, design calculations and considerations which required to meet specific solar dryer design directives.

3.4.1. Moisture contents, temperature and collector efficiency

For the purpose of design the initial moisture content of banana *(M_i)* was taken to be 82% as described earlier in literature review. Although during experiment this value for each sample of banana fruits purchased will be determined and averaged through standard method. In contrast, the final moisture contents *(M_f)* which prevent banana fruits from spoilage was taken to be <20%. The maximum allowable drying temperature *(T_d)* for fruits with high sugar content is taken to be 338K (Abdullahi et al., 2013). To avoid quality degradation and brownish of end products the drying temperature value of 333K which is a bit lower than and closer to the maximum allowable drying temperature was chosen to be the drying temperature for this design's calculations.

Also for the purpose of design, an estimate of 50% was assumed to be the efficiency of the collector. This value is in line with the range of 30% to 50% described by (Ampratwum and Dorvlo, 1998) and (Sodha, 1987). It was assumed to be based on the lower and upper efficiency of 26% to 65% of solar collector efficiency reported by (Jairaj et al., 2009) . However, the actual efficiency of the flat plate collector will be determined during experiment and it is anticipated to be in a range closer or higher to this value. Table 3.2 shows some preliminary design parameters of the banana solar dryer, the data includes the physical properties of banana and geographical conditions of Gaborone, Botswana.

Table 3. 2 Summary of preliminary design parameters

Banana Properties	Symbol	Value	Unit
Number of banana fruits per batch	N_{batch}	15	-
Mass of banana fruits to be dried	M_b	3.69-4	kg
Weight of a single banana fruit	W_b	0.246	kg
Thickness of banana slice	δ_b	0.003-0.005	m
Maximum allowable drying Temp.	T_{Max}	60	K
Ambient Temperature	T_a	35	K

Initial moisture contents	M_i	75-82	%
Final moisture contents	M_f	13-16	%
Solar collector Efficiency (assumed)	η	0.50	%
Geographical conditions			
Collector tilt angle	β	29 due north	degree
Botswana Incident Solar Radiation	I	10-21	$MJ/m^2/day$
Sunshine hours per day	S_d	8-9	h
Latitude of Gaborone, Botswana	ϕ	24.67	^0S

3.4.2. Amount of moisture to be removed from banana fruits

Banana fruits like other AP's have two parts, dry part and wet part. The total amount of water (wet part) present inside the 4kg of banana fruits to be dried was calculated using Equation [3.1] as it is suggested by (Ehiem et al., 2009, Ampratwum and Dorvlo, 1998).

$$M_w = M_b * \frac{M_i - M_f}{100 - M_f} \text{..... [3.1]}$$

$$= 3.69\text{kg} * \frac{82 - 16}{100 - 16} = \mathbf{2.89kg}$$

Therefore the dry part of 4kg of banana fruits is given by

3.69kg – 2.89kg = 0.781kg (21.68%)

3.4.3. Energy required to effect moisture losses

From the literature review (Mercer, 2007) described two formulae [3.2] and [3.3] used for calculating heat energy required to remove amount of water from different fruits. The formula consisted of two stage process,

(a) The first stage

By increasing the temperature of the wet materials (in this case banana fruits) to the level at which the amount of moisture contents can be removed. The heat required was given by:

$$Q_a = M_b * C_p * \Delta T \text{ ..... [3.2]}$$

The value of specific heat capacity *(C_p)* of banana fruits is calculated using the formula below as stated by (Mercer, 2007).

$$C_p = 1.424m_c + 1.549m_p + 1.675m_f + 0.837m_a + 4.187m_w + 2.0505m_i \ldots\ldots \text{[3.2a]}$$

Whereby according to (Mercer, 2007)

m_c is the mass fraction of carbohydrate

m_p is mass fraction of protein

$m_{f\,is}$ mass fraction of fat

m_a is mass fraction of ash

m_w is mass fraction of water

m_i is mass fraction of ice (for fruits stored in freezers)

In (Kasa and G/Yohanis, 2017) the authors provided the value of chemical composition of banana fruits. By using these values in Equation [3.2a] the value of specific heat capacity *(C_p)* of banana fruits was calculated as follows:

$$C_p = 1.424 * 23.43 + 1.549 * 1.03 + 1.675 * 0.48 + 0.837 * 0.8 + 4.187 * 74.26 + 2.0505 * 0$$

$$C_p = \mathbf{3.47kJ/kg^0C}$$

Note: This value seems to agree with the value computed by (Mercer, 2007) a shown in Appendix II

Therefore;

$$Q_a = 3.69\text{kg} * 3.47\ \text{kJ/kg}^0\text{c} * (60 - 35)^0\text{C} = \mathbf{251kJ}$$

(b) The second stage

The heat required to evaporate the moisture contents of the products after being warmed up. The heat required to evaporate is calculated using Equation [3.3] below as follows:

$$Q_b = M_w * (h_g - h_f) \text{ ……..…… [3.3]}$$

From steam table at drying temperature of 333K:

The enthalpy of water as a liquid h_g = 2906.6kJ/kg

The enthalpy of water as a vapor h_f=251.13kJ/kg

$$Q_b = 2.89\text{kg} * (2906.6 - 251.13)\,\text{kJ/kg} = \mathbf{7,674kJ=7.672MJ}$$

Therefore, the total useful energy required to remove amount of water of 2.89kg from 3.69kg of banana fruits is the summation of the heat required to increasing the temperature of the wet materials (in this case banana pulps) and the heat required to evaporate the moisture contents of the products, and is given as follows:

$$Q = Q_a + Q_b = 251 + 7674 = 7925\text{kJ} = \mathbf{7.93MJ}$$

3.4.4. Sizing the flat plate collector

From the total useful energy (Q_u) required to evaporate the amount of moisture contents and the total net radiation (I) received by the tilted flat plate collector around Gaborone, the area of the solar collector (A_c) required to generate and supply the useful energy to the drying chamber was calculated using Equation [3.4] as described by (Sodha, 1987).

$$A_c = \frac{Q_u}{I_T \eta_c} \text{ ……..…….. [3.4]}$$

By assuming the collector efficiency (η) of 50% which is within the range of 30% to 50% as suggested in (Ampratwum and Dorvlo, 1998) and (Sodha, 1987), and by taking the minimum value of total average global irradiation for Botswana (*I)* of 12MJ/m^2 which is within the range of 21 MJ/m^2 and 10 MJ/m^2 as reported in (Ketlogetswe and Mothudi, 2009) and (Andringa, 2017) respectively, the collector area can be calculated as follows:

$$A_c = \frac{7.93\text{MJ}}{12MJ/m^2 * 0.5} = \mathbf{1.32}\boldsymbol{m^2}$$

Hence, an area of a solar collector (absorber plate) was taken to be 1.36m^2 in order to account accommodate fins attached on absorber plate, which also increases collector surface area. This size was also chosen due to the fact that in (Forson et al., 2007), the authors highlighted hat the length to width ratio of a flat plate solar collector should be in a range between 1-2.5. Therefore by taking the ratio of 2.1 to be used for this design to determine dimensions of collector, the actual length (L_C) and width (w) of the solar collector was chosen to be 1.7m x 0.8m = 1.36m^2. It should be put in mind that during actual fabrication of the collector, the width of the collector which is also taken to be the width of the absorbing plate will be 0.784 instead of 0.8 to account for the depth of 0.016mm of the grooves to be used to secure the edges of both top and bottom glasses in each sides of the solar collector as shown on Figure 3.5a.

3.4.5. Airflow passages/channels

Air passage is one of the important component of solar flat collector. (Scanlin, 1997) pointed on the air velocity of a dryer to be between 0.5m/s to 5.08m/s. The author also argues on the depth of the air channel to be between $1/15$ to $1/20$ of the lengths of a collector in order to ensure aerodynamic flow of air along the collector.

Therefore by assuming factor of depth of air channel to be 1/20 (0.05) as recommended by (Scanlin, 1997), multiplying this factor with the length of solar collector, the air depth of air passage was obtained as follows:

The depth of air passage = 0.05 * 1.6m = 0.08m

In the reference (Irtwange and Adebayo, 2009), the authors suggested that the fluid depth or channel between absorber plate and cover plates should be between 0.04m to 0.08m. For the purpose of this design, both the fluid depths were taken to be 0.08m, this mean that, the top air channel was chosen to be 0.08m and the bottom channel which has a gap between the bottom glass and absorber plate to be 0.060m, leaving 0.02m air gap space underneath of absorber plate (seen on figure 3.9).

3.4.6. Absorber surface area

The size of the surface area of the absorber plate (A_{ab}) was assumed equivalent to the solar collector surface area,

$$A_{ab} = A_c = L_C * W_c$$

$$A_{ab} = 1700 * 800 = 1.36m^2$$

The thickness of the absorber plate to be used in design was calculated using Equation [3.5] as described by (Abubakar and Isiyaku, 2014). The thickness is approximated as the ratio of the of heat transfer coefficient (0.2W/m^2 K) to thermal conductivity of the aluminum plate which is 210W/m. K, therefore the thickness of the plate is given by

$$\delta p = \frac{0.2}{K} \quad \text{..... [3.5]}$$

$$\delta p = \frac{0.2W/m^2K}{210W/mK} = 0.000952m$$

Under this design, the value of thickness of absorber plate was taken to be slightly high than the calculated one due to the fact that the absorber plate was expected to carry fins on its middle surface area. In order to avoid bending of absorber plate and effect of expansion during high solar radiation the value was taken to be 0.0016m which is one of the standard aluminum thicknesses recommended by ISO.

3.4.7. Tilt angle of solar collector

Since the location of University of Botswana is in the southern hemisphere at the latitude of 24.67^{0}S, the flat plate collector orientation angle *(β)* of 29^0 facing north was considered as the optimum slope to be used in design of collector and during experiment as described by (Jacobson and Jadhav, 2018). However, in order to allow proper and safe maintenance, the solar collector was designed in such a way that it can be tilted to various angles, this will help to bring the collector to the horizontal position in order to remove glass, to do proper internal

inspections, cleanness and other maintenances to be done inside the collector. On the other hand, this variations of angle can helps a researcher in performing research study on performance of solar collector for various inclination angles in Botswana.

3.4.8. Volumetric flow and mass flow rate

To ensure air is not restricted within solar collector, the solar collector inlet is employed and the volumetric flow is calculated by multiplying the area of the inlet hole (the inlet hole was assumed to have diameter 80mm, equivalent to the height of the top passage)

$$\text{Inlet Area } (A_i) = \pi r^2 = \pi * 0.04^2 = \mathbf{0.00503 m^2}$$

Volumetric and Mass flow rate are given by:

Volumetric = inlet area * air Velocity

Mass flow rate = $A_i \rho \upsilon$ = 0.00503*1.13υ (Kg/s) =0.00568υ……. [3.6]

Assuming air inlet velocity of 1.5m/s which is between 0.5m/s -5.08m/s as recommended by (Scanlin, 1997)

$$\text{Volumetric flow rate} = 0.00503 m^2 * 1.5\ {}^{m}/_{S} = \mathbf{0.00755 m^3/_s}$$

$$\dot{m} = \text{Volumertic flow rate} * \text{density of air}$$

$$= 0.00754\ (m^3/s) * 1.13\ (kg/m^3) = \mathbf{0.00851\ kg/s}$$

Note: These values are for the design purposes, the actual values will be obtained during experiments, since it is obvious that the volumetric flow and mass flow rates are both dependent on the value of velocity of air that goes inside the solar collector.

3.4.9. Average drying time

The average drying time was calculated using Equation [3.7]

$$M_{dr} = \frac{M_w}{t_d} \text{……. [3.7]}$$

$$= \frac{2.89kg}{8hrs} = \mathbf{0.361kg/h}$$

$$= \mathbf{0.361\,kg/h} * \frac{\mathbf{1hr}}{\mathbf{3600}} = \mathbf{1.0028e^{-4}kg/s}$$

3.5. Descriptions of the design components of a solar dryer

The designated solar dryer shown in Figure 3.3 is made up of three components namely: the Drying unit, Collector units and the Frame. A detailed descriptions of all components is as shown in the following section.

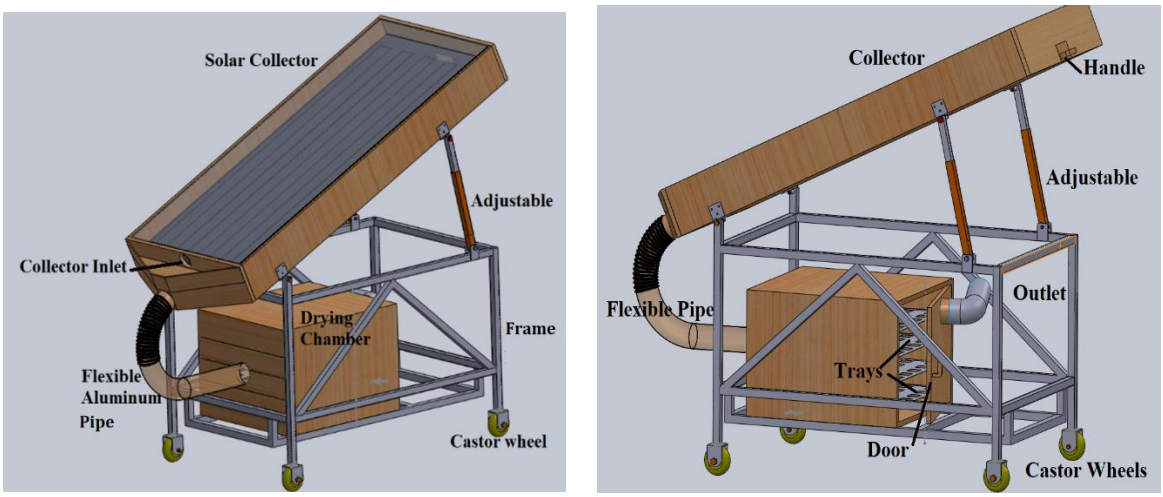

Figure 3. 3 Isometric views of the designated solar dryer.

3.5.1. Collector unit and its configurations

The designed solar collector shown in Figure 3.4 is the double pass flat plate collector type with two air flow passages. The collector unit has an external overall dimension of 1.8m x 0.840m. The collector unit is made up of Plywood with 16 to 20mm thickness. The solar collector unit has two air passages, two glasses and one aluminum sheet. The top channel which is in-line with the air inlet hole is between the top and bottom glass while the second passage is confined between the bottom glass and the absorber plate, Figure 3.5a and 3.5b illustrate. The reason for designing this type of collector is due to the reported description by (Ramani et al., 2010)**.** The report shows improvement of thermal performance of solar collector through airflow passage

arrangement, which reduces significantly heat losses coefficient on the top surface and the channel between glass cover and absorber plate. Under this configuration the inlet air is pre-heated first in the top channel, increases its temperature above ambient temperature before re-heated again with absorber plate in the bottom air channel.

The collector unit is also designed to be equipped with fins attached on the absorber plate along the second air passage. Five fins were used under this design. The fins on top of absorber plate are anticipated to increase heat transfer coefficient by capturing and transferring properly the heat energy from the absorber plate to the flowing air within the system (Daliran and Ajabshirchi, 2018). Attaching fins on absorber plate means increasing absorber heat transfer surface area resulting in increasing airflow turbulences along the passage, hence high solar collector outlet temperature can be achieved**.** The efficiency of solar collector depends significantly on the solar radiation and mass flow rate. Mass flow rate is enhanced by fins on surface geometry of a collector**.** Different shapes of the fins such as u-shape, flat shape and vertical or longitudinal inclined shape have been used on solar collector airflow passage by (Chabane et al., 2013), (Daliran and Ajabshirchi, 2018) and (Mahfoud et al., 2013) respectively to enhance heat transfer phenomena. The top or first air channel of the designated solar collector has the depth of 0.08m while the bottom passage has the depth of 0.06m. Both channels have the width of 0.784m. When removed and unfolded a single fin has a surface area of 0.15x 1.25 = 0.1875m^2. It is made up of aluminum material of a thickness of 1.6mm. Five fins attached on absorber plate increase surface area of absorber plate by 69%. These fins are placed in line with direction of flow and at a distance of 0.08m to each other.

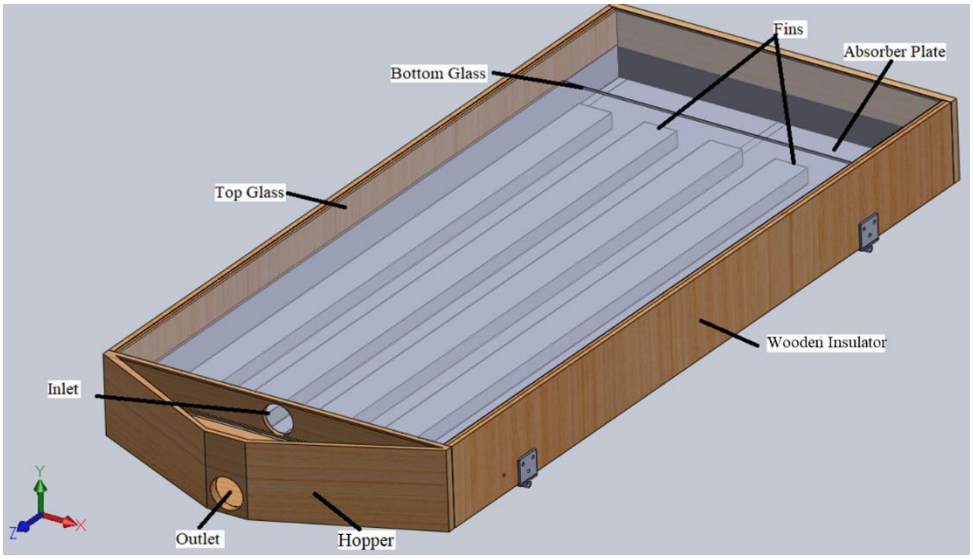

Figure 3. 4 Isometric view of the designated solar collector

For the purpose of maintenance and access to the internal components of the solar collector, the collector unit has been designed with a hopper (see Figure 3.4 above) having both air inlet and outlet holes on one side of the collector. The hopper can be closed or opened, locked or unlocked by the two latches fixed in both sides of the collector (see also Figure 3.6f). The shape of the hopper is also designed in such a way that it prevent wind with elevated speeds to go inside the solar collector. The solar collector unit is also designed to be placed on top of the frame having adjustment that allow the unit to be tilted to an angle between 0^0 and 35^0 at an interval of 5^0.

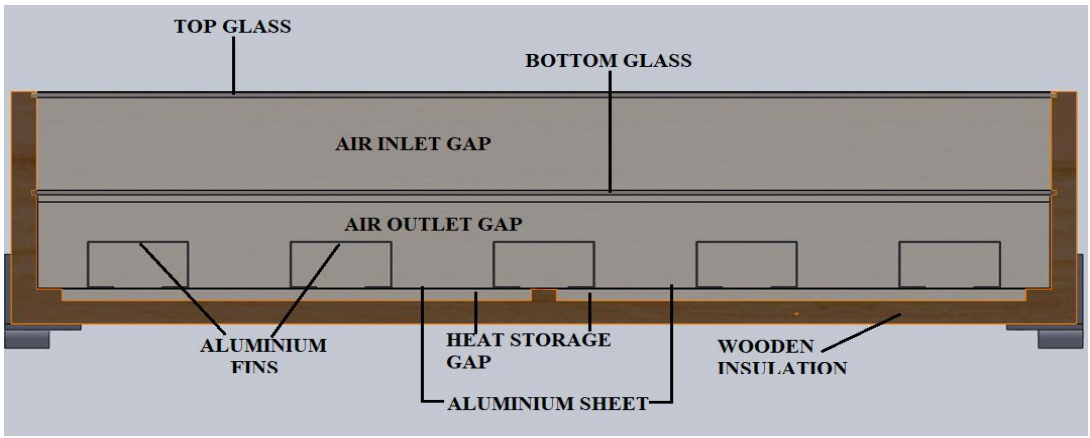

(a)

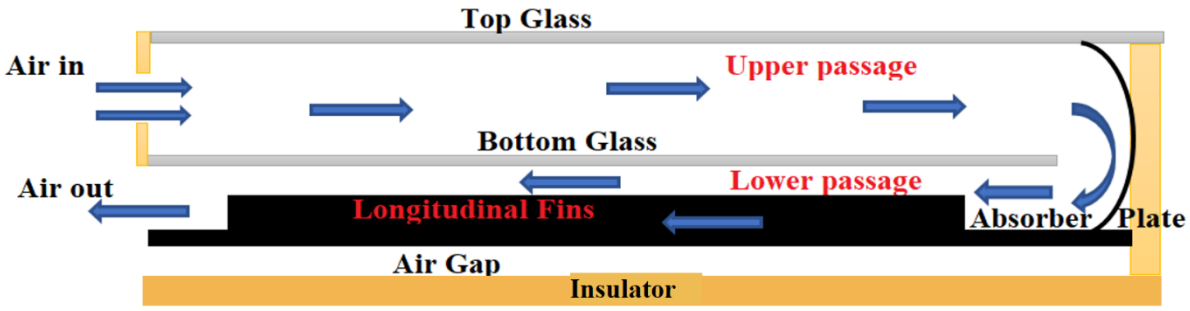

(b)

Figure 3. 5 Cross section of a collector (a), Airflow inside passages of solar collector (b)

Table 3.3 shows different properties of materials used in designing, developing and simulating the banana solar dryer. The materials shown in table 3.3 are the main materials used in this design, and most of them are available in local market around Gaborone. The properties of each material were obtained from various literatures, other properties were measured direct on the material during purchased or fabrication.

Table 3. 3 Materials and their properties used for fabricating Solar Collector

Name of Material	Thermal properties	Thickness (m)	References
Transparent Glasses	λ = 0.18W/m K, τ = 0.85, α = 0.96, ε =0.94	0.004	(Prabhu et al., 2018)
Aluminum	λ = 210W/m K, ε = 0.090	0.0016	(Jelle, 2011), (Brunner et al., 2006)
Plywood (Wood)	λ = 0.1-0.2W/m K, ε = 0.90	0.016-0.020	(Brunner et al., 2006)
Matt Black Paint	ε = 0.96, α = 0.95 - 0.96	-	(Ekechukwu and Norton, 1999a)

3.5.2. Drying chamber (cabinet)

A drying chamber Figure 3.6 is the tray type cabinet, having four number of trays designed to accommodate banana fruits to be dried. For tray type cabinet solar dryers, the drying chamber is designed by taking into account the loading capacity, which depends on the product to be

loaded and its moisture contents, the airflow rate and conditions of drying air based on one of the following rules as mentioned in section 2.3.2.

A. Solar collector area, A_c = 0.75 x Total tray area in meter square
B. Loading capacity = 4kg of fresh products per meter square of tray area,
C. Airflow rate = 0.75m^3/m for every square meter of tray

Rule A:

Since the area of collector (A_c) calculated in section 3.44 was 1.36m^2, the total area of trays is 1.36m^2/0.75=**1.8m^2**, therefore for a dryer with 4 trays, the area of one tray = 1.8m^2/4 = **0.45m^2**

Rule B:

If approximately 4kg was to be chosen to be the loading capacity for the dryer as discussed in section 3.42, the total area of trays is chosen to be **1m^2**, therefore for a dryer with 4 trays, the area of one tray = **0.25m^2**

Rule C:

Since the proposed dryer employs a convective fan mechanism, this rule is achieved through the specifications of a fan and the airflow rate across the dryer.

For the purpose of this study, rule B was selected, and therefore, four trays each with length and width of 0.534m and 0.468m were selected to be used in the drying chamber. This rule was selected due to the area which has a minimum loading capacity that allows exposure of product surfaces to drying airflow. Therefore, four trays having dimensions as mentioned above occupy an internal space of 0.648m, 0.468m and 0.528m for the length, width and height of a drying chamber respectively. The trays are centered and leaving clearances between the fan and the door of the drying chamber as it can be seen on Figure 3.9. In order to prevent heat losses from inside the drying chamber to the outside, all internal side wall of the drying chamber were insulated using Polyethylene foam sheets covered with aluminum foil and form a thickness of the insulator to be 0.01m. Since the drying chamber is made up of plywood of thickness of

0.016m, the total thickness of the insulator was 0.026m, and therefore the external overall dimensions of the drying chamber was 700x520x 580mm for length, width and depth respectively as shown in figure 3.9. The drying chamber is equipped with removable trays on which banana slices are spreads, they are easier to be removed for loading and unloading, cleaning and to access the inside environment of drying chamber. The trays are constructed using wooden frame and netting materials which allows hot air to cross through from bottom to top across banana slices, the properties of plywood, nets and flexible pipe used in developing drying chamber can be seen in Table 3.4.

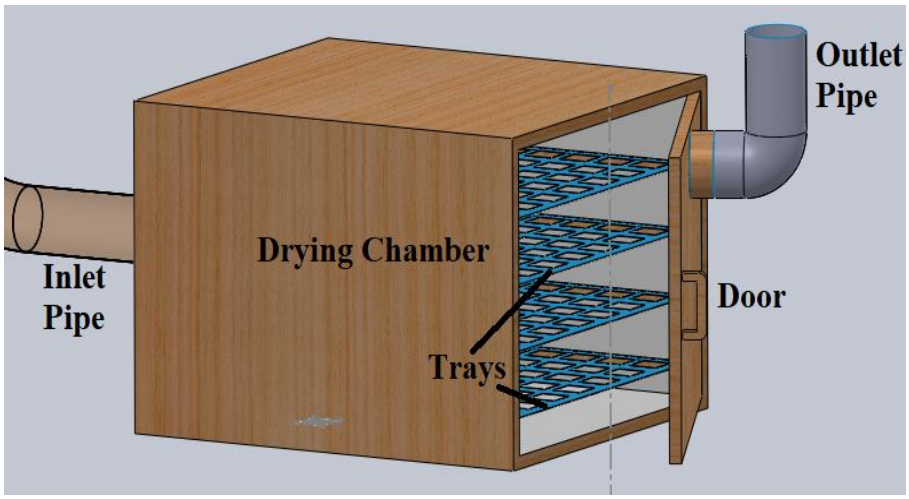

Figure 3.6 Designated drying chamber.

The hot air is coming from the collector to the drying chamber through an aluminum flexible pipe shown on Figure 3.3 which connect the outlet of the solar collector and the inlet to the drying chamber. Inside the drying chamber at the inlet side a fan is fixed, the fan is able to withstand the temperature of up to 343K and is powered by a small solar panel of 15W. This fan save two purposes: One it acts as a suction fan to suck hot air from the collector unit, second it radially distribute the fumes of hot air evenly across the trays where banana slices are placed, hence allowing easy moisture diffusion from the core of the banana slices to the product surface, from the surface to the hot air then taken away to outside the dryer.

Table 3. 4 Some materials and their properties used for fabricating solar dryer

Material	Properties:	Temperature range	References
Polyethylene foam	λ=0.02 – 0.027 W/m K	-323K-393K	(Papadopoulos, 2005)
Aluminum Flexible hose	λ=210W/m K, α=0.96	-	(Jelle, 2011), (Brunner et al., 2006)
Plywood (Wood)	λ=0.1- 0.2W/m K	-	(Jelle, 2011)
Nets			

3.5.3. Outlet pipe

In order to evacuate hot air carrying moisture from the drying chamber to the outside environment, the exhaust pipe is attached to the drying chamber access door as shown of Figure 3.6 and 3.3. The outlet pipe is the elongated pipe, it was constructed using the plastic pipe. The whole structure of the dryer was mounted on a movable frame which makes an overall dimension of the system to be 1572 x 870 x 1340mm length, width and height respectively (see Appendix XII).

3.5.4. Design description of support and Adjustment

The structure of the designated solar dryer consists of three main components namely, the solar collector, the drying chamber and the, frame. The framework or the structure of the solar dryer was designed by taking into account the following factors Weight, inclination angle, Materials, Maintenance, flexibility and mobility. The solar collector and drying chamber were measured and found to have weight of 64kg and 32kg respectively, the two components were centered on framework in order to have equal distribution of weight on castor wheels. This weight served as preliminary load to the framework. Since the drying chamber was supposed to sit on the bed-frame underneath of solar collector, the height from ground was taken to be 0.02m and that of the drying chamber was taken to be 0.580m, the height of 0.740m of the solar collector when inclined at 29º were added to form the overall height of 1.340m.

For the purpose of maintenance, the length of the dryer was taken to be 1.572m in order to fit within the overall length of 1.7m of a collector, when tilted in horizontal position. The

adjustment of the collector was made in order to allow horizontal positioning of collector when performing maintenance such as removal of upper and inner glasses. Square steel tube of dimension of 32x32x1.6mm was chosen for making framework,

3.6. Fabrication of the dryer

The solar dryer together with its components designed in the previous sections were fabricated in the workshops of the Department of Mechanical Engineering, University of Botswana. Fabrication procedures were categorized in four steps namely: Fabrication of Frame, Fabrication of solar collector, Fabrication of the drying chamber and lastly was assembly of all components mentioned above.

3.6.1. Frame and solar collector

A wooden cabinet Figure 3.7a with two slots on its side's wall was fabricated first. The slots were later used to secure glazing glasses. The wooden cabinet shown on Figure 3.7a was secured with four angle-line supporters and inclined at an angle on top of the fabricated frame shown on Figure 3.7b. The frame was made up of 32x32x1mm square tubes welded together to form a complete frame. Figure 3.7c shows the aluminum sheet 1.6mm attached with five fins. The whole structure was placed inside a wooden cabinet to form a sub-assembly as shown on Figure 3.7d.

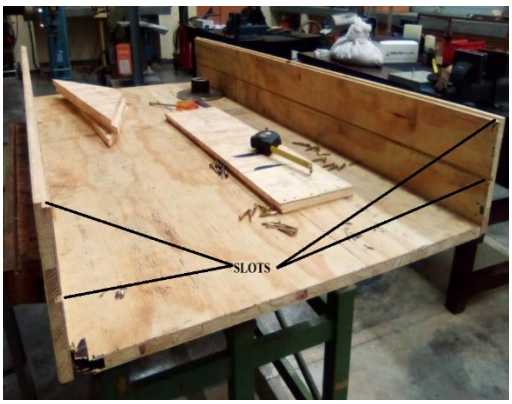

(a)

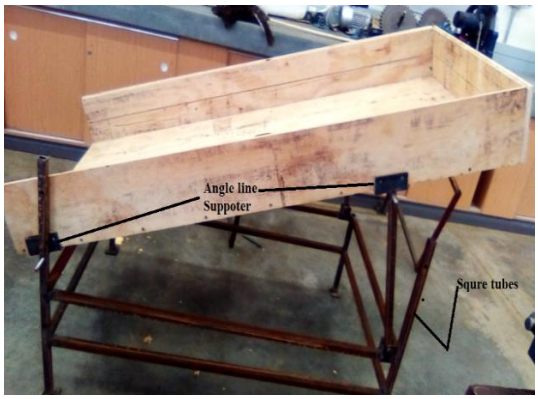

(b)

(c)

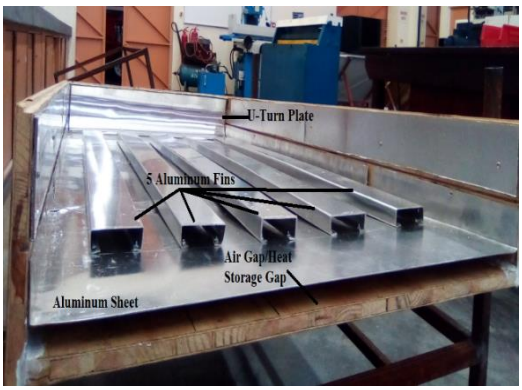

(d)

(e)

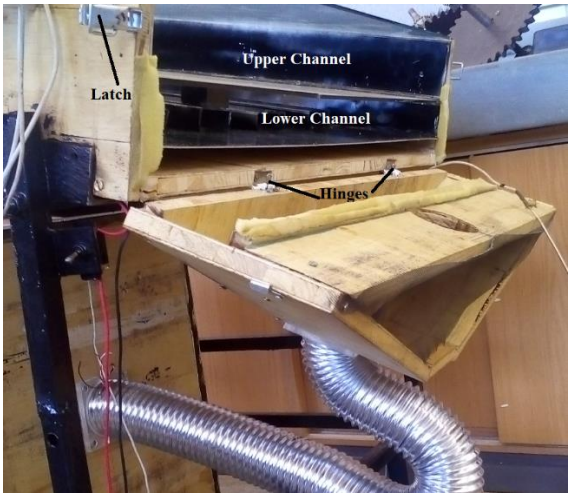

(f)

Figure 3. 7 Pictures showing the Fabrication procedure of the solar Collector

3.6.2. Drying chamber

Fabrication of the drying chamber Figure 3.8 having an overall dimension of 700x520x580 as designed in section 3.5.2 was done. The drying chamber was made up of plywood fastened with long screws, every joint on a drying chamber structure was sealed with silicon sealant in order to prevent heat and air leakage during experiment. The drying chamber was made up with one door to facilitate the loading and offloading of banana together with access to internal components. One hole having diameter of 80mm was drilled in one side opposite to the door, the door itself was also drilled with a hole positioned up, the hole on the door served as an outlet and other on opposite side served as an inlet to the drying chamber.

Figure 3. 8 Fabrication of drying chamber

3.6.3. General details of the developed solar dryer

The solar dryer has the overall dimensions of 1572 x 870 x 1340mm length, width and height. Underneath of the solar collector is the drying chamber lying on a bed made up of square pipes welded together. The dryer is designed in such a way that the solar collector can be titled to any angle between 0^0 and 35^0 in order to receive maximum solar radiation. On the other hand the dryer can be moved from one location to another and swayed to a direction of sun when necessary.

3.6.4. Solar dryer operation

The operation and testing of the newly constructed banana solar dryer system was evaluated in the Industrial and design workshop of the University of Botswana during summer season months of February and March. The weather conditions were favorable to run tests in order to investigate the preliminary thermal behaviors and performance of the banana solar dryer prior to drying. The air having an ambient temperature enter solar collector through the inlet hole to the top passage which is between the top and bottom glass, while flowing in this passage the temperature of air increases above ambient temperature. At the end of the top passage the air makes a downward U-turn into the bottom passage (see Figure 3.5b). The air is further heated by both the absorber plate and fins. The hot air is forced to exit the solar collector through a

flexible aluminum pipe by the suction of the fan fixed inside the dryer. The aluminum flexible pipe is insulated with wool material to prevent heat loss when hot air passing through the pipe. Within the drying chamber, the hot air having enough drying temperature is forced to pass through the trays loaded with banana slices. The banana slices are forced to dry through a convection heat transfer mode and the air carrying moisture is forced to exit the drying chamber through the exhaust pipe, as long as the solar power or radiation exists the circle keep on repeating until the products are dried.

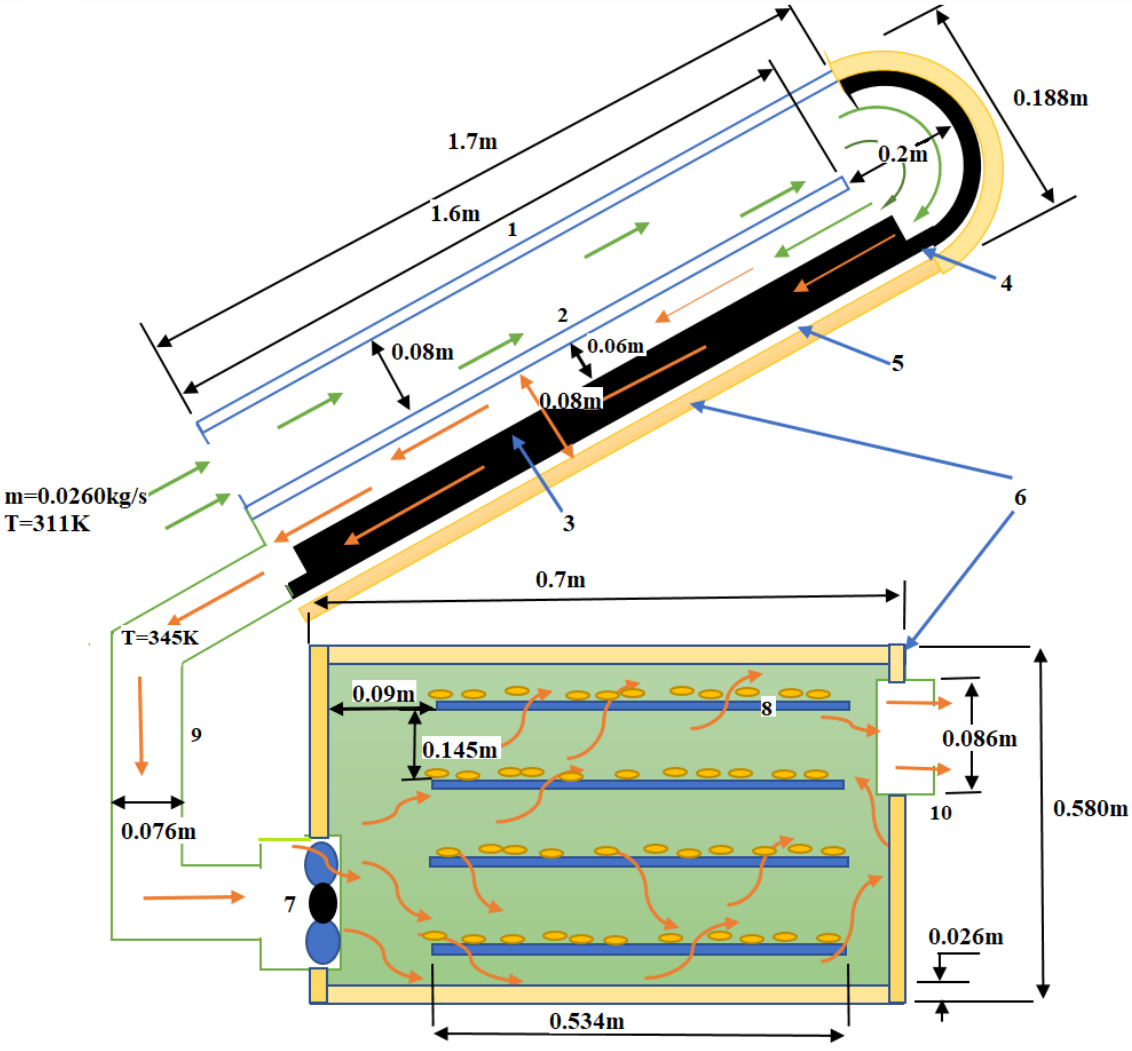

Figure 3.9. An outlay of solar dryer 1. Top glass, 2. Bottom glass, 3. Fin, 4. Absorber plate, 5. Air gap, 6. Insulators, 7. Fan, 8. Tray, 9. Aluminum pipe, 10. Outlet air

CHAPTER FOUR: EXPERIMENTAL SETUP AND SYSTEM EVALUATION

4.1. Introduction

An experimental setup and test were done in order to determine the performance of the developed banana solar dryer and compare different parameters to see how they correlate among each other. The experimentation was done in the Faculty of Engineering of the University of Botswana between February and March, 2019. Different experiments were conducted in different days, each experiment was carried out for eight to nine hours each day from 8am to 5pm. The developed drying system was made up of plywood to prevent heat losses through the surroundings. As said above the air enters the system by a suction force generated by the fan mounted in the drying chamber, the fan is powered by the 15W solar panel as shown on Figure 4.2. The system does not need electrical power from the grid therefore it is 100% green technology.

4.2. Instrumentation and measurements

The measurement of drying parameters of the developed banana solar dryer was carried out for 8 to 9hrs from 08am to 5pm each day in different days. Setting up of all measuring devices were done before testing/drying as it can be seen in Figure 4.2. The most important data to be recorded during testing were solar radiation (W/m^2), inlet and outlet airflow, wind speed (m/s), relative humidity (%) and temperatures (^0C). On these parameters, only temperatures were recorded automatically through data harvest and computer, while other parameters were recorded manually in every hour.

A Data logger (Easy Vision Data Harvest) was connected as it can be seen on Figure 4.1. Six (6) NiCr-Ni thermocouple sensors capable of measuring temperature between -303K to 383K were distributed in various places of the system for measuring absorber plate temperature, bottom glass temperature, top glass temperature, outlet and inlet temperature for both collector and drying chamber, ambient temperature and trays temperatures. The sensors were connected

to the Easy vision data harvester. The real time temperatures were recorded in the computer via the Easy Vision data logger (See Appendices III-VI).

The air velocity of the inlet, outlet and outside the dryer system were recorded using anemometer instrument type AVM09 Model 506-9666 having a measuring range of 0.3-45m/s. Relative humidity of the inlet and outlet air together with the surrounding environment was recorded on an hourly basis using the environment meter type MT 941 having the range between 2.5% to 95% with an accuracy of ±5%RH. The solar radiation was measured every hour using anemometer type CM3-025778 manufactured by KIPP & ZONEN LTD having sensitivity accuracy of 23.89x 10^{-6} W/m^2. All measuring devices mentioned above are available at the workshops of the Faculty of Engineering and are tabulated in Table 4.1 and shown in Figure 4.1.

A general instrumentation setup of all measuring devices was done as shown in Figure 4.2 and evaluation of the performance of the system was carried with and without load in order to examine the behavior and performance of both solar collector and drying chamber.

Table 4. 1 Summary of measuring instruments and their specifications

Instrument	Designer/Manufacturer	Measuring Parameter	Specifications	Quantity
Anemometer	AVM09 Model 506-9666 DIGITAL PROVA, **TAIWAN**	For measuring velocity of fluid (m/s) flowing in the system	Accuracy of data hold range of 0.3-45m/s.	1
Data logger/Harvest	Easy Vision, Leighton Buzzard, UK	For Harvesting temperatures data	Temperature between -30^{0}C to 110^{0}C	1
Pyrometer	Model:CM3, S/N 025778, KIPP & ZONEN LTD, Delft Holland	For measuring solar radiation	Sensitivity: 23.89x 10^{-6} W/m	1
Environment Meter	Type MT 941, MAJOR TEC, Insando 1600, SA	For measuring Temperature (^{0}C) and Relative Humidity (%)	Accuracy ±5% RH. Range between 2.5% to 95%	1
Digital Balance	Model: GP-30K S/N: 14717414	For measuring weights (kg)	Precision: 0.1g	1

Temperature sensors		For measuring temperatures (^{0}C)	Temperature between -30^{0}C to 110^{0}C	6

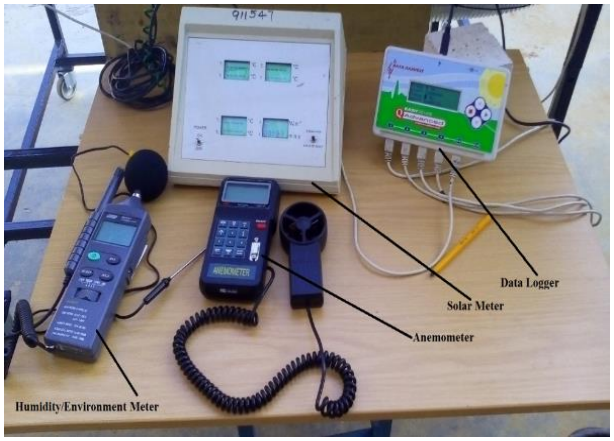

Figure 4. 1 Photograph showing some measuring devices used.

Figure 4. 2 Photographs showing experimental set up of the system and internal view of drying chamber.

4.3. Drying of banana fruits

Fresh ripe banana fruits were bought from the market a day before the experiment. The fruits were cleaned, manually peeled and sliced to a thickness of about 3 to 5mm. For the purpose of maintaining the color, taste and avoid banana slices to become dark/brown during drying, lemon juice was used and every banana slice was dipped into the lemon juice. Prior to loading the total weight of the peeled banana (pulp) was recorded using digital weighing machine as shown in Figure 4.3a below and few samples of banana slices were selected at random in order to measure the initial moisture content using standard way of oven drying.

One tray can carry approximately 3-4 pulps of banana fruits and therefore 12 to 15 banana weigh approximately 2.5 -3.6kg when sliced to a thickness range of 3-5mm and spread evenly on four trays as shown in Figure 4.3b. For the purpose of achieving uniform drying of slices, attention was observed to not overlap the slices while on trays, and therefore banana slices were positioned 5-8mm apart from each other.

(a)

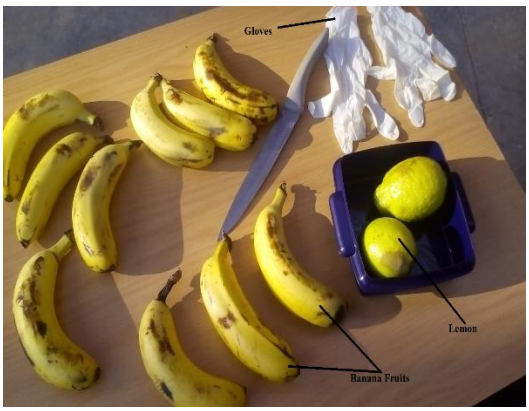

(c)

(b)

(d)

Figure 4. 3 Weighing, peeling, slicing and loading process of banana prior to drying

After loading, the drying chamber was closed and the whole system was exposed under the sunlight. The drying process was carried out in the morning around 08:40am. The dryer was switched on to activate the fan which sucks hot air from the collector and blow it across slices.

4.4. Energy flow and heat transfer coefficients of the system

The solar dryer system was designed, developed and tested in the workshop of the Faculty of Engineering of the University of Botswana situated between latitude -24.67^{0}S and longitude 25.92^{0}E. As describe earlier, the solar collector which is the main source of heat to be used is the double pass solar collector type having two transparent glasses one fixed on top and the other fixed between the absorber plate and the top glass. All these together with the plywood form a prominent components of the dryer.

During experiment the dryer was subjected to different environmental conditions like wind velocity, ambient temperature etc. Under these circumstances, the variations of drying parameters were inevitable and therefore heat transfer coefficients induced by various external forces that surround the dryer were taken into account as follows.

4.4.1. Energy balance around the solar collector

In order to model the energy balance of a double pass solar collector, the heat energy flux around the top cover, bottom and absorber plate need to be evaluated. Different equations have

been used to evaluate the energy balance correlation of a DPSC. Convective and radiative heat transfer coefficients induced by surrounding environment together with heat losses are correlations discussed in this section

4.4.1.1. Energy flux around the top transparent glass

The flow of air in the first channel of the developed solar collector can be seen in Figure 4.4. During experiment the temperature of the top glass and ambient temperature were measured using sensors, one attached on the top glass and another being held on the surrounding environment. The top glass of the solar collector is subjected to radiative and convective heat transfer

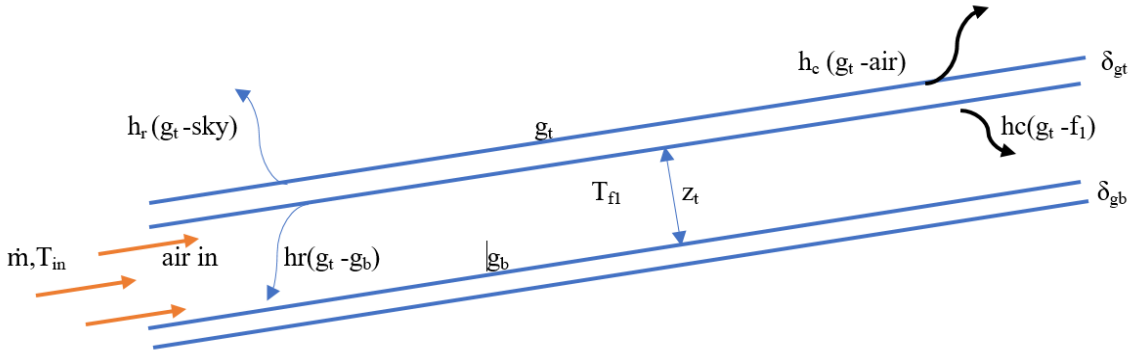

Figure 4. 4 Schematic diagram of the airflow & energy flux around the first channel

The energy balance on the surface of the top glass together with the convective heat transfer in the upper passage when air if flowing are expressed as shown on the Equation [4.1a&b] as described by (Ho et al., 2018).

$$\alpha_{gt} I A_{gt} = A_{gt}\left[h_{c(tg-air)}\left(T_{gt} - T_{air}\right) + h_{c(gt-f1)}\left(T_{gt} - T_{f1}\right) + h_{r(gt-gb)}\left(T_{gt} - T_{gb}\right) + h_{r(gt-air)}\left(T_{gt} - T_{gb}\right)\right] \quad [4.1a]$$

$$\dot{m} C_p \frac{d(T_{f1} - T_{air}}{dt} = \left[h_{c(gt-f1)}\left(T_{gt} - T_{f1}\right) + h_{c(gb-f1)}\left(T_{gb} - T_{f1}\right)\right] A_{gt} \quad [4.1b]$$

4.4.1.2. Energy flux around the bottom transparent glass

The flow of air in the second channel of the developed solar collector can be seen in figure 4.5. The bottom channel is between the bottom glass and the absorber plate, the energy balance is calculated taking into account the energy flow of both surfaces of the bottom glass (i.e. top &

bottom surfaces of bottom glass) and the energy gained by the moving air in the channels.

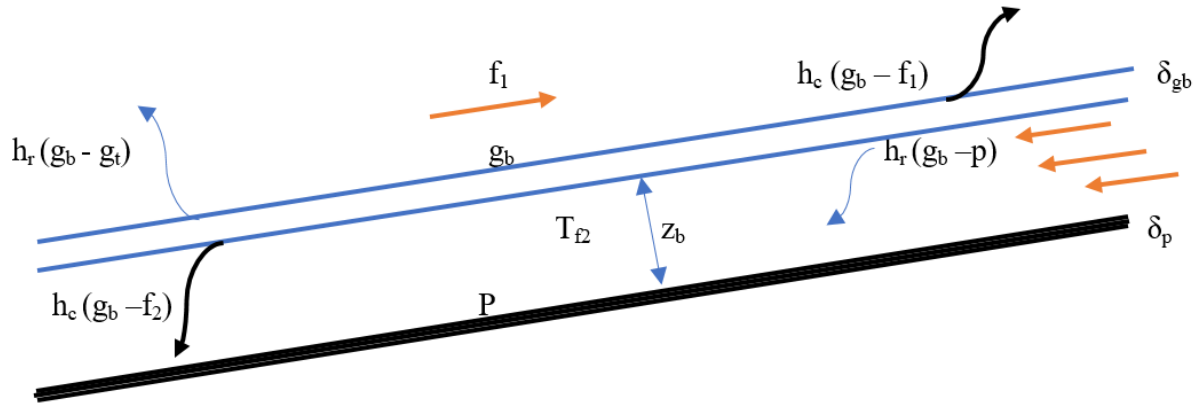

Figure 4. 5 Schematic diagram of the energy flux around the second channel

Equation [4.2a&b] serves the energy balance between the bottom glass and the absorbing plate in the second channel of the solar collector.

$$\tau_{gt}\alpha_{gb}IA_{gb} = A_{gb}\left[h_{c(gb-f1)}\left(T_{gb} - T_{f1}\right) + h_{c(gb-f2)}\left(T_{gb} - T_{f2}\right) + h_{r(gb-gt)}\left(T_{gb} - T_{gt}\right) + h_{r(gb-p)}\left(T_{gb} - T_{p}\right)\right] \quad [4.2a]$$

$$\dot{m}C_p\frac{d(T_{f2}-T_{f1})}{dt} = A_{gb}\left[h_{c(gb-f2)}\left(T_{gb} - T_{f2}\right) + h_{c(p-gb)}\left(T_p - T_{f2}\right)\right] \quad [4.2b]$$

4.4.2. Heat transfer coefficients

During experiment, the heat flux coefficient caused by the blowing wind on top of the glass was calculated using Equation [4.3] below as described by (Klein, 1975) and (Kareem et al., 2017c).

$$h_w(W/m^{2\,0}C) = 8.55 + 2.56v_w \quad [4.3]$$

Whereby v_w is the velocity of wind in m/s that blow on top of the glass cover

The mean velocity of the outside environment during experiment was measured and found to be in a range between 3.35m/s and 4.91m/s (see Table 6.1). Equation [4.3] above was used to find the heat flux coefficient caused by wind blowing on top of the glass, this is due to the fact

that (Kareem et al., 2017c) suggested to use this equation for the wind velocity of less or equal to 5m/s. Therefore by taking the average wind speed of 4.03m/s the convective heat flux coefficient due to the moving wind around the collector was calculated to be:-

$$h_w = 8.55 + 2.56\,x\frac{3m}{s} = \mathbf{18.87\ W/m^2}$$

4.4.2.1. Heat loss coefficient on top glass

Klein (Klein, 1975) and Ho et al., (Ho et al., 2005) described the Equation [4.4] below for the determination of the heat loss expected from the top glass of the solar collector as follows. Appendix XII shows the heat loss coefficient on top of glass for the developed solar dryer.

$$U_t = \left[\frac{1}{h_w} + \frac{N_g}{\frac{C}{T_p}\left(\frac{T_p - T_{air}}{\zeta + N_g}\right)^{\omega}}\right]^{-1} + \frac{\sigma(A_c)(T_p^4 - T_{air}^4)}{\frac{1}{0.00591(N_g)(h_w)+\varepsilon_p} + \frac{\zeta+2N_g-1+0.133\varepsilon_p}{\varepsilon_g} - N_g} \quad \text{..... [4.4]}$$

Whereby:

$N_g =$ the number of transparent glasses $= 2$

$C = 520(1 - 0.000051)(\theta^2)$ but $0^0 < \theta < 70^0$, (in this study $\theta = 29^0$)

= 520(1-0.000051) (29) = **498**

$$\omega = 0.43\left(1 - \frac{100}{T_p}\right)$$

$$\zeta = (1 + 0.07866N_g)(1 + 0.089h_w - 0.1166\varepsilon_p h_w)$$

ε_p = Absorber plate emissivity = 0.09

ε_g = Glass emissivity = 0.94

h_w = Heat flux coefficient on top glass = 18.87W/m^2

4.4.2.2. Radiative heat transfer between the top glass and sky

This can be described and calculated taking into account the temperature of the top glass and temperature of the sky or ambient. (Srinivasan, 2016,) arrived to the point of using Equation [4.6] below together with Equation [4.6a] to obtain this value. (Akhtar and Mullick, 2007) also used the formula [4.6a] to describe the value of radiation between the clouds or sky and the top

glass of the solar collector. Therefore the radiative heat transfer between the top and sky was calculated as shown on Appendix XII.

$$h_r = \frac{\sigma\varepsilon_{gt}(T_{gt}^4 - T_{sky}^4)}{T_{gt} - T_{amb}} \quad \text{[4.6]}$$

$$T_{sky} = 0.05552(\ T_{air/sky}) = 0.0552 T_a^{1.5} \quad \text{[4.6a]}$$

4.4.2.3. Radiative heat transfer coefficient between glasses

In (Khoukhi and Maruyama, 2006) and (Kareem et al., 2017c) proposed to use Equation [4.6b] below to determine the radiative heat transfer coefficient between glasses of a double pass solar collector. Therefore the value for the coefficient of radiative between glasses of the developed solar collector was calculated using this equation as shown on Appendix XII.

$$h_r = \frac{\sigma(T_{gb}^2 - T_{gt}^2)(T_{gb} - T_{gt})}{\left\{\frac{1}{\varepsilon_{gt}} + \frac{1}{\varepsilon_{gb}} - 1\right\}} \quad \text{[4.6b]}$$

Whereby;

σ = Stefan Boltzmann constant ($5.67 x 10^{-8} W/m^2K^{-4}$)

T_{gt} = Temperature of Top glass

T_{gb} = Temperature of Bottom glass

ε = Emissivity of Top and bottom glass

4.4.2.4. Radiative heat transfer between bottom glass and absorber plate

In (Srinivasan, 2016,) suggested to use Equation [4.6c] for the radiative heat transfer coefficient between the bottom glass and the absorber plate of a double pass solar collector. The value for the coefficient of radiative was therefore calculated using this formula:

$$h_r = \frac{\sigma(T_{ab}^2 + T_{gb}^2)(T_{ab} + T_{gb})}{\left\{\frac{1}{\varepsilon_{gb}} + \frac{1}{\varepsilon_{ab}} - 1\right\}} \quad \text{[4.6c]}$$

4.4.2.5. Convective heat transfer between glasses

The developed solar collector employed two glasses upper and lower glass, so according to the Hottel's empirical equation cited by (Ho et al., 2018) the convective heat transfer coefficient of the air moving between the upper and lower glass in a double pass solar collector was calculated using Equation [4.7]. This value was calculated for the devolved dryer as shown on Appendix XII.

$$h_{co(gt-gb)} = 1.25(T_{gb} - T_{gt})^{0.25} \quad \text{..... [4.7]}$$

4.4.2.6. Convective heat transfer between bottom glass and absorber plate

The convective heat transfer coefficient between the glass cover and absorber plate of a double pass solar collector is the value which is governed by the thermal conductivity *k* of the absorbing plate (in this case, aluminum plate). The characteristic length or sometimes called hydraulic diameter of the rectangular channel l_c as computed in the Equation 4.8a and the distance x moved by the moving fluid (in this case air) from the inlet passing through the top channel to the bottom channel. The value can be computed using Equation [4.8] as described by (Kareem et al., 2017c).

$$h_{co} = \frac{k}{l_c}\left[(2.92 + 0.00181Re)exp\left(\frac{-0.03795x}{l_c}\right) + (0.0158Re^{0.8})\right] \text{..... [4.8]}$$

$$l_c = \frac{4wH}{2(w+H)} \text{..... [4.8a]}$$

$$l_c = \frac{4x0.784x0.06}{2(0.784 + 0.06} = \mathbf{0.111469m}$$

4.4.2.7. Hydrodynamic boundary layer on absorber plate

For laminar flow the value of Reynold number is less than 3000 and for turbulent flow it is greater than 3000 (Kareem et al., 2017a). Since the developed dryer has a double pass solar collector having rectangular cross-section and is the forced convection collector, the value for Reynold, Nusselt and Prandtl number needed to be calculated taking into consideration the

characteristic length (l_c) by which the fluid (air) is moving. The characteristic length for the rectangular flat channel was given by Equation [4.8a] above. The collector has two channels the upper and the bottom channels. The Reynolds number for the airflow within channels was calculated using Equation [4.9] below as shown in Appendix XII.

$$R_e = \frac{v l_c \rho}{\mu} \quad \text{..... [4.9]}$$

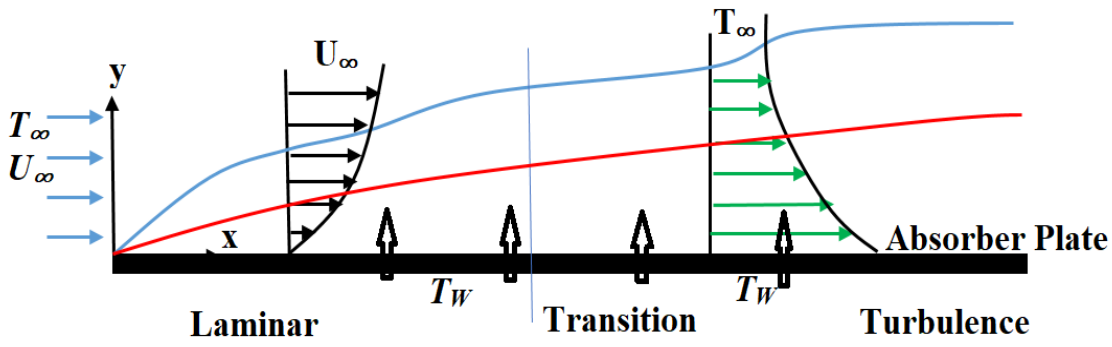

Figure 4. 6 Hydrodynamic and thermal boundary layers on hot absorber flat plate

The Figure 4.6 above shows the absorber flat plate and the moving fluid on top of it, how the relationship between the heats diffuse from the absorber plate into the moving fluid (air) within the solar collector occurs. Plandtl, Nusselt and Reynolds number in this case are needed to be known in order to account for the molecular diffusivity of heat and momentum. This will help to know which molecular diffuse much faster than the other amongst the two (Bird, 2002). If Plandtl number is greater than one it means the heat flux diffuses much slowly than the airflow movement and vice versa. Plandtl number can be calculated using Equation 4.9d. The Nusselt number is the dimensionless temperature gradient on the surface of the absorber plate. For a convection flow the Nusselt number depends mostly on Reynolds and Prandtl number (Bird, 2002), it is used to calculate the heat transfer coefficient and help to define whether the heat is transferred more by convection or conduction means. The low value of Nusselt number means the higher the heat transferred by conduction than convection, the higher the value of Nusselt number will be the heat transferred by convection than conduction. It can be obtained using any

of the Equation [4.9a-c] as suggested by different authors. All these dimensionless values were calculated for the developed solar dryer as they can be seen in Appendix XII.

$$Nu = \frac{hl_c}{k} \quad \text{[4.9a]}$$

$$Nu = 0.00755(Re^{0.8})(Pr^{0.33}) \quad \text{[4.9b]}$$

$$Nu = \frac{0.0606\left\{(Re)(Pr)\frac{l_c}{l_p}\right\}^{1.2}}{1+0.0909(Pr^{0.17})\left\{(Re)(Pr)\frac{l_c}{l_p}\right\}^{0.7}} + 4.9 \quad \text{[4.9c]}$$

$$Pr = \frac{Molecular\ diffusivity\ of\ Momentum}{Molecular\ diffusivity\ of\ Heat} = \frac{\mu C_p}{k} \quad \text{[4.9d]}$$

Whereby:

$\upsilon =$ is the velocity of airflow in the system m/s

$\rho =$ is the density of the air at a specific temeperature kg/m^3

$\mu =$ is the dynamic viscosity of air $kg/m.s$

w and H are width and height (depth)of a channel as shown on Figure 4.7

$C_p =$ Specific heat capacity

$\frac{l_c}{l_p} =$ is the ratio of the characteristic lenght to the length of absorber plate

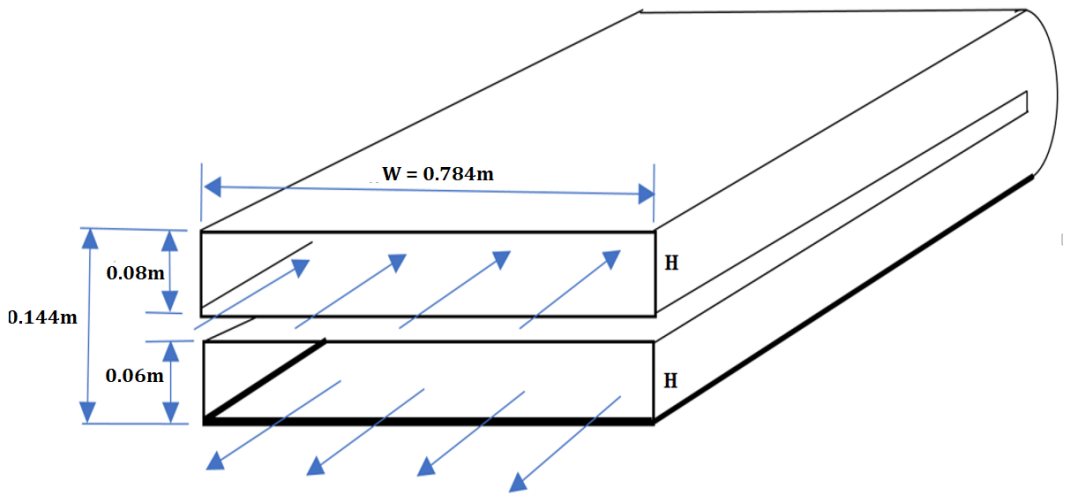

Figure 4. 7 Schematic view of airflow going in and coming out the solar collector

4.4.3. Properties of air leaving collector under various temperatures

Air flowing in and leave the collector vary linearly with respect to change in temperatures and time spent within the solar collector. Therefore to account for its physical properties like density, specific heat, viscosity and thermal conductivity, the following Equations [4.11a-d] were used to govern the physical properties of the air leaving solar collector as described by (Rasham, 2018). T_{out} and T_{in} being collector outlet and inlet temperatures respectively. These values for the developed solar dryer can be seen in Appendix XII.

$$\text{Viscosity } (\mu)\frac{m^2}{s} = 1.983 - 0.00184[T_{out} - T_{in}]x10^{-5} \ldots\ldots\ldots\ldots\ldots\ldots\ldots\ldots\ldots\ldots\ldots 4.11a$$

$$\text{Density } (\rho), kg/m^3 = 1.1774 - 0.00359[T_{out} - T_{in}] \ldots\ldots\ldots\ldots\ldots\ldots\ldots\ldots\ldots\ldots\ldots 4.11b$$

$$\text{Specific heat } (C_p), \frac{J}{kg}.K = 1.0057 + 0.000066[T_{out} - T_{in}] \ldots\ldots\ldots\ldots\ldots\ldots\ldots\ldots\ldots 4.11c$$

$$\text{Thermal conductivity}(k), W/m^0C = 0.02624 - 0.0000758[T_{out} - T_{in}] \ldots\ldots\ldots\ldots 4.11d$$

4.5. Evaluation of the thermal performance of the System

The developed solar system uses solar radiation as a main source of heat for generating hot air to be used for drying banana products. Therefore the rates of utilizing thermal energy from the sun as an input to the developed solar dryer is the measure of the performance of the dryer. For the better design of the dryer, analysis of the hydraulic and thermal performances of the dryer is of great importance since the two criteria normally help in identifying the pressure drop and heat transfer within the system (Ho et al., 2018).

4.5.1. Collector thermal performance

In (Fudholi et al., 2014, Kareem et al., 2017c, Kareem et al., 2017a) as described in literature review, the thermal performance of the solar collector is evaluated by calculating the efficiency of the solar collector, efficiency of the dryer and the pick-up efficiency. The measure of how efficiency is the available energy within the solar collector from the solar radiation that can be

harnessed or captured by the flowing air under steady state condition is what referred to the collector efficiency. In order to determine the performance of the collector the Hottel-Whillier-Bliss equation [4.12a] was used as reported by (Duffie and Beckman, 1980, Struckmann, 2008, Klein, 1975) to evaluate the useful energy gained by the flowing air inside the solar collector

$$Q_u = A_c F_R\left[I\{\alpha\tau\}_g - U_L\{T_i - T_a\}\right] \quad \text{..... [4.12a]}$$

$$F_R = \frac{mC_p(T_o - T_i)}{A\left[I\alpha\tau - U_{L(T_i - T_a)}\right]} \text{..... [4.12b]}$$

Whereby:

τ = Being the transmission coefficient of glazing

α = Being the absorption coefficient of plate

Sometimes the value of heat gained by the moving air within the solar collector (Q_u) can also be calculated using equation [4.12b]

$$Q_u = hA_c\{T_p - T_a\} = \dot{m}C_p\{T_{out} - T_{in}\} \text{ ..... [4.12c]}$$

The value of efficiency of the solar collector was calculated using equation [4.13] below

$$\eta_c = \frac{\dot{m}C_p(T_{out} - T_{in})}{A_c I} = \frac{Q_u}{A_c I} \text{..... [4.13]}$$

Whereby;

F_R = is the Heat Removal factor

U_L = is the overall heat loss coefficient

$\dot{m} = \rho A_i V$

C_p = Specific heat capacity (J/kg K)

ρ = Density of air at inlet temperature (kg/m^3)

T_{out} = Collector mean outlet temperature (K)

T_{in} = Collector inlet temperature (K)

T_p = Absorber plate temperature (K)

T_a = Ambient temperature (K)

Q_u = Useful Heat gain (W)

A_c = Collector surface area (m^2)

$\dot{m}$ = Mass flowrate (kg/s)

V = Velocity at inlet (m/s)

I = Mean solar radiation (W/m^2)

The evaluation values of efficiency, useful heat gained and the total heat received by the collector of the developed solar dryer can be seen on Table 6.2.

CHAPTER FIVE: THE CFD ANALYSIS OF DEVELOPED SOLAR DRYER

5.1. Introduction

In order to take into account the governing equations of the transport phenomena of the fluid flowing within the dryer numerically, the ANSYS Fluent program based on the finite volume method under pressure-based and transient simulation was used. The CFD tool helps in making analysis and comparison of the heat and fluid flow transfer through provision of numerical solution of various governing equations. The major processing steps in CFD simulation as mentioned in the literature review are basically Geometry of the flow domain of the system; meshing of the modeled geometry; performing solver settings; initializing; running calculations and lastly visualization and validation of the model. In this study the finite volume method was applied independently in two main components of the system, namely the solar collector and the drying chamber.

5.2. Numerical Modeling of developed double pass solar collector

Solar collector in this study is taken as the main source of heat for drying banana slices. The collector consists of three main parts: Two glasses, absorber plate and the wooden cabinet. In this study an attempt was made to carry out CFD simulation using ANSYS Fluent for the streams of air flowing along the solar collector in order to study the heat transfer phenomena. The fluid domain of the solar collector was modelled in the ANSYS design model following exactly the internal wall geometry of the real developed solar collector where hot air is flowing though from inlet to the outlet holes.

5.2.1. The Geometry and airflow of solar collector

Since the model for the developed solar dryer particularly solar collector has been discussed experimentally, a 3D geometry of a solar collector having an air inlet hole, top & bottom glasses, absorber plate together with outlet hole as shown in Figure 5.1 was modelled using ANSYS 18.2 academic version software. The flow of air starts form the inlet holes, passes

through the top channel and enters the bottom channel with a U-turn motion downwards to the surface of the solar absorber (see figure 3.5b). As it enters in the bottom channel from the top channel the stream of air get heated up by the absorbing plate.

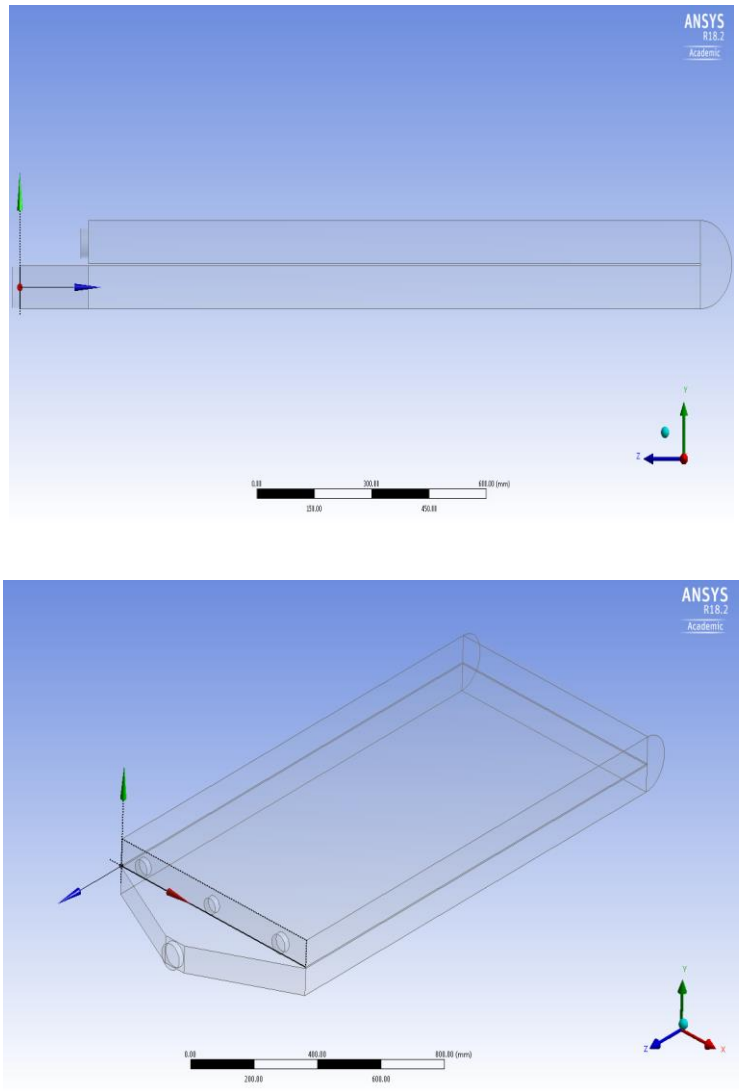

Figure 5. 1 Extracted Geometry of the volume of double-pass solar collector

5.2.2. Meshing of solar Collector

Meshing as discussed in the literature is the discretization of flow domain into number of small elements. Meshing of the whole solar collector domain as shown in Figure 5.2a was done using ANSYS software. By using mesh controls like body and edge meshing techniques, the mesh refinement was applied to the critical zones and sharp corners of the collector flow domain, Figure 5.2b. In order to maintain the quality of the mesh the element quality, skewness and the

aspect ratio were checked as they can be seen in Figure 5.3. The element size of 0.001mm having tetrahedral shape for the individual edges and body meshing was created, while the inlet and outlet element size of 0.002mm was considered. The total number of elements of 3,816,337 with nodes of 746,255 were generated in order to enhance convergence of the simulation. Since the ANSYS program installed at the University of Botswana is the research version and has no limitations to economize the number of elements, the sizes and number of elements were chosen to be more desirable in order to account for the laminar sub layers along and near walls of the solar absorber, therefore having better prediction of the internal flow. Fine mesh of high density were also applied to all boundaries like inlet and outlet, region on top of the absorber plate and corners of the solar collector geometry.

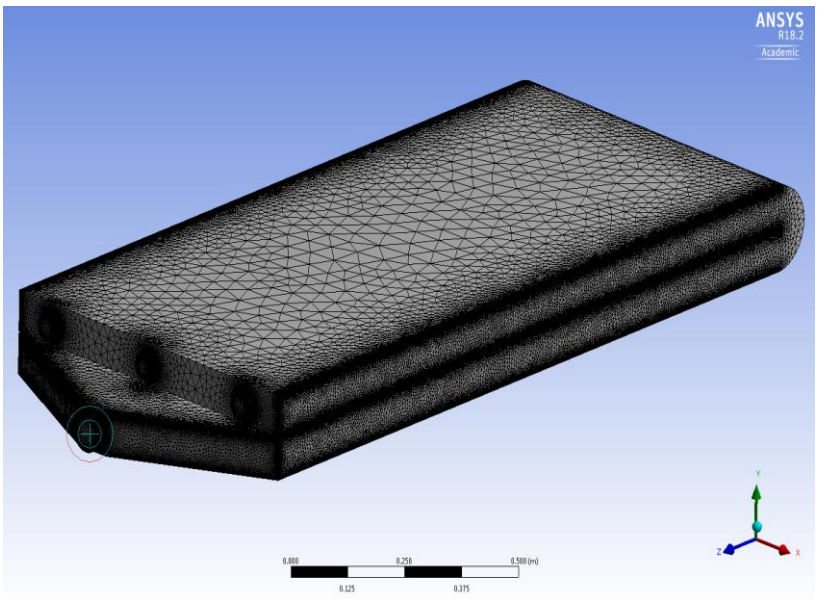

(a) Body meshing

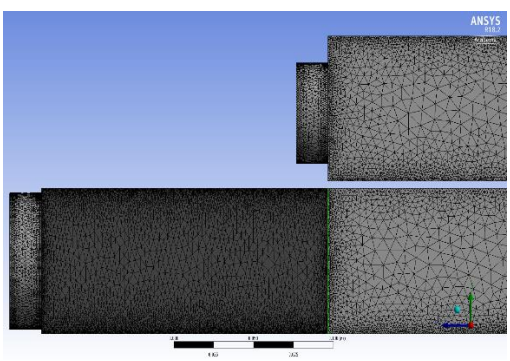

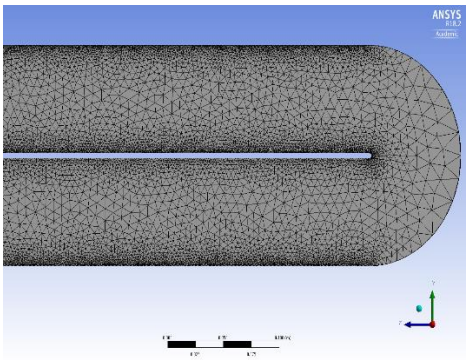

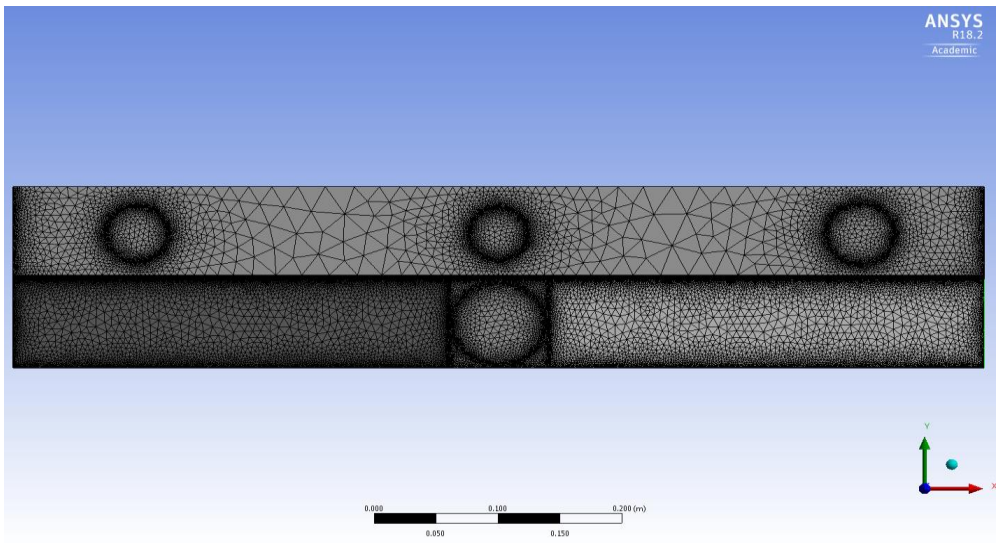

(b). Fine mesh on corners, curve, rounds and edges of the solar collectors

Figure 5. 2 Different Meshing techniques of the double pass solar collector

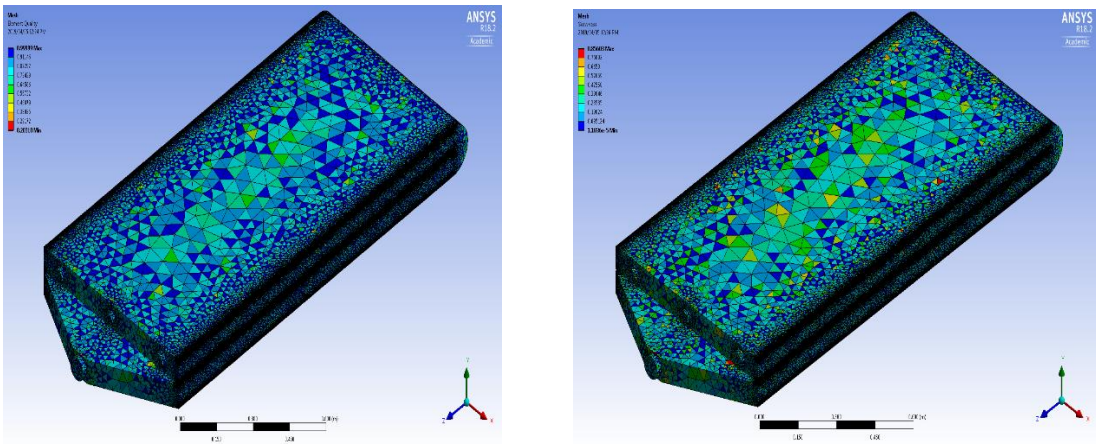

(a) (b)

Figure 5. 3 A 3D element quality (a) and skewness (b) of the double pass solar collector

5.2.3. Fluent setup and boundary conditions of a solar collector

Based on literature review in chapter three, the simulation under pressure based solver was selected in the ANSYS setup. To account for viscous flow and momentum turbulences, the RNG k-ε turbulence model was used in this study. ANSY Fluent incorporated with a model that calculate the effects of sun's rays that go in the computational domain of the solar collector. This utility help to model sun's location in a specified day of the year by providing the global location, date, sunshine factor and domain orientation. During experiment the solar collector

was subjected to solar heat from solar radiations. Therefore in CFD Fluent settings, the energy equation and the Discrete Transfer radiation Model (DTRM) was energized for simulating the heat transfer due to the solar radiations. The solar load calculator was energized for the geographical locations of the University of Botswana (24.67^0S and longitude 25.92^0E) where experiment was done. Due to the position of the collector in ANSYS modeler the grid orientation for North was set in +y axis and East in -x axis and fair whether condition by default was picked.

It should be noted that the developed solar dryer is the forced convection dryer with an axial fan powered by the 15W solar panel. Therefore the system it is not free from turbulences effects, as it can be seen in experimental results (see Appendix XII) whereby the Reynold number was greater than 3000. Since the hot air was flowing within the system the heat equations was energized in transient state. Physically the solar collector was made up of top and bottom glazing glasses, therefore during CFD setup the material properties for both glasses were set as semi-transparent materials of 0.85 and 0.96 transmissivity and absorptivity respectively. The same applies to the absorber plate, all properties of aluminum were selected from the database of the Fluent. The heat losses through walls of the collector made up of wood were neglected and assumed adiabatic conditions. The following boundary conditions were used to govern the simulation.

Table 5. 1 Some input parameters for the solar collector simulation

Parameter	Value & unit
Inlet velocity/mass flow rate	3.86m/s (0.0253kg/s)
Inlet air temperature	311.84K
Density of air	1.18kg/m^3
Specific heat capacity of air	1005J/kg K
Insulation (wall temp)	Ambient Temp 310.86K
Avg. absorber plate temperature	359K
Outlet	By default was assumed gauge Pressure = 0

During CFD simulation using ANSYS the convergence criteria for the turbulence k-ε, x, y & z velocity components, continuity and energy equations were monitored by setting the residuals as shown on the Table 5.2 below

Table 5. 2 Convergence criteria of the collector CFD simulation

Convergence Criterion	Set Value
continuity equation	$10e^{-4}$
x - velocity	$10e^{-4}$
y - velocity	$10e^{-4}$
z - velocity	$10e^{-4}$
energy	$10e^{-7}$
k	$10e^{-7}$
omega/epsilon	$10e^{-7}$

5.3. Numerical Modeling of drying chamber

Drying chamber in this study is the components of the banana solar dryer which serves two main purpose, firstly, it acts as the carrier and temporary storage of banana products during drying process, secondly, is the receiver of hot air generated from the solar collector.

The CFD Simulation of a rotating fan in the drying chamber was done to examine flow of hot air from the inlet to the outlet/chimney of the dryer. The air was forced to pass through the banana slices placed on the tray (not shown in CFD Geometry). The reason for performing CFD in drying chamber was to account for the turbulence flows and examine the volume rendering of velocity and temperature distributions within the drying chamber, showing out areas that receive high/low airflow or temperature.

5.3.1. Geometry of drying chamber and fan

The geometry of the drying chamber having the volume of 0.648x0.468x0.520m was modeled exactly the same as the developed drying chamber, the fan having radial diameter of 0.090m Figure 5.4 was designed using SOLIDWORK program and imported into ANSYS software as an “STP file”. This was due to the complexity of designing blades feature within the ANSYS. Figure 5.4 below shows the geometry of the drying chamber as a fluid domain having inlet,

outlet and fan. With the help of boolean operation in ANSYS workbench, the fan case and trays are enclosed and operationally subtracted from the flow domain so that they don't have effects to the simulation.

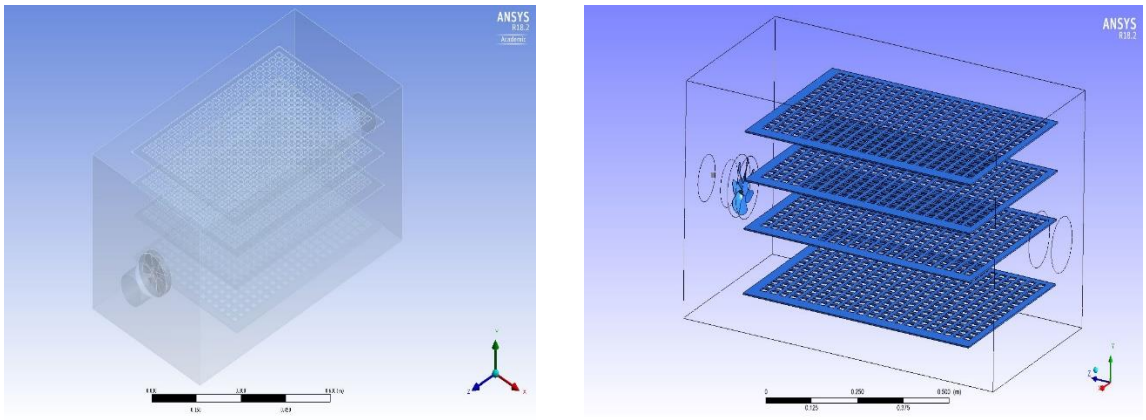

Figure 5. 4 The geometry of the drying chamber as a flow domain

5.3.2. Meshing of the drying chamber

Discretization of the domain of the drying chamber into number of elements was done in different parts of the domain. This was not due to the complexity of the model but due to the application of rotating fan within the flow domain of the drying chamber. An independent meshing to the coved edges of corners, outlet and inlet holes and the rotating case of the fan were applied. The aim of doing so is to make sure every zone within the drying chamber is captured and refined to the extent that the solver can be able to solve the flow problem easily.

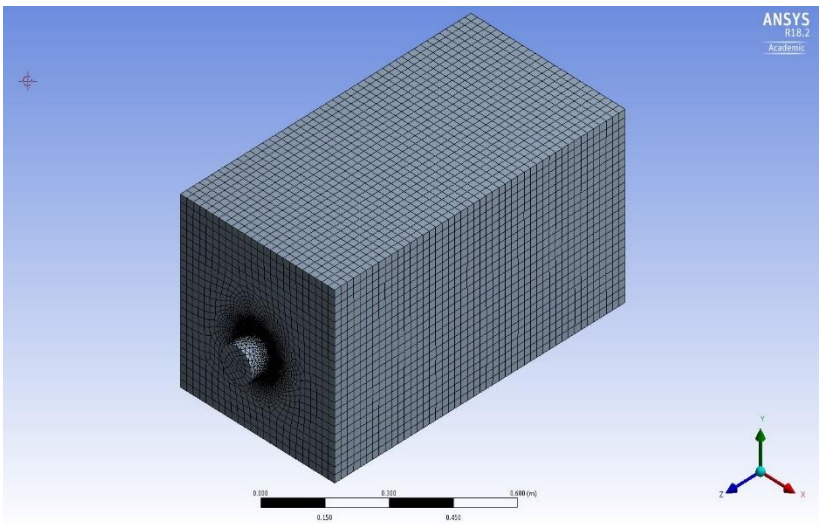

Figure 5. 5 Meshing of the drying chamber flow domain

5.3.3. The Boundary conditions of drying chamber

It is obvious that convergence of the simulation and the stability of the computational fluid is governed by the boundary conditions and set up of the solver. The setting up of the fluid domain for the drying chamber was done using ANSYS Fluent program. As said earlier on, the drying chamber is equipped with a fan which draws air from the collector, flows it radially and distributed all over within the internal zone of the drying chamber, therefore the boundary conditions for the drying chamber are described in Table 5.3.

The drying chamber is made up of plywood, therefore the density, thermal conductivity and the specific heat of the wood were taken to be 700kg/m^3, 0.173W/m K and 2310J/kg K respectively. These values are already programmed within the ANSYS database. According to (ANSYS, 2017) the trays within the drying chamber can be taken as porous materials for air flow during simulation and therefore the trays ware modeled using standard fluid flow equations by adding momentum sources term. The convergence was obtained after number of iterations and time steps and visualization of results were the last process

Table 5. 3 Boundary conditions for the drying chamber

Parameter	Value & unit
Inlet air velocity	2.8m/s or 0.0186kg/s
Inlet air temperature	337K
Density of air	1.14kg/m^3
Specific Heat capacity of air	1007J/kg K
Insulation (wood)	Opaque, under ambient Temp
Outlet	Assumed gauge Pressure, by default

5.3.4. Fluent solver and sliding meshing settings of a Fan

A transient simulation of the rotating fan within the drying chamber was done through the sliding mesh method. This technique was done in order to simulate the mesh motion effects of the fan having seven blades fixed on back wall inside the drying chamber (see Figure 5.4).

Sliding mesh methods helps in analyzing the transient flow and account for the static and rotating motion of both components, the outer case and blades of the fan respectively. It allows all meshes closer to the rotor blade to have a rotation motion relative to those meshes associated with the stationery part of the blade (Fluent, 2015). Through the application of the volume rendering features of the ANSYS software, the visualization of the fan motion and fumes distributions of hot air within the drying chamber was done. The flowchart Figure 5.6 was designed and used to make setup and procedures to be followed when dealing with sliding meshing of the rotating fan. This flowchart can be used as the benchmark for other fan simulation in drying process or other industrial purposes.

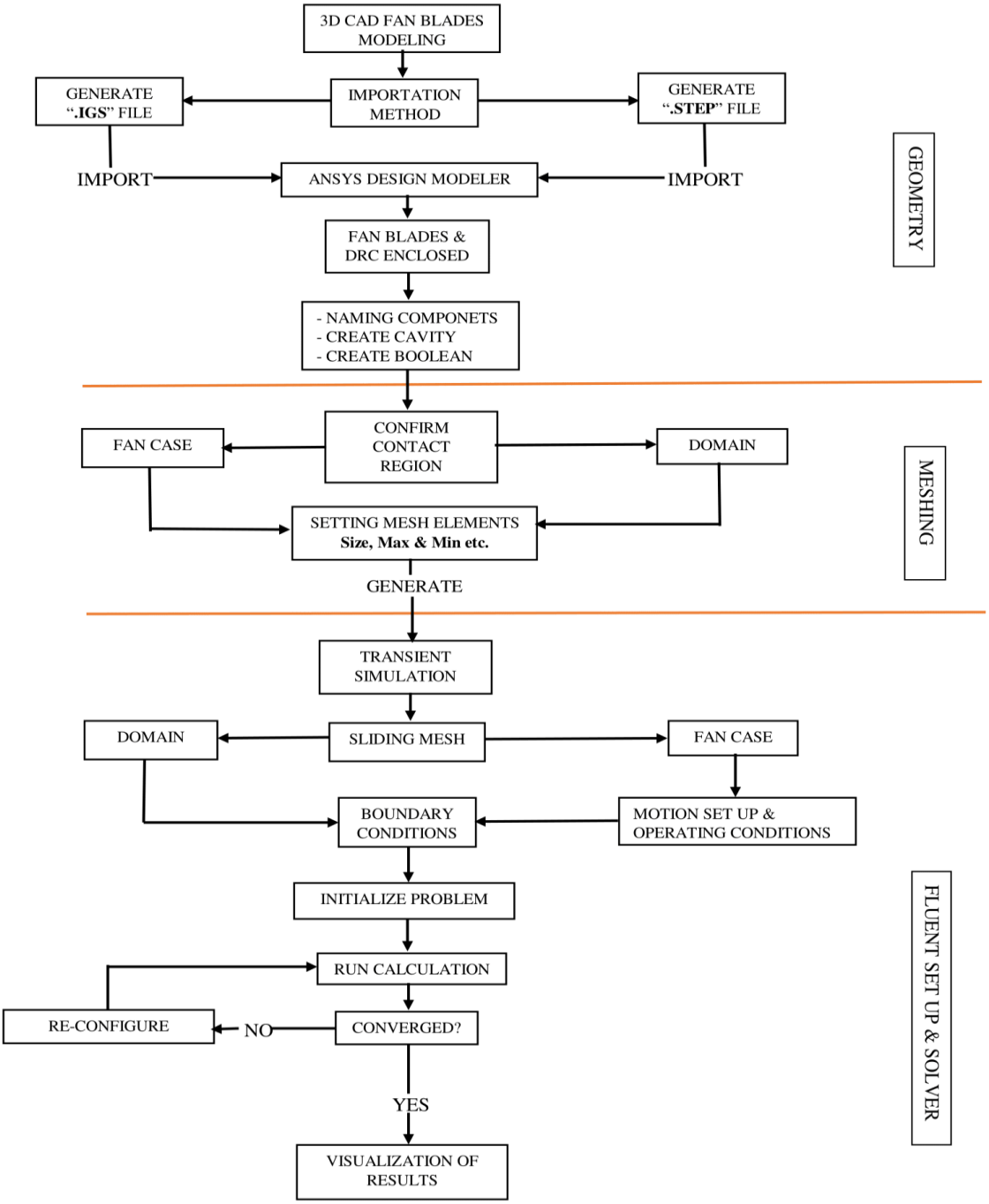

Figure 5. 6 Flow chart scheme

CHAPTER SIX: RESULTS AND DISCUSSIONS

6.1. Introduction

The results and discussions of the experiments conducted on the developed dryer are presented and discussed in this chapter. These includes the testing of the dryer under no load, climate conditions during the experiments, the effect of solar radiation on the system, temperature distribution and efficiency of the system, heat loss coefficients and useful energy obtained. It further discussed the quality control of end products and evaluation of dryer in reduction of banana losses. Results from computational fluid dynamic modeling of the developed solar dryer comparison with experimental results will also form part of this chapter.

6.2. No load testing results

In trying to investigate the performance of the solar dryer, the developed drying system was tested without load on 26/02/2019 at the workshop of Faculty of Engineering of the University of Botswana. This was the first test which aimed to check the performance of the dryer, the test took only five hours starting at 10am to 3pm. The test was conducted without load in different mass flowrates between 0.0162kg/s and 0.0298kg/s from 10:25am to 15:25pm. Appendix III shows the some of the data harvested. During this first tests some of drawback were observed and solved before the actual drying tests. One of the drawback raised was the leakage of air to the surroundings nearby the collector outlet. The problem was solved by sealing all unnecessary leakages. Also it was observed that the fan employed fail to draw enough air from the collector. This was caused by the presence of only one inlet hole at the collector, and it was solved by employing three inlet holes distributed around the entrance wall of the solar collector (see Figure 5.1 in the previous chapter).

In the dates 27/02/2017, 01/03/2019 and 03/03/2019 experimental drying tests were conducted with banana slices loaded into the drying chamber following all the preliminary drying procedure as discussed in section 4.2. The data were recorded as it can be depicted in Appendix

IV, V and VI respectively. On 05/03/2019, 08/03/2019 and 12/03/2019 experimental drying testing's were also done, during testing all measuring devices were attached to the system for measuring parameters of interest as it can be seen on the Figure 6.1 according to the measuring procedures described in section 4.1.

Figure 6. 1 Setting up and recording of parameters and final developed solar dryer.

6.3. Environmental observation

During all experimental testing, there were heat loss on top of the solar collector due to the direction and speed of the wind blowing around the experimental area and the dryer. Therefore the effects of wind on the solar collector was inevitable, although the effect of it to the dryer was not high. These effects were observed due to the temperature fluctuation on the top glass which was observed to be higher than external temperature recorded during experiments as it can be seen clearly in Appendices III-VI, where the top glass temperature line (green line) was more sinusoidal than other temperatures.

The mean velocity of the outside environment during experiment was measured and found to be in a range between 3.35m/s to 4.91m/s. From the experiment the solar radiation increases as approaching toward afternoon (mid of a day), with a maximum solar irradiance recorded at 12:00pm of 983W/m^2. Table 6.1 below illustrates some environmental properties measured during experiments.

Table 6. 1 Some environmental data recorded in 03/0/2019 during the experiment

Time of the Day	Solar Radiation	Ambient Air Temp	Air Relative Humidity	Wind Velocity
Hrs	W/m^2	K	(%)	m/s
08:40AM	511	306.8	44.5	3.35
09:00AM	584	305.4	45.9	4.91
10:00AM	787	309.5	33.2	4.84
11:00AM	907	308.1	26.6	4.27
12:00PM	983	311.3	17.9	3.94
13:00PM	965	313	16.2	3.82
14:00PM	842	313.5	15.4	3.78
15:00PM	860	314.2	13.6	4.31
16:00PM	701	314.7	15.2	3.6
16:40PM	529	313.8	15.7	3.48

6.4. Experimental observations

6.4.1. Solar radiation effects on the collector unit

Out of all drying tests, the one conducted on 03/03/2019 shows the optimal drying tests among all others. Table 6.2 shows the results of some drying parameters of the test which include solar radiations, temperatures and airflow velocities. The mass flowrates, efficiencies and heat gain of the collector were calculated using Equating [3.6], [4.13] and [4.12c] respectively.

Table 6. 2 Drying experiment conducted on 03/03/2019 from 8:40am to 16:40pm

Time	Solar Radiation	Absober Plate Temp	Bottom Glass Temp	Top Glass Temp	Collector Outlet Air Temp	Drying Chamber outlet Temp	Collector Inlet airflow	Collector Inlet Air Temp	Mass Flowrate	Collector Efficiency	Usefull Heat Gain [Eq. 5.12c]	Total Heat Received by Collector [Eq. 2.9]	Pacentage of Heat Collected by the Colletor
	W/m2	K	K	K	K	K	m/s	K	Kg/s	%	W	W	%
08:40AM	511	331	326	317	314	309.20	2.78	303.80	0.0182	28.28	185	534	35
09:00AM	584	336	327	316	318	313.00	2.89	302.70	0.0189	38.96	292	610	48
10:00AM	787	350	334	317	326	320.30	3.77	307.40	0.0247	45.60	460	822	56
11:00AM	907	361	344	323	335	329.00	3.92	310.90	0.0257	53.15	618	947	65
12:00PM	983	370	353	330	342	336.40	3.96	310.90	0.0260	63.85	805	1027	78
13:00PM	965	374	357	327	345	340.30	3.86	312.49	0.0253	66.92	828	1008	82
14:00PM	842	368	353	326	345	341.00	3.31	315.60	0.0217	58.87	636	879	72
15:00PM	860	367	348	327	345	341.50	3.92	316.20	0.0257	66.38	732	898	82
16:00PM	701	358	349	330	341	338.60	3.65	315.40	0.0239	68.32	614	732	84
16:40PM	529	348	342	324	335	333.80	3.69	315.00	0.0242	72.51	492	553	89

During the drying experiment it was measured that the air velocity sucked into the solar collector V_{in} was between 2.78 – 3.96m/s having the temperature range between 302K to 316K. The minimum and maximum solar radiation were measured to be 529W/m^2 at 08:40am and 983W/m^2 at 12:00noon respectively. The maximum collector outlet temperature was 345K, this value occurred at 13:00, 14:00 and 15:00pm while the absorber plate temperatures at that time

were 375K, 368K and 367K respectively. The maximum efficiency of the solar collector was 72.50%. All these values together with the intermediaries' values during drying can be depicted from the Table 6.2 above or in Appendix VII. The effects of solar radiation was also experienced on inlet airflow velocities, this was due to the fact that during morning especially before 10am the solar radiation was low, therefore suction of air into the solar collector by the fan was low due to the low rotation speed caused by the low power output of the solar panel. However this was not the case after 10:00am and during afternoon whereby the fan rotates at its maximum speed, as now the solar panel produces enough power.

6.4.2. Temperature distributions on collector unit

Figure 6.2 show the graph of the top glass, bottom glass and absorber plate temperatures around the solar collector and how they deviate with solar radiation. All the temperatures were dependent on solar radiation. The graph shows the discrepancy between the top and bottom glass temperatures, the temperature of the bottom glass is higher than the top glass. This portrays a good picture that there is heat captured by the flowing air between the glasses, therefore the air in the upper channel is pre-heated, accumulate heat energy before enters the bottom channel.

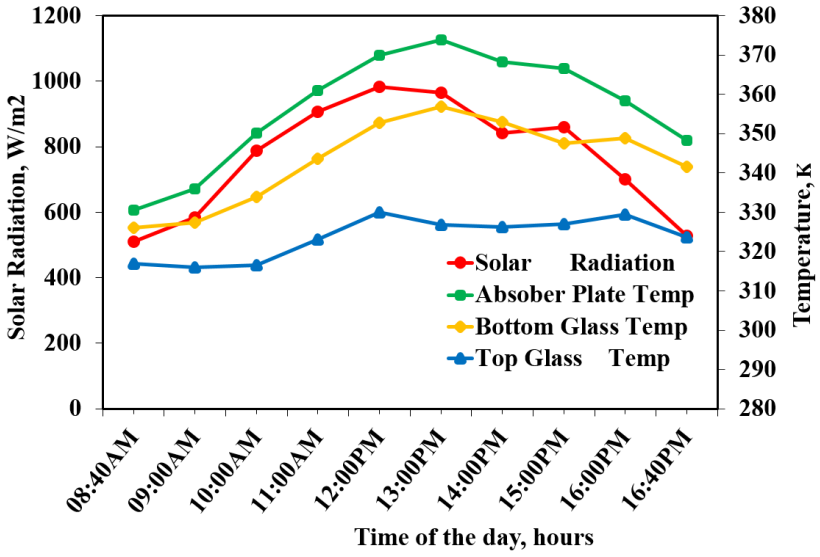

Figure 6. 2 Temperature distributions of solar collector during drying process.

Figure 6.3 shows the graph of inlet and outlet temperatures of the solar collector. From the graphs it can be observed that at 15:00 pm the solar radiation starts to drop down very rapidly but the drop of outlet temperature of the collector was gradually slow. In other words, a drop of 436W/m^2 solar radiation makes a drop of just 283K of the outlet temperature within an hour. This phenomena of slow release of heat to the collector outlet is caused by good design and configurations of the collector. It is healthy to the system since it help the solar collector maintaining its thermal properties for a while during sun drop.

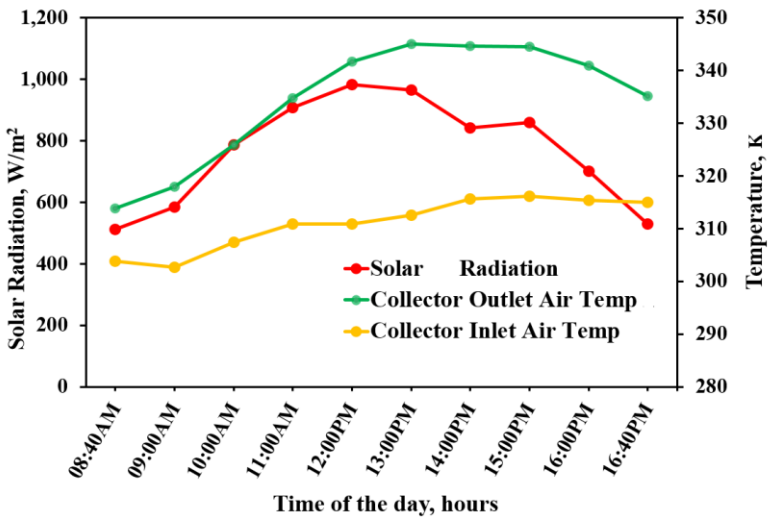

Figure 6. 3 Inlet and outlet temperatures of the solar collector

6.4.3. Mass flowrates Vs efficiency of the collector unit

During the experiment and from the Table 6.2 the efficiency of the collector showed improvement. The efficiency of the collector rose with the rise in mass flow rates and time, but it keeps on stabilizing even when mass flow rates dropped as shown on the graph Figure 6.4. A good predication from Figure 6.4 is that the application of the air gap underneath the absorber plate helped to maintain and stabilize the percentage increase of efficiencies of the collector by releasing extra stored heat especially during low solar radiation. However, the efficiency was

under 50% from 08: 40am to 11:00am due to the fact that, the fan was running under direct power from a PV panel. The airflow rate and velocity of the fan goes high at 11:00pm and therefore high suction of air from the collector led to poor heat dispassion and lead to difference between inlet and outlet temperature of collector, as these two parameters contribute to the efficiency of collector. This phenomena can also be observed in Table 6.2. On the other hand, Table 6.1 shows that the surrounding wind velocity was high from 08:40am to 11:00am, so there was cooling on aluminum flexible pipe where temperature sensor was fixed, as the pipe was not insulated.

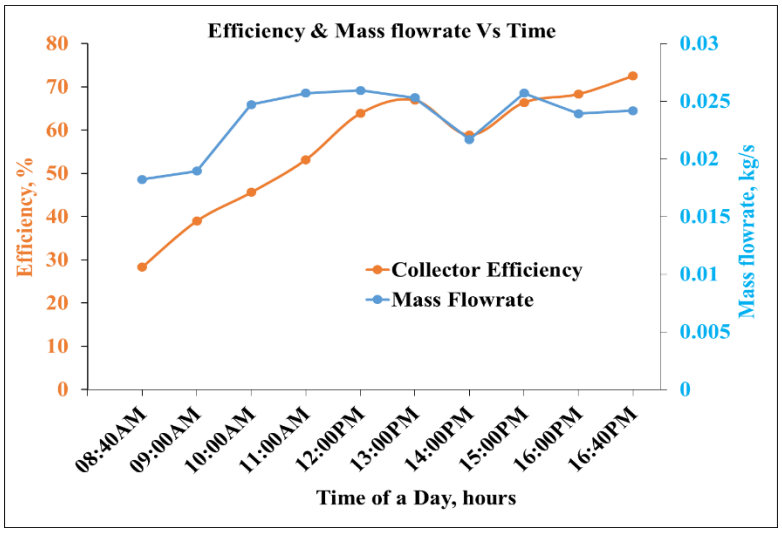

Figure 6. 4 The effect of collector configurations, mass flowrates and time on collector efficiency

6.4.4. Collector useful heat Gain

From Table 6.2 and by using Equation 4.12c the maximum useful heat gained by the solar collector (Q_u) from the solar radiation was 828.21W (see Figure 6.5), this value was obtained at 13pm when the solar radiation was 965W/m^2. Figure 6.5 below shows the trend of the useful heat against solar radiation for 8hrs of drying. Figure 6.6 illustrates the percentage of the useful heat gained by the moving air in the solar collector against the heat collected from the sun by the solar collector. From the graph we can conclude that in seven hours of drying out of eight

hours in a day at least 50% up to the average of 69% of the heat collected by the solar collector were taken to be used for drying in all seven hours of drying.

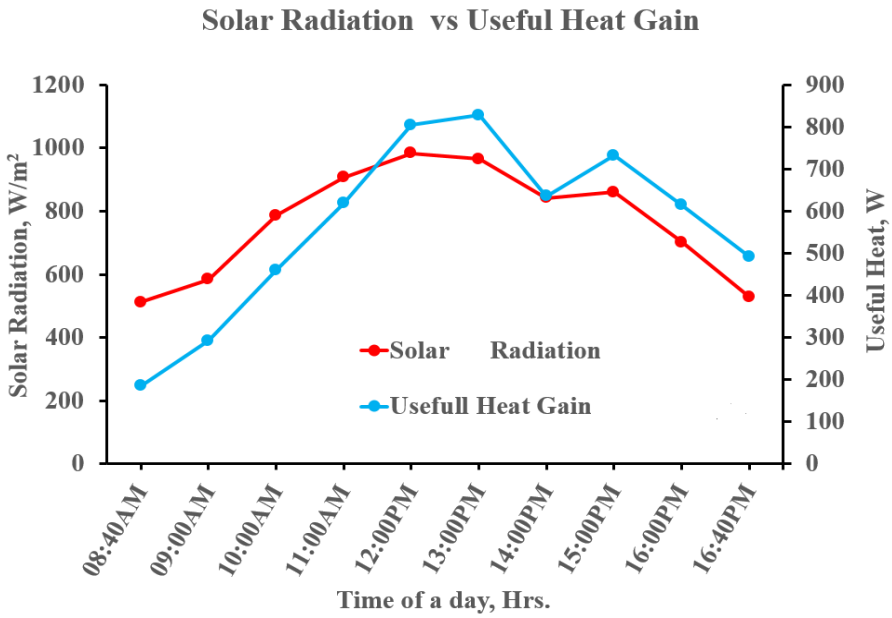

Figure 6. 5 Relationship between the useful heat gained, radiation vs Time of the day

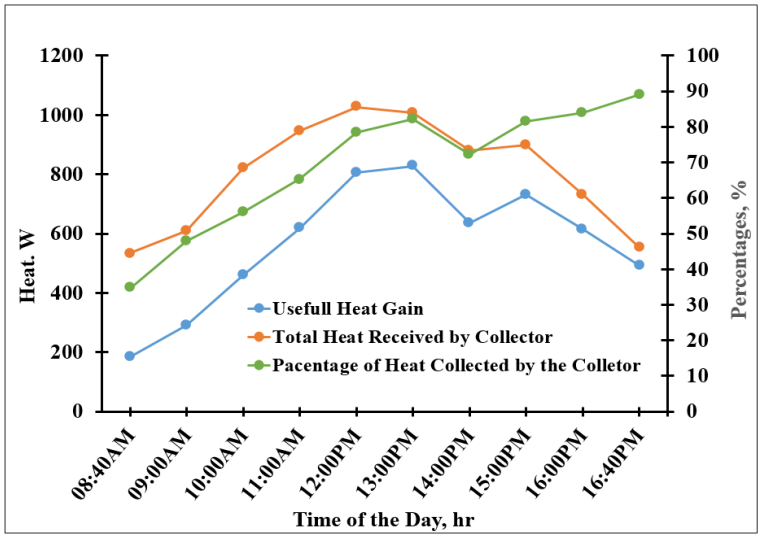

Figure 6. 6 Relationship between the Heat collected and Heat Gained by the collector

6.4.5. Radiative and Convective heat transfer coefficients

Radiative and convective heat transfer coefficients are the driver of the heat loss in the system. These includes the coefficient heat transfer due the wind blowing on the system [Eq.4.3], temperature emissivity due to the radiative coefficients on top and bottom glasses together with

collector absorbing plate [Eq. 4.4 – 4.6c] described on section 4.3.2. Figure 6.7 below shows the graph of heat loss coefficients and heat transfer coefficients. During high solar radiation (between 11am and 16:40pm) the heat loss to the environment was high, however there were small trend on heat losses due to radiative heat transfer coefficients during that time. From the trend of the graph, it shows us that the performance of solar collector can be enhanced during solar hours, as this time the degree of hotness of the system if a bit high due to high solar radiation.

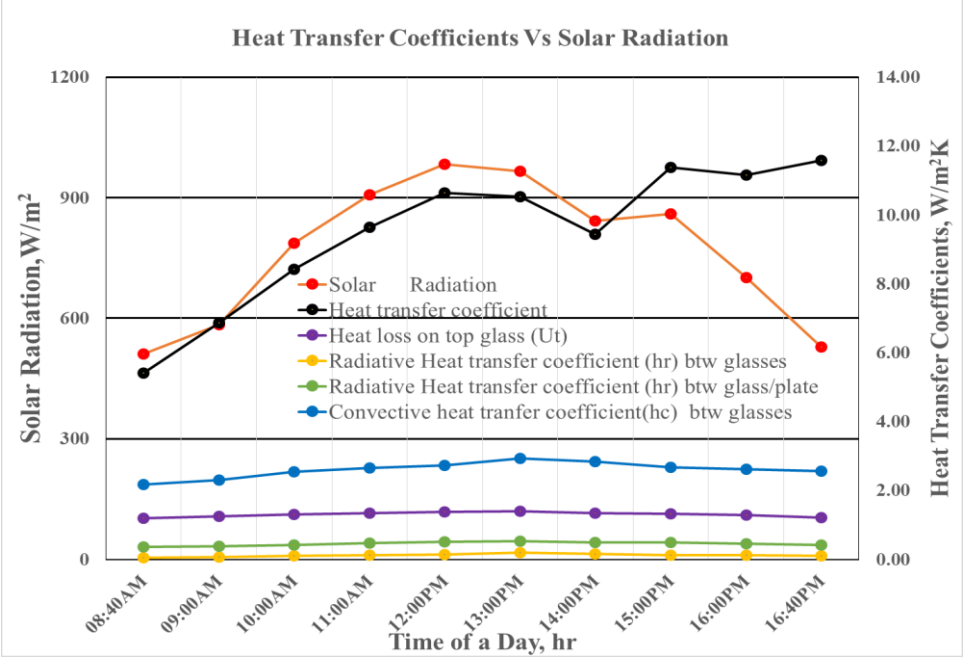

Figure 6. 7 Graph of convective & radiative heat transfer coefficient and heat loss against time and solar radiation

From the above experimental results of this study, the solar dryer has shown good thermal improvements and performance of a double pass solar collector as compared to other literature studies done the same design and development of a double pass solar collector. From the results of this study, it can be depicted that, the maximum instantaneous efficiency of a double pass solar collector was 72.50% which is 3.5% and 10% high than that reported by (Pramanik et al., 2017) and (Mahmood et al., 2015) which were recorded to be 69% and 62.50% respectively . The value of efficiency of this study was also high than the one reported by (Kareem et al.,

2017b) and (Kareem et al., 2017c) which were 64.08% and 58.73% respectively. A close agreement of efficiency of this study was observed with that reported by (Fudholi et al., 2013) which was recorded to be between 70-80% respectively. By comparing the useful heat gain, the value of useful heat gain recorded in this study Figure 6.6 was 69% nearly close to the one reported in (Pramanik et al., 2017) which was found to be about 60% to 70%.

6.5. Computational Fluid Dynamic (CFD) results

In this section the effects of solar radiation in thermal properties of the double pass solar collector was evaluated under different boundary conditions, temperatures and mass flow rates. The ANSYS Fluent software were used to extract and portray results in the form of graph, table and pictures as can be seen in the following sections

6.5.1. Solar collector

Figure 6.8 Shows the CFD results of the temperatures distribution contour on the surface of the absorber plate. From this figure we can see the temperature is not uniformly distributed around the plate. The high heated area/zone was found at the middle of the plate approximately 384K was generated. This is due to the distances from the side-walls of the solar collector which are normally close to the outside environments, so the heat was lost in side-walls of the solar collector. It can be depicted from the Figure 6.8 that the high temperature zones start approximately 0.3m from the entrance of the bottom channel and distribute toward the outlet of the solar collector. This can be due to the fact that at the entrance of the bottom channel, the air with low amount of temperatures from the top channel tried to lower down the temperature of the absorber plate since there is a relationship between the air flowing on top of the plate and the temperature distribution on the plate.

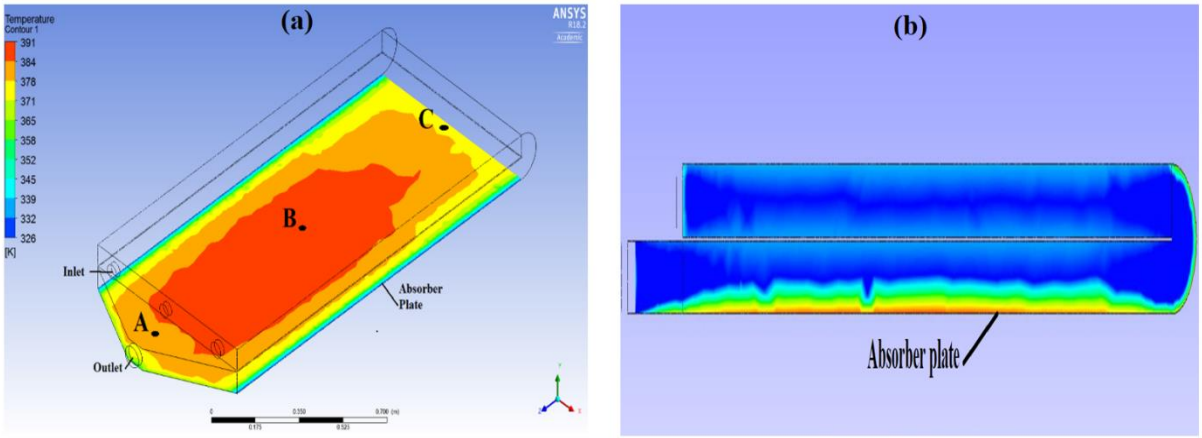

Figure 6. 8 Temperature distribution on absorber plate surface (a), Contour of static temperature or temperature gradient near wall of absorber plate (b)

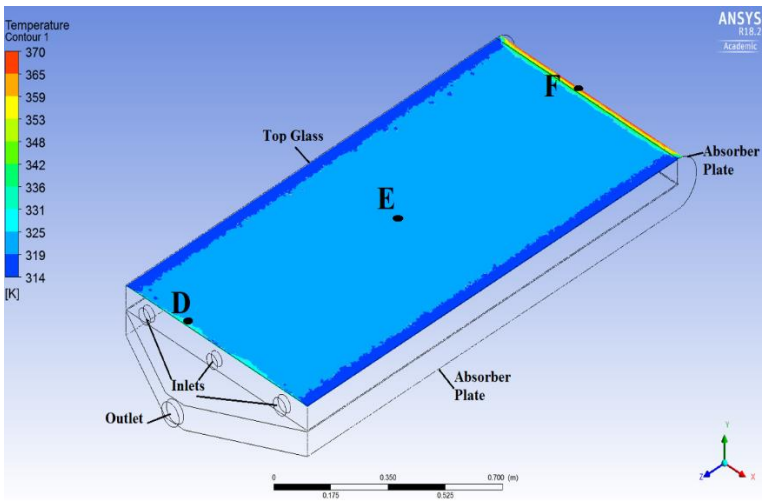

Figure 6. 9 Temperature distribution on top glass of the double pass solar collector

Table 6. 3 Comparison in temperature distributions on absorber plate and top grass from the CFD modeling and experiment results

Temperatures (K)						
Area	**Absorber Plate (Fig. 6.8)**			**Top Glass (Fig. 6.9)**		
Location	**A**	**B**	**C**	**D**	**E**	**F**
Simulation	378.9	**384.1**	371.5	**330.2**	324.3	359.6
Experiment	373.4	**374.8**	369.4	**330.0**	323.4	358.8
Difference	5.5	9.3	2.1	0.2	0.9	0.8

The level of agreement between the CFD and experimental results conducted, as far as the solar collector is concerned is on the maximum temperature generated by the absorber plate during experiments, and the maximum temperatures at different points (A, B and C) of the absorber plate generated by CFD simulations, as shown of the Figure 6.8a. During the experiment the maximum temperature of the absorber plate was 374.8K while that of CFD results was 384.1K. Table 6.3 shows comparison and variation of temperatures in various points on absorber plate and top glass of a solar collector. Figure 6.8b shows a contour of a temperature in a middle section of the solar collector. It shows the temperature gradient on a sub-layers of the absorber plate and how it grows towards up above the hot plate. This is a good indication that heat can be captured or transferred into a moving fluid (in this case air) passing on a flat plate (absorber plate).

Figure 6.9 shows the temperature distribution on the top glass of the solar collector. From the experimental result (see Figure 6.2 or Table 6.2 and 6.3) the maximum temperature reached was 330K, the maximum temperature reached on CFD result shown on Figure 6.9 is approximately 324.3-330.2K, this make good comparison among the temperatures obtained through both approaches. However, slight discrepancies and variations among the temperatures were inevitable due to the fact that the CFD does not take considerations of wind and other environmental effects during the simulation, this is not the case for the experimental approach whereby the temperatures recorded by sensors can change due the environmental effects. Figure 6.9 shows also the temperature increase of up to 359.6K at the end of the top glass, this is due to the fact that during manufacturing, the end of the collector was made up of aluminum plate, it was curved to join the upper and lower channels of the collector, so the same design was done during modeling of the geometry in CFD. In this case the wall of the glass closer to the curved surface at the end of the collector will experience temperature almost the same or slightly lower than absorber temperature, as it can be seen on Figure 6.9

Figure 6.10 shows volume rendering to velocity distributions across trays within the drying chamber. The distribution was not uniform to all the four trays in the fists design whereby the top three trays experienced more drying effects than bottom tray, this was also experienced during experiments investigation whereby banana slices put on the bottom tray took more time to dry than those on other three top trays. However it was decided to solve this problem by making the fluid inlet and outlet holes of the drying chamber sandwich trays for better performance. Therefore the fluid inlet hole was placed below the bottom tray and the fluid out hole be above the top tray. This phenomena has led to proper drying of banana slices uniformly, hence reduces drying time of banana fruits.

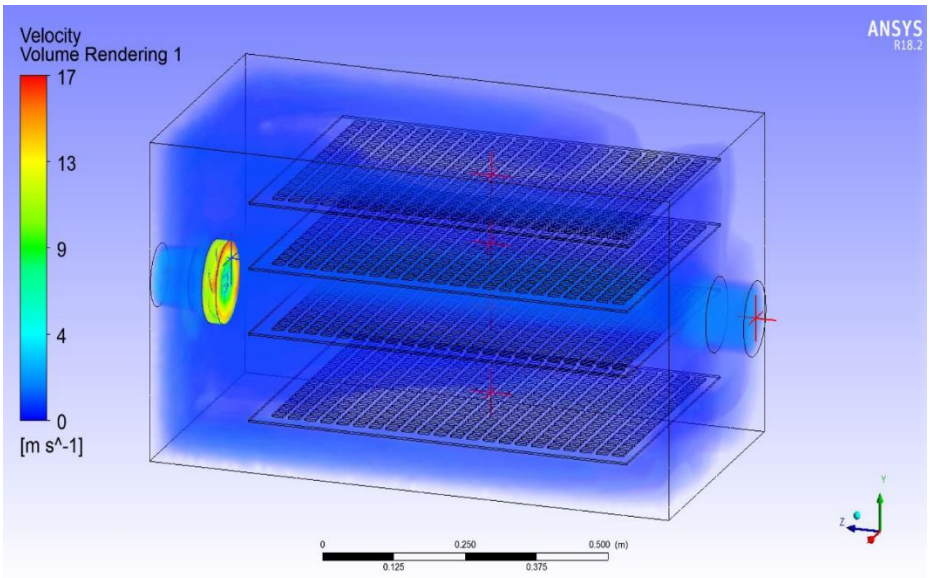

Figure 6. 10 Volume rendering to velocity profile across the trays within the drying chamber

6.6. Quality of End products

The quality of end dried products like banana flakes are determined through number of properties like color and teste. Drying process of agricultural products normally tends to modify simultaneously food properties, therefore the change in product properties like size, shape, color and aroma or test during drying process is quite inevitable and can influence consumer's demand perception (Kumar et al., 2014). In this section the quality of dried banana is evaluated in terms of color, teste and physical deformation.

6.6.1. Color and teste of banana flakes

Drying processes were conducted in different number of days between February and March under different treatments conditions. During and after drying process it was observed that banana flakes treated with lemon juice were having little bending shapes compare to those not treated with lemon juice, also they maintained color and with better test compared to the untreated one. From this results it can be concluded that treatment of banana fruits prior to drying can led to the good quality of end products, therefore various treatment reagents can also be applied and evaluated to see the best treatment reagent that can give out good product. Figure 6.11 below shows banana flakes as the end products of the developed solar dryer.

Figure 6. 11 Solar Dried banana flakes

6.6.2. Shrinkage of banana flakes

Shrinkage or bending behavior of drying product has effects during drying. It increases drying time because some parts of a slice will not receive enough temperature of hot air for water activity to take place easy therefore increases drying time. During the drying of banana slices using the developed solar dryer, shrinkage behavior was also investigated. It was observed that shrinkage behavior of banana slices during drying can at least be reduced through the use of nets in making drying trays, instead of using wire mesh as most of drying process normally do. Nets materials tend to make banana slices stick on it temporarily when they are still wet, as the drying process continue and water is being removed from banana slices, the stickiness behavior tends to lose its capability, therefore banana slices become dry and easy to be removed from the trays. The only precaution to be observed when using netting trays is to avoid elevated drying temperatures of more than 353K, otherwise the temperatures more than this may affect or cause welding behavior and closing up of netting perforated holes. Appendix VIII shows some drying parameters and properties of banana flakes dried using the developed solar dryer

6.7. Dryer evaluation in reduction of banana losses

The developed solar dyer in this study was designed purposely for experimental procedures and it was able to accommodate the loading capacity of approximately 2-4kg of banana fruits within a drying chamber having a volume capacity of $0.21m^3$. However, a bigger dryer with large size more than this can be designed to accommodate large loading capacity of banana fruits. For the purpose of estimating the losses of banana fruits served by the dryer within a month (30days) aiming to reduce (PHL), below are assumptions.

a) The weight of banana fruits to be dried that would otherwise become waste 3.69kg
b) Drying time is 13hrs (see Appendix VIII), meaning two typical drying days, so for a month it means 15days of fully drying.

$$\text{Drying Runs} = \frac{\text{Total days of drying in a month}}{\text{Drying time in days}} = \frac{30\text{days}}{2\text{days}} = 15$$

$$\text{Losses Reduction} = \text{Dryer Capacity x drying runs} = 3.69\text{kgx}15$$

$$= \mathbf{55.35kg/month\ per\ dryer}$$

From **Appendix X** and by considering the above assumptions more savings can be achieved when large dryers of different volumes employed as it can be seen on the appendix mentioned above. Materials costs for developing this dryer are shown on **Appendix IX.**

CHAPTER SEVEN: CONCLUSION AND RECOMMENDATION FOR FUTURE WORK

A low cost forced convection solar dryer with a double pass solar collector capable of drying banana has been designed and constructed. From the study the general performance evaluation of the developed solar dryer having a double pass solar collector and convective air drying chamber was studied through experimental and numerical approach. The whole structure of the solar dryer was easy to develop/construct using simple and affordable materials and can be implemented at very low costs. Due to the uniqueness configuration of the solar collector having double channels and absorber plate, being not directly exposed to the ambient surroundings, the system was able to achieve high operational efficiency. From the experiment conducted, the maximum efficiency of the solar collector was obtained to be 72% which fairly promising that the dryer can generate enough drying temperature for even other products with lower moisture content than banana fruits. The heat storage gap underneath of the absorber plate helped to improve efficiency of the collector and avoid rapid drop of the outlet temperature of the solar collector at low sunshine, this phenomena help to keep and maintain the drying temperature for a period of time.

From the experiments conducted with fresh banana fruits it was found that the average initial moisture content of a banana ranges from 75-82% (w.b), this value was dropped down to an average of less than 20% final moisture content within 8 to 13 hours depending on the solar radiation and loading capacity of the dryer. The optimal drying temperature designed for this dryer is between 333K and 338K. During experiment this temperature reached optimal drying temperature within short time and sometimes went up by 1K to 7K as shown in Appendices III-VI. Therefore, the developed dryer was good to produce enough drying temperature.

In this study the numerical model was developed and validated with experimental data obtained from developed solar dryer. A good agreement between experimental and numerical data was observed in temperature distributions on absorber plate and top glass. Slight differences were

also observed in various locations on the solar collector. Therefore the CFD model can produce and predict temperature and velocity distribution within the solar collector and drying chamber.

In a developed dryer, attention should be paid to not dry products at an elevated temperatures for long time. This may result to degradation of the products. Under this situation an auxiliary system for controlling temperature can be employed to this dyer in order to maintain drying parameters to the optimal level, however, care must be taken to avoid the system being more sophisticated and therefore deviate from a green technology concept of view.

The dryer also can later be improved by adding/adjusting or change fins shapes in a way that can lengthen the air flow movement within the collector, this will create more turbulences flow within a collector and therefore increases the rate of heat transfer from the absorbing plate. A dryer can also be changed to a hybrid drying system by employing an auxiliary solar heating system to generated and maintain drying temperature and velocity.

Furthermore, in this developed solar dryer the quality of end products (taste, color, and appearance) were checked and preserved. From the experiments it was observed that banana dried on netting trays can at least remain with their spheroidal shape without being heavier degraded or deformed to another shape. This was due to the fact that banana while wet tried to stick on netting trays, as the drying continued, the stickiness behavior disappeared and left slices of banana in good shape and easy to be removed. On the other hand, lemon juice was applied prior to drying, the experiment shows that the taste of banana fruits remained attractive to the user and the banana slices remain with their color without being darkened as seen in Figure 6.11.

With regards to the uniformity of the drying air within a drying chamber, a blowing fan of high blowing rate that will dissipate air uniformly within trays can also be considered in further work. This will alleviate periodic exchange of the trays, since it was observed during

experiment that slow drying occurred to the tray just below the inlet or below the fan within drying chamber.

This study was done by designing the dryer particular solar collector that can be tilted to various angles, for the purpose of future study, this design feature can helps in performing research study on performance of solar collector in various inclination angles in Botswana that can allow maximum solar radiation in a particular area or season.

In the CFD section under this study, the prediction of moisture diffusing from the banana materials to the flowing air within drying chamber was not examined. It is an area of great important and I suggest to be done in future work, especially with the current and new products of CFD software which are able to generate and accept user define function and capture the mass or moisture diffusion of a product.

REFERENCES

ABANO, E. & SAM-AMOAH, L. 2011. Effects of different pretreatments on drying characteristics of banana slices. *APRN Journal of Engineering and Applied Science,* 6**,** 121-129.

ABDULLAHI, Y., MOMOH, M., GARBA, M. M. & MUSA, M. 2013. Design and construction of an adjustable and collapsible natural convection solar food dryer. *Int J Comput Eng Res,* 3**,** 1-8.

ABUBAKAR, M. & ISIYAKU, D. 2014. Development of a par-boiled rice solar dryer. *Bayero Journal of Pure and Applied Sciences,* 7**,** 1-7.

ADEGOKE, C. & BOLAJI, B. O. 2000. Performance Evaluation of Solar–Operated Thermosyphon Hot Water System in Akure.

AHMAD, S., NASIR, M. A., ANWAR, Z. & THOMPSON, A. 2007. Effect of fruit size and temperature on the shelf life and quality of ripe banana fruit. *Sarhad Journal of Agriculture,* 23**,** 45.

AKHTAR, N. & MULLICK, S. 2007. Computation of glass-cover temperatures and top heat loss coefficient of flat-plate solar collectors with double glazing. *Energy,* 32**,** 1067-1074.

AKPINAR, E. K. 2006. Mathematical modelling of thin layer drying process under open sun of some aromatic plants. *Journal of Food Engineering,* 77**,** 864-870.

ALAM, M. S. 2014. Modeling of thin layer drying kinetics of grape juice concentrate and quality assessment of developed grape leather. *Agricultural Engineering International: CIGR Journal,* 16**,** 196-207.

ALONSO-TORRES, B., HERNÁNDEZ-PÉREZ, J. A., SIERRA-ESPINOZA, F., SCHENKER, S. & YERETZIAN, C. 2013. Modeling and validation of heat and mass transfer in individual coffee beans during the coffee roasting process using computational fluid dynamics (CFD). *CHIMIA International Journal for Chemistry,* 67**,** 291-294.

AMER, B., HOSSAIN, M. & GOTTSCHALK, K. 2010. Design and performance evaluation of a new hybrid solar dryer for banana. *Energy conversion and management,* 51**,** 813-820.

AMPRATWUM, D. B. & DORVLO, A. S. 1998. Evaluation of a solar cabinet dryer as an air-heating system. *Applied Energy,* 59**,** 63-71.

AMRAOUI, M. A. & ALIANE, K. 2017. Three-dimensional Analysis of Air Flow in a Flat Plate Solar Collector. *Periodica Polytechnica Mechanical Engineering,* 62**,** 126-135.

AMRUTKAR, S. K., GHODKE, S. & PATIL, K. 2012. Solar flat plate collector analysis. *IOSR Journal of Engineering,* 2**,** 207-213.

ANANDHARAMAKRISHNAN, C. 2013. *Computational Fluid Dynamics Applications in Food Processing*.

ANDRINGA, J. 2017. Some characteristics of the pattern of solar radiation in Botswana. *International Energy Journal,* 11.

ANSYS, I. 2011. ANSYS FLUENT user's guide. *Canonsburg, PA*.

ANSYS, I. 2017. ANSYS LS-DYNA user's guide. ANSYS. Inc. Pennsylvania, US.

AREGBESOLA, O., OGUNSINA, B., SOFOLAHAN, A. & CHIME, N. 2015. Mathematical modeling of thin layer drying characteristics of dika (Irvingia gabonensis) nuts and kernels. *Nigerian Food Journal,* 33**,** 83-89.

ASHGRIZ, N. & MOSTAGHIMI, J. 2002. An introduction to computational fluid dynamics. *Fluid Flow Handbook, McGraw-Hill Professional***,** 24.1-24.52.

BAINI, R. & LANGRISH, T. 2007. Choosing an appropriate drying model for intermittent and continuous drying of bananas. *Journal of Food Engineering,* 79**,** 330-343.

BALA, B., MONDOL, M., BISWAS, B., CHOWDURY, B. D. & JANJAI, S. 2003. Solar drying of pineapple using solar tunnel drier. *Renewable Energy,* 28**,** 183-190.

BELESSIOTIS, V. & DELYANNIS, E. 2011. Solar drying. *Solar energy,* 85**,** 1665-1691.
BHAGORIA, A. S. Y. J. L. 2013. A CFD (computational fluid dynamics) based heat transfer and fluid flow analysis of a solar air heater provided with circular transverse wire rib roughness on the absorber plate. *Energy*.
BHASKARAN, R. & COLLINS, L. 2002. Introduction to CFD basics. *Cornell University-Sibley School of Mechanical and Aerospace Engineering*.
BIRD, R. B. 2002. Transport phenomena. *Applied Mechanics Reviews,* 55**,** R1-R4.
BOLAJI, B. O. 2005. Performance evaluation of a box-type absorber solar air collector for crop drying.
BOLAJI, B. O. & OLALUSI, A. P. 2008. Performance evaluation of a mixed-mode solar dryer.
BRADLEY, R. L. 2010. Moisture and total solids analysis. *Food analysis.* Springer.
BRENNDORFER, B., KENNEDY, L., BATEMAN, C., TRIM, D., MREMA, G. & WEREKO-BROBBY, C. 1987. Solar dryers—their role in post-harvest technology.
BRUNNER, S., GASSER, P., SIMMLER, H. & WAKILI, K. G. 2006. Investigation of multilayered aluminium-coated polymer laminates by focused ion beam (FIB) etching. *Surface and Coatings Technology,* 200**,** 5908-5914.
CÂRLESCU, P.-M., ARSENOAIA, V. & ROȘCA, R. 2017. CFD simulation of heat and mass transfer during apricots drying. *LWT-Food Science and Technology,* 85**,** 479-486.
CHABANE, F., MOUMMI, N. & BENRAMACHE, S. 2013. Experimental analysis on thermal performance of a solar air collector with longitudinal fins in a region of Biskra, Algeria. *Journal of Power Technologies,* 93**,** 52-58.
CHAUHAN, N. & JETHVA, K. 2016. Drying Characteristics of Banana Powder. *Indian Journal of Science,* 23**,** 75-88.
CHAUHAN, P. S., KUMAR, A. & TEKASAKUL, P. 2015. Applications of software in solar drying systems: a review. *Renewable and Sustainable Energy Reviews,* 51**,** 1326-1337.
CORZO, O., BRACHO, N., VÁSQUEZ, A. & PEREIRA, A. 2008. Energy and exergy analyses of thin layer drying of coroba slices. *Journal of Food Engineering,* 86**,** 151-161.
D.C, W. 2008. Formulation of the k-omega turbulence model revisited *AIAAJ*.
DA ROSA, A. V. 2012. *Fundamentals of renewable energy processes*, Academic Press.
DA SILVA, W. P., E SILVA, C. M., GAMA, F. J. & GOMES, J. P. 2014. Mathematical models to describe thin-layer drying and to determine drying rate of whole bananas. *Journal of the Saudi Society of Agricultural Sciences,* 13**,** 67-74.
DA SILVA, W. P., E SILVA, C. M. & GOMES, J. P. 2013. Drying description of cylindrical pieces of bananas in different temperatures using diffusion models. *Journal of Food Engineering,* 117**,** 417-424.
DALIRAN, A. & AJABSHIRCHI, Y. 2018. Theoretical and experimental research on effect of fins attachment on operating parameters and thermal efficiency of solar air collector. *Information Processing in Agriculture*.
DHANUSHKODI, S., WILSON, V. H. & SUDHAKAR, K. 2014. Thermal Performance evaluation of Indirect forced cabinet solar dryer for cashew drying. *American-Eurasian Journal of Agricultural and Environmental Science,* 14**,** 1248-1254.
DUFfiE, J. A. & BECKMAN, W. A. 1980. Solar engineering of thermal processes. *John Willey & Sons, New York*.
DUFFIE, J. A. & BECKMAN, W. A. 1974. Solar energy thermal processes. University of Wisconsin-Madison, Solar Energy Laboratory, Madison, WI.
DURUSOJU, M., GOYAL, C., SHEIKH, I., DONGRE, A., MARBATE, L., ROHIT, K. & KATEKAR, V. An Experimental Investigation of Thermal Performance of Solar Air Heater with 'W'Wire Mesh.
ECONOMICS, T. 2018. *Trading Economics* [Online]. Available: https://tradingeconomics.com/botswana/imports/mozambique/bananas-plantains-fresh-dried [Accessed 18/10/2018 2018].

EHIEM, J., IRTWANGE, S. & OBETTA, S. 2009. Design and development of an industrial fruit and vegetable dryer. *Research Journal of Applied Sciences, Engineering and Technology,* 1**,** 44-53.

EKECHUKWU, O. & NORTON, B. 1996. Design and measured performance of a solar chimney for natural circulation solar energy dryers. *Journal of solar energy engineering,* 118**,** 69-71.

EKECHUKWU, O. & NORTON, B. 1999a. Review of solar-energy drying systems III: low temperature air-heating solar collectors for crop drying applications. *Energy Conversion and Management,* 40**,** 657-667.

EKECHUKWU, O. V. & NORTON, B. 1999b. Review of solar-energy drying systems II: an overview of solar drying technology. *Energy conversion and management,* 40**,** 615-655.

EL-KHAWAJAH, M., ALDABBAGH, L. & EGELIOGLU, F. 2011. The effect of using transverse fins on a double pass flow solar air heater using wire mesh as an absorber. *Solar energy,* 85**,** 1479-1487.

EL-SEBAII, A., ABOUL-ENEIN, S., RAMADAN, M., SHALABY, S. & MOHARRAM, B. 2011. Thermal performance investigation of double pass-finned plate solar air heater. *Applied Energy,* 88**,** 1727-1739.

ESQUIVEL, R. S., VINDAS, M. R., TRETO, P. C. & RAMÍREZ, K. S. 2018. Cfd Applied in the Optimization of A Dryer For Parchment Coffee Drying (Coffeaarabica L.) By Forced Ventilation.

EVANS, J. 1994. Food Refrigeration and Process Engineering Research Centre. *Food Science and Technology Today,* 8**,** 50-4.

FADHEL, M., ABDO, R. A., YOUSIF, B., ZAHARIM, A. & SOPIAN, K. Thin-layer drying characteristics of banana slices in a force convection indirect solar drying. Proceedings of the 6th IASME/WSEAS International Conference on Energy and Environment (EE 2011), 2011. World Scientific and Engineering Academy and Society Press, 310-315.

FAO 2013. *FAO Statistical Yearbook: World Food and Agriculture*, FAO.

FAYOSE, F. & HUAN, Z. 2016. Heat Pump Drying of Fruits and Vegetables: Principles and Potentials for Sub-Saharan Africa. *International journal of food science,* 2016.

FERGUSON, P. D. B. S. N. L. R. I. 2005. *Computational Fluid Dynamics: Applications in Environmental Hydraulics*.

FLUENT, A. 2015. Theory guide. *Ansys Inc*.

FORSON, F., NAZHA, M., AKUFFO, F. & RAJAKARUNA, H. 2007. Design of mixed-mode natural convection solar crop dryers: application of principles and rules of thumb. *Renewable Energy,* 32**,** 2306-2319.

FUDHOLI, A., SOPIAN, K., OTHMAN, M. Y., RUSLAN, M. H. & BAKHTYAR, B. 2013. Energy analysis and improvement potential of finned double-pass solar collector. *Energy Conversion and Management,* 75**,** 234-240.

FUDHOLI, A., SOPIAN, K., YAZDI, M. H., RUSLAN, M. H., GABBASA, M. & KAZEM, H. A. 2014. Performance analysis of solar drying system for red chili. *Solar Energy,* 99**,** 47-54.

GUPTA, B., WAIKER, J. K., MANIKPURI, G. P. & BHALAVI, B. S. 2013. Experimental analysis of single and double pass smooth plate solar air collector with and without porous media. *American Journal of Engineering Research,* 2**,** 144-149.

HEGDE, V. N., HOSUR, V. S., RATHOD, S. K., HARSOOR, P. A. & NARAYANA, K. B. 2015. Design, fabrication and performance evaluation of solar dryer for banana. *Energy, sustainability and Society,* 5**,** 23.

HO, C.-D., CHANG, H., HSIAO, C.-F. & HUANG, C.-C. 2018. Device performance improvement of recycling double-pass cross-corrugated solar air collectors. *Energies,* 11**,** 338.

HO, C., YEH, C. & HSIEH, S. 2005. Improvement in device performance of multi-pass flat-plate solar air heaters with external recycle. *Renewable Energy,* 30**,** 1601-1621.

HOSSAIN, M. & BALA, B. 2007. Drying of hot chilli using solar tunnel drier. *Solar Energy,* 81**,** 85-92.

INGLE, P., PAWAR, A., DESHMUKH, B. & BHOSALE, K. 2013. CFD analysis of solar flat plate collector. *International Journal of Emerging Technology and Advanced Engineering,* 3**,** 337-342.

IRTWANGE, S. & ADEBAYO, S. 2009. Development and performance of a laboratory-scale passive solar grain dryer in a tropical environment. *Journal of Agricultural Extension and Rural Development,* 1**,** 042-049.

JACOBSON, M. Z. & JADHAV, V. 2018. World estimates of PV optimal tilt angles and ratios of sunlight incident upon tilted and tracked PV panels relative to horizontal panels. *Solar Energy,* 169**,** 55-66.

JAIRAJ, K., SINGH, S. & SRIKANT, K. 2009. A review of solar dryers developed for grape drying. *Solar Energy,* 83**,** 1698-1712.

JANJAI, S., LAMLERT, N., INTAWEE, P., MAHAYOTHEE, B., BALA, B., NAGLE, M. & MÜLLER, J. 2009. Experimental and simulated performance of a PV-ventilated solar greenhouse dryer for drying of peeled longan and banana. *Solar Energy,* 83**,** 1550-1565.

JARIWALA, H. J. & SYED, H. S. Study on Use of Fruit Peels Powder as a Fertilizer. *RAESET-2016,* 1**,** 106.

JELLE, B. P. 2011. Traditional, state-of-the-art and future thermal building insulation materials and solutions–Properties, requirements and possibilities. *Energy and buildings,* 43**,** 2549-2563.

JERCAN, A. S. 2006. The simplified calculus of the flat plate solar collector. *Annals of the University of Craiova, Electrical Engineering series*.

KADAM, D., GOYAL, R. & GUPTA, M. 2011. Mathematical modeling of convective thin layer drying of basil leaves. *Journal of Medicinal Plants Research,* 5**,** 4721-4730.

KADER, A. A. Increasing food availability by reducing postharvest losses of fresh produce. V International Postharvest Symposium 682, 2004. 2169-2176.

KAREEM, M., GILANI, S., HABIB, K., IRSHAD, K. & SAHA, B. B. 2017a. Performance analysis of a multi-pass solar thermal collector system under transient state assisted by porous media. *Solar Energy,* 158**,** 782-791.

KAREEM, M., HABIB, K., RUSLAN, M. H. & SAHA, B. B. 2017b. Thermal performance study of a multi-pass solar air heating collector system for drying of Roselle (Hibiscus sabdariffa). *Renewable energy,* 113**,** 281-292.

KAREEM, M., HABIB, K., SOPIAN, K. & RUSLAN, M. 2017c. Multi-pass solar air heating collector system for drying of screw-pine leaf (Pandanus tectorius). *Renewable Energy,* 112**,** 413-424.

KARIM, M. A. & HAWLADER, M. 2005. Drying characteristics of banana: theoretical modelling and experimental validation. *Journal of food engineering,* 70**,** 35-45.

KASA, T. & G/YOHANIS, F. 2017. Chemical Composition and Nutritional Effect of Pineapple, Mango, Banana, Avocado and Orange: A Review Article. *Chemical and Process Engineering Research,* 54, 2017**,** 1-6.

KETLOGETSWE, C. & MOTHUDI, T. 2009. Solar home systems in Botswana—Opportunities and constraints. *Renewable and Sustainable Energy Reviews,* 13**,** 1675-1678.

KHOUKHI, M. & MARUYAMA, S. 2006. Theoretical approach of a flat-plate solar collector taking into account the absorption and emission within glass cover layer. *Solar Energy,* 80**,** 787-794.

KLEIN, S. 1975. Calculation of flat-plate collector loss coefficients. *Solar energy,* 17**,** 79.

KUCUK, H., MIDILLI, A., KILIC, A. & DINCER, I. 2014. A review on thin-layer drying-curve equations. *Drying Technology,* 32**,** 757-773.

KUMAR, C., KARIM, M. & JOARDDER, M. U. 2014. Intermittent drying of food products: A critical review. *Journal of Food Engineering,* 121**,** 48-57.

LABED, A., MOUMMI, N., BENCHABANE, A., AOUES, K. & MOUMMI, A. 2012. Performance investigation of single-and double-pass solar air heaters through the use of various fin geometries. *International Journal of Sustainable Energy,* 31**,** 423-434.

LEON, M. A., KUMAR, S. & BHATTACHARYA, S. 2002. A comprehensive procedure for performance evaluation of solar food dryers. *Renewable and Sustainable Energy Reviews,* 6**,** 367-393.

LUHANGA, P. 1995. Solar uv radiation at Gaborone, Botswana. *Renewable energy,* 6**,** 795-799.

MACKAY, M. E. 2015. *Solar energy: An introduction*, OUP UK.

MAHFOUD, O., ZEDAYRIA, M., MOUMMI, A. & MOUMMI, N. 2013. Numerical 2D study of air flow controlled by passive technique in solar air collectors. *Revue des Energies Renouvelables,* 16**,** 159-170.

MAHMOOD, A., ALDABBAGH, L. & EGELIOGLU, F. 2015. Investigation of single and double pass solar air heater with transverse fins and a package wire mesh layer. *Energy Conversion and Management,* 89**,** 599-607.

MAISNAM, D., RASANE, P., DEY, A., KAUR, S. & SARMA, C. 2017. Recent advances in conventional drying of foods. *Journal of Food Technology and Preservation,* 1**,** 1-10.

MALALASEKERA, H. K. V. A. W. 1995. *An introduction to computational fluid dynamics,* Essex, England, Pearson Education Ltd.

MALEKJANI, N. & JAFARI, S. M. 2018. Simulation of food drying processes by Computational Fluid Dynamics (CFD); recent advances and approaches. *Trends in Food Science & Technology*.

MARKETING", D. 2017. A Profile of the South African Banana market value chain.

MASKAN, A., KAYA, S. & MASKAN, M. 2002. Hot air and sun drying of grape leather (pestil). *Journal of food engineering,* 54**,** 81-88.

MATHEW, S., VISAVALE, G. & MALI, V. 2016. CFD Analysis of a Heat Collector Element in a Solar Parabolic Trough Collector. Retrieved.

MERCER, D. G. 2007. An intermediate course in food dehydration and drying. *Department of Food Science, University of Guelph, Ontario, Canada*.

MOSTAGHIMI, N. A. J. An Introduction to Computational Fluid Dynamics,. *Fluid Flow Handbook.*

MUIRURI, P. I. & MOTSAMAI, O. S. 2018. Three Dimensional CFD Simulations of A Wind Turbine Blade Section; Validation. *Journal of Engineering Science & Technology Review,* 11.

NIJEGORODOV, N., KHARE, D. & THOMAS, T. SIMULATION OF THE MEAN MONTHLY AND MEAN YEARLY OPTIMUM SLOPES FOR BOTSWANA AND SADC COUNTRIES. Proceedings of the Second IASTED Africa Conference. 8.

NIJEGORODOV, N. & MONOWE, P. 2011. Simulation of solar radiation conditions in coastal and continental areas by using a new algorithm.

NORTON, T., GRANT, J., FALLON, R. & SUN, D.-W. 2010. Improving the representation of thermal boundary conditions of livestock during CFD modelling of the indoor environment. *Computers and Electronics in Agriculture,* 73**,** 17-36.

NWAKUBA, N., ASOEGWU, S., NWAIGWE, K. & CHUKWUEZIE, C. 2017. DESIGN AND DEVELOPMENT OF A HYBRID SOLAR-ELECTRIC DRYER FOR SLICED VEGETABLE CROPS. *JOURNAL OF AGRICULTURAL ENGINEERING AND TECHNOLOGY (JAET) EDITORIAL BOARD,* 23**,** 48.

NWAKUBA, N. R., ASOEGWU, S. & NWAIGWE, K. 2016. Energy requirements for drying of sliced agricultural products: a review. *Agricultural Engineering International: CIGR Journal,* 18**,** 144-155.

OMOLOLA, A. O., JIDEANI, A. I. & KAPILA, P. F. 2015. Drying kinetics of banana (Musa spp.). *Interciencia,* 40**,** 374-380.

ONWUDE, D. I., HASHIM, N., JANIUS, R. B., NAWI, N. M. & ABDAN, K. 2016. Modeling the thin-layer drying of fruits and vegetables: A review. *Comprehensive reviews in food science and food safety,* 15**,** 599-618.

ORBEGOSO, E. M., SAAVEDRA, R., MARCELO, D. & LA MADRID, R. 2017. Numerical characterisation of one-step and three-step solar air heating collectors used for cocoa bean solar drying. *Journal of environmental management,* 203**,** 1080-1094.

OSUNDE, Z. D. 2017. Effect of pretreatments and drying methods on some qualities of dried mango (Mangifera indica) fruit. *Agricultural Engineering International: CIGR Journal,* 19**,** 187-194.

PAPADOPOULOS, A. M. 2005. State of the art in thermal insulation materials and aims for future developments. *Energy and buildings,* 37**,** 77-86.

PRABHU, C., SUDHAKAR, P., BALAJI, G. & CHERALATHAN, M. Analysis of solar flat plate collector with straight and helical flow path heat tube using mathematical modeling and java based simulation. IOP Conference Series: Materials Science and Engineering, 2018. IOP Publishing, 012110.

PRAMANIK, R. N., SAHOO, S. S., SWAIN, R. K., MOHAPATRA, T. P. & SRIVASTAVA, A. K. 2017. Performance analysis of double pass solar air heater with bottom extended surface. *Energy procedia,* 109**,** 331-337.

PURKAYASTHA, M. D., NATH, A., DEKA, B. C. & MAHANTA, C. L. 2013. Thin layer drying of tomato slices. *Journal of food science and technology,* 50**,** 642-653.

RAMANI, B., GUPTA, A. & KUMAR, R. 2010. Performance of a double pass solar air collector. *Solar Energy,* 84**,** 1929-1937.

RANGABABU, J., KUMAR, K. & RAO, S. 2015. Numerical Analysis and Validation of Heat Transfer Mechanism of Flat Plate Collectors. *Procedia Engineering,* 127**,** 63-70.

RASHAM, M. A. A. M. 2018. Thermal Analysis of Double-Pass Solar Air Collector with Different Materials of Absorber Plate and Different Dimensions of Air Channels. *Article in International Journal of Science and Research (IJSR)*.

ROMERO, V., CEREZO, E., GARCIA, M. & SANCHEZ, M. 2014. Simulation and validation of vanilla drying process in an indirect solar dryer prototype using CFD Fluent program. *Energy Procedia,* 57**,** 1651-1658.

SANGHI, A., AMBROSE, R. K. & MAIER, D. 2018. CFD simulation of corn drying in a natural convection solar dryer. *Drying Technology,* 36**,** 859-870.

SAXENA, A. & GOEL, V. 2013. Solar air heaters with thermal heat storages. *Chinese Journal of Engineering,* 2013.

SAYIGH, A. 1979. ESTIMATION OF TOTAL RADIATION INTENSITY-UNIVERSAL FORMULA. *Journal of Engineering Sciences,* 5**,** 43-56.

SCANLIN, D. 1997. Indirect, Through-Pass, Solar Food Dryer. *Home Power. February*.

SCHEEPENS, P., HOEVERS, R., ARULAPPAN, F. X. & PESCH, G. 2011. Storage of agricultural products. *Wageningen: CTA*.

SHARMA, A., CHEN, C. & LAN, N. V. 2009. Solar-energy drying systems: A review. *Renewable and sustainable energy reviews,* 13**,** 1185-1210.

SHEWEN, K. G. T. H. A. E. C. 1981. Optimization of Flow Passage Geometry for Air-Heating, Plate-Type Solar Collectors. *Journal of Solar Energy Engineering* Volume 103, Issue 4.

SMITABHINDU, R., JANJAI, S. & CHANKONG, V. 2008. Optimization of a solar-assisted drying system for drying bananas. *Renewable Energy,* 33**,** 1523-1531.

SODHA, M. S. 1987. Solar crop drying.

SOLTANI, M., ALIMARDANI, R. & OMID, M. 2011. Modeling the main physical properties of banana fruit based on geometrical attributes. *Int J Multidiscip Sci Eng,* 2**,** 1-6.

SOPIAN, K., ALGHOUL, M., ALFEGI, E. M., SULAIMAN, M. & MUSA, E. 2009. Evaluation of thermal efficiency of double-pass solar collector with porous–nonporous media. *Renewable Energy,* 34**,** 640-645.

SOPIAN, K., DAUD, W. R. W., OTHMAN, M. Y. & YATIM, B. 1999. Thermal performance of the double-pass solar collector with and without porous media. *Renewable Energy,* 18**,** 557-564.

SRINIVASAN, T. B. R. A. K. Heat Transfer Analysis on Finned Plate Air Heating Solar Collector for its Application in Paddy Drying. International Conference on Recent Advancement in Air Conditioning and Refrigeration, RAAR 2016

2016, India. Elsevier Ltd.

STATISTICS, B. 2015. BOTSWANA POPULATION PROJECTIONS (2011 – 2026). Botswana.

STRUCKMANN, F. 2008. Analysis of a flat-plate solar collector. *Heat and Mass Transport, Project Report, 2008MVK160*.

SUN, D.-W. 2007. *Computational Fluid Dynamics in Food Processing*, Taylor & Francis Group.

TOMAR, V., TIWARI, G. & NORTON, B. 2017. Solar dryers for tropical food preservation: Thermophysics of crops, systems and components. *Solar Energy,* 154**,** 2-13.

TOOLBOX, T. E. Dry Air Properties.

TUNDE-AKINTUNDE, T. Y. & OGUNLAKIN, G. O. 2011. Influence of drying conditions on the effective moisture diffusivity and energy requirements during the drying of pretreated and untreated pumpkin. *Energy Conversion and Management,* 52**,** 1107-1113.

VERSTEEG, H. K. & MALALASEKERA, W. 2007. *An introduction to computational fluid dynamics: the finite volume method*, Pearson Education.

WASALA, W., DHARMASENA, D., DISSANAYAKE, T. & THILAKARATHNE, B. 2012. Physical and mechanical properties of three commercially grown banana (Musa acuminata Colla) cultivars in Sri Lanka.

WEC, W. E. C. 2018. *Energy Resouces* [Online]. Available: https://www.worldenergy.org/data/resources/ [Accessed June, 14 2018].

XIA, B. & SUN, D.-W. 2002. Applications of computational fluid dynamics (CFD) in the food industry: a review. *Computers and electronics in agriculture,* 34**,** 5-24.

YEARBOOK, F. S. 2013. World Food and Agriculture. Food and Agriculture Organization of the United Nations, Rome.(2013).

YOUCEF-ALI, S., MESSAOUDI, H., DESMONS, J., ABENE, A. & LE RAY, M. 2001. Determination of the average coefficient of internal moisture transfer during the drying of a thin bed of potato slices. *Journal of Food Engineering,* 48**,** 95-101.

Appendix I: The physical properties of air at 1 Atmosphere

Temperature (K) (deg C)	Specific Heat - c_p - (kJ/kgK)	Specific Heat - c_v - (kJ/kgK)	Ratio of Specific Heats - k - (c_p/c_v)	Dynamic Viscosity - μ - (10^{-5} kg/m s)	Thermal Conductivity (10^{-5} kW/m K)	Prandtl Number	Kinematic Viscosity[1] - ν - (10^{-5} m^2/s)	Density[1] - ρ - (kg/m^3)	Thermal Diffusivity - α - (10^{-6} m^2/s)
175	1.0023	0.7152	1.401	1.182	1.593	0.744	0.586	2.017	
200	1.0025	0.7154	1.401	1.329	1.809	0.736	0.753	1.765	10.17
225	1.0027	0.7156	1.401	1.467	2.020	0.728	0.935	1.569	
250	1.0031	0.7160	1.401	1.599	2.227	0.720	1.132	1.412	15.67
275	1.0038	0.7167	1.401	1.725	2.428	0.713	1.343	1.284	
300	1.0049	0.7178	1.400	1.846	2.624	0.707	1.568	1.177	22.07
325	1.0063	0.7192	1.400	1.962	2.816	0.701	1.807	1.086	
350	1.0082	0.7211	1.398	2.075	3.003	0.697	2.056	1.009	29.18
375	1.0106	0.7235	1.397	2.181	3.186	0.692	2.317	0.9413	
400	1.0135	0.7264	1.395	2.286	3.365	0.688	2.591	0.8824	36.94
450	1.0206	0.7335	1.391	2.485	3.710	0.684	3.168	0.7844	
500	1.0295	0.7424	1.387	2.670	4.041	0.680	3.782	0.7060	
550	1.0398	0.7527	1.381	2.849	4.357	0.680	4.439	0.6418	
600	1.0511	0.7640	1.376	3.017	4.661	0.680	5.128	0.5883	
650	1.0629	0.7758	1.370	3.178	4.954	0.682	5.853	0.5430	
700	1.0750	0.7879	1.364	3.332	5.236	0.684	6.607	0.5043	
750	1.0870	0.7999	1.359	3.482	5.509	0.687	7.399	0.4706	
800	1.0987	0.8116	1.354	3.624	5.774	0.690	8.214	0.4412	
850	1.1101	0.8230	1.349	3.763	6.030	0.693	9.061	0.4153	
900	1.1209	0.8338	1.344	3.897	6.276	0.696	9.936	0.3922	
950	1.1313	0.8442	1.340	4.026	6.520	0.699	10.83	0.3716	
1000	1.1411	0.8540	1.336	4.153	6.754	0.702	11.76	0.3530	
1050	1.1502	0.8631	1.333	4.276	6.985	0.704	12.72	0.3362	
1100	1.1589	0.8718	1.329	4.396	7.209	0.707	13.70	0.3209	
1150	1.1670	0.8799	1.326	4.511	7.427	0.709	14.70	0.3069	
1200	1.1746	0.8875	1.323	4.626	7.640	0.711	15.73	0.2941	
1250	1.1817	0.8946	1.321	4.736	7.849	0.713	16.77	0.2824	
1300	1.1884	0.9013	1.319	4.846	8.054	0.715	17.85	0.2715	
1350	1.1946	0.9075	1.316	4.952	8.253	0.717	18.94	0.2615	
1400	1.2005	0.9134	1.314	5.057	8.450	0.719	20.06	0.2521	
1500	1.2112	0.9241	1.311	5.264	8.831	0.722	22.36	0.2353	
1600	1.2207	0.9336	1.308	5.457	9.199	0.724	24.74	0.2206	
1700	1.2293	0.9422	1.305	5.646	9.554	0.726	27.20	0.2076	
1800	1.2370	0.9499	1.302	5.829	9.899	0.728	29.72	0.1961	
1900	1.2440	0.9569	1.300	6.008	10.233	0.730	32.34	0.1858	

Source: (Toolbox)

Appendix II: Thermal properties of food products

Material	Moisture Content (by weight)	Specific Heat Above Freezing (kJ / kg K)	Specific Heat Below Freezing (kJ / kg K)	Freezing Point (°C)	Latent Heat of Fusion (kJ / kg)
Apples	84%	3.651	1.892	-1.1	280.18
Dried Apple	24%	1.641	1.139	not available	not available
Bananas	75%	3.349	1.779	-0.8	250.16
Grapes	82%	3.584	1.867	-1.6	273.51
Peaches	89%	3.818	1.955	-0.9	296.86
Dried Peach	25%	1.675	1.151	not available	not available
Bread	34%	1.993	1.271	-2.2	106.74
Water	100%	4.187	2.050	0	333

Source: (Mercer, 2007)

Appendix III: Data recorded in every 10seconds on 26/02/2019 for 5hrs

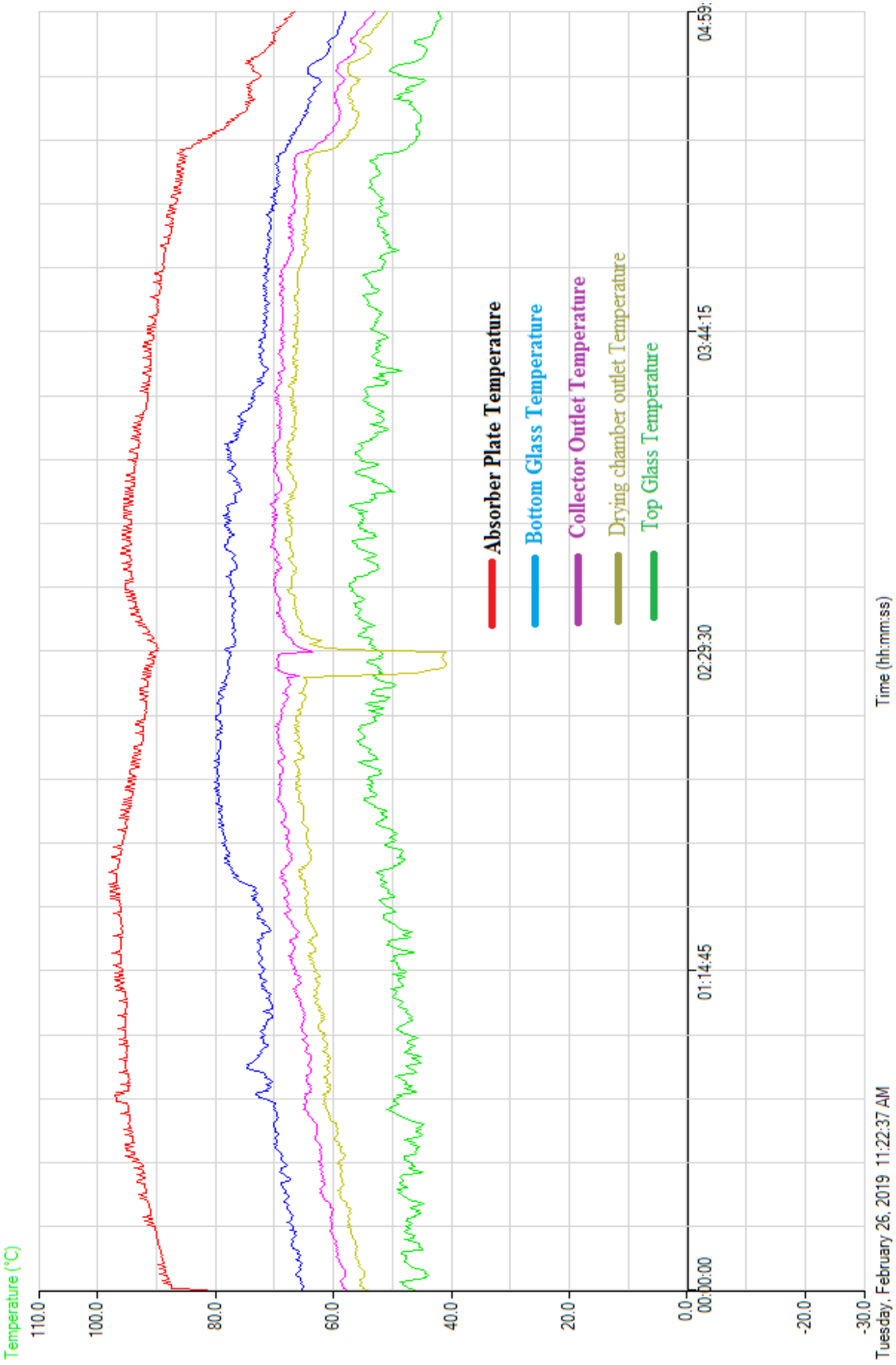

Appendix IV: Data recorded in every 10seconds on 27/02/2019 for 8hrs

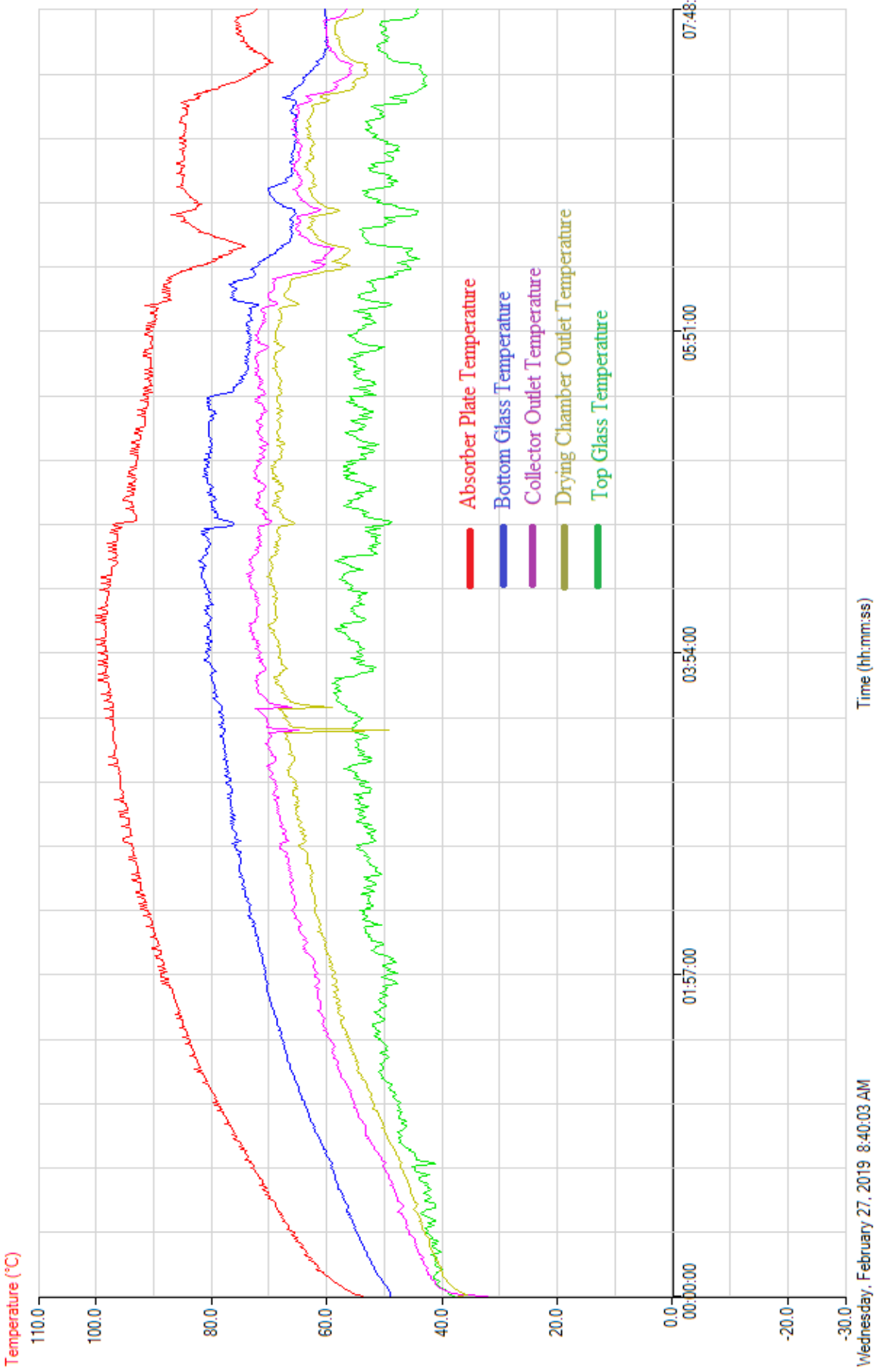

Appendix V: Data recorded in every 10seconds on 01/03/2019 for 8hrs

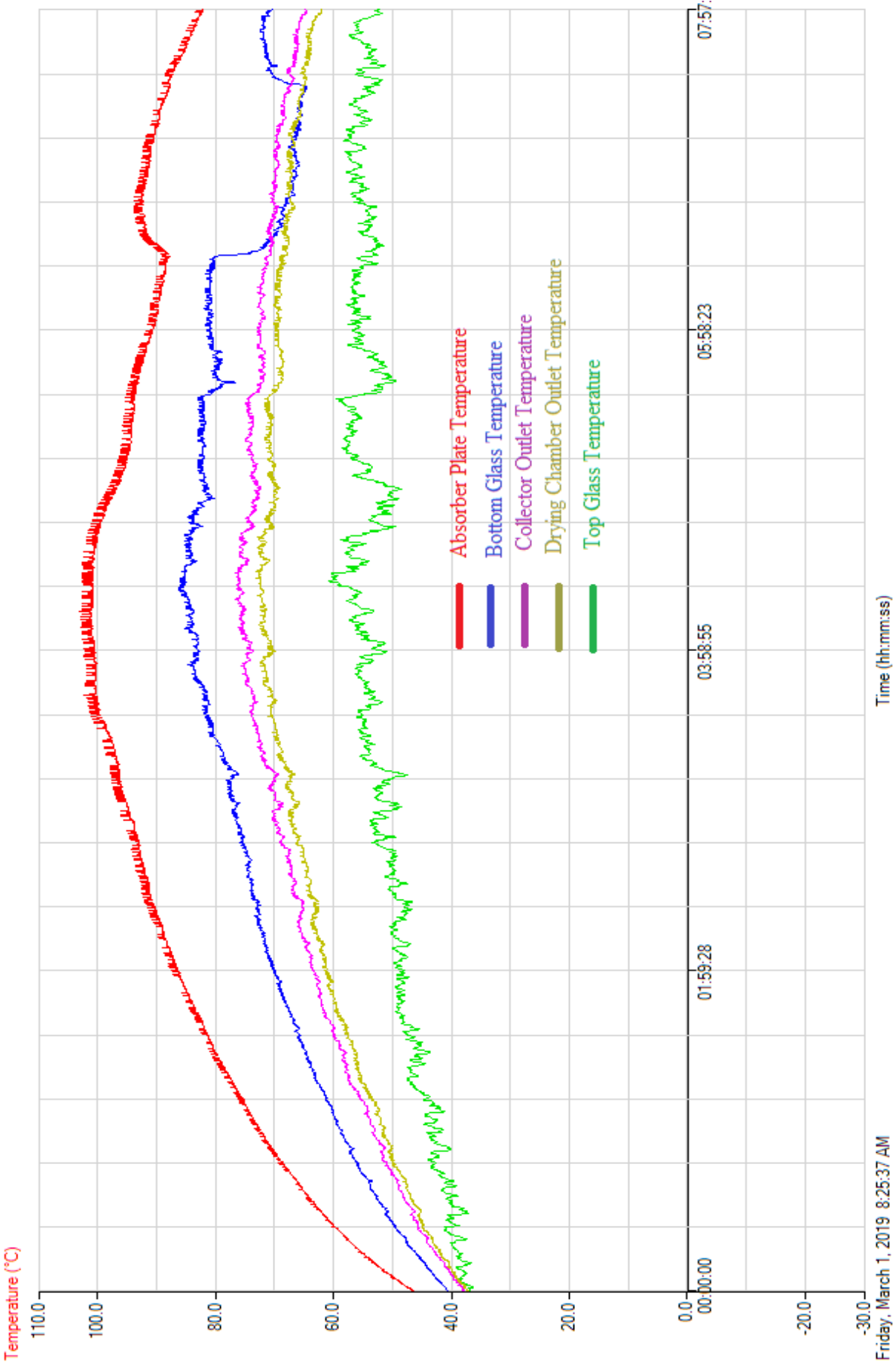

Appendix VI: Data recorded in every 10seconds on 03/03/2019 for 8hrs

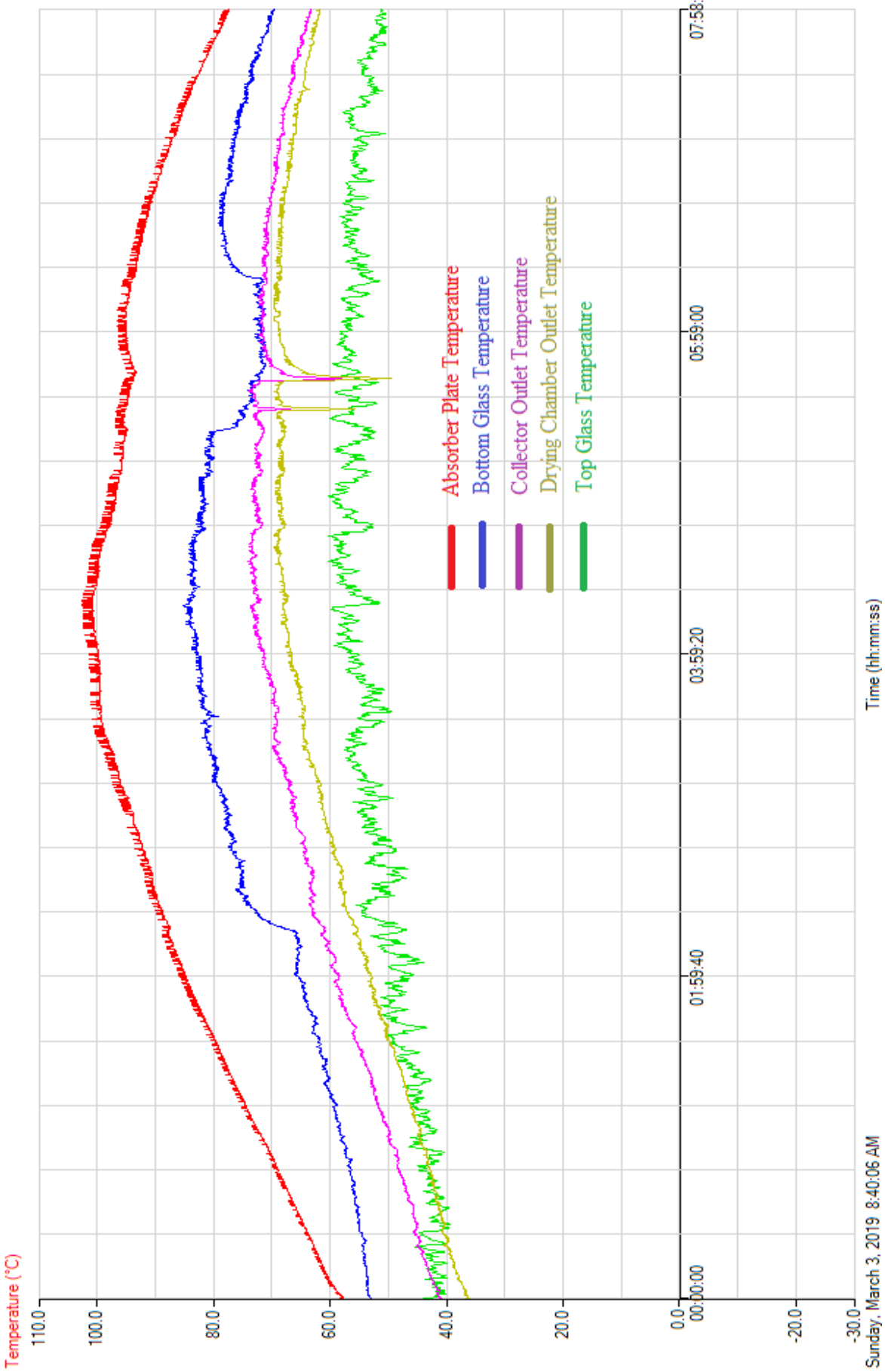

Appendix VII: Experimental measured values from developed solar dryer

Time	Solar Radiation	Absober Plate Temp	Bottom Glass Temp	Top Glass Temp	Collector Outlet Air Temp	Drying Chamber outlet Temp	Collector Inlet airflow	Collector Inlet Air Temp	Mass Flowrate [Eq. 4.6]	Collector Efficiency [Eq. 5.13]	Usefull Heat Gain [Eq. 5.12c]	Total Heat received by collector [Eq. 2.9]	Pacentage of Heat Collected by the Colletor
Hrs	W/m2	°C	°C	°C	°C	°C	m/s	°C	kg/s	%	W	W	%
08:40AM	511	58	53	44	41	36.20	2.78	30.80	0.0182	28.28	185.31	533.73	34.72
09:00AM	584	63	54	43	45	40.00	2.89	29.70	0.0189	38.96	291.83	609.98	47.84
10:00AM	787	77	61	44	53	47.30	3.77	34.40	0.0247	45.60	460.31	822.01	56.00
11:00AM	907	88	71	50	62	56.00	3.92	37.90	0.0257	53.15	618.33	947.34	65.27
12:00PM	983	97	80	57	69	63.40	3.96	37.90	0.0260	63.85	804.97	1026.72	78.40
13:00PM	965	101	84	54	72	67.30	3.86	39.49	0.0253	66.92	828.21	1007.92	82.17
14:00PM	842	95	80	53	72	68.00	3.31	42.60	0.0217	58.87	635.71	879.45	72.28
15:00PM	860	94	75	54	72	68.50	3.92	43.20	0.0257	66.38	732.16	898.25	81.51
16:00PM	701	85	76	57	68	65.60	3.65	42.40	0.0239	68.32	614.28	732.18	83.90
16:40PM	529	75	69	51	62	60.80	3.69	42.00	0.0242	72.51	491.94	552.53	89.03

Appendix VIII: Samples taken in different days showing properties of dried Banana Flakes

DATE: 12/03/2019

TOTAL WEIGHT (PEEL &PULP): 4.79KG	
PULP WEIGHT:	3.69 KG
PEELS WEIGHT:	1.10 KG ≈ 30%
FINAL WEIGHT:	0.481 KG
INITIAL M/C:	75-81%
FINAL M/C:	13%
DRYING TIME:	13HRS

DATE: 01/03/2019

TOTAL WEIGHT (PEEL &PULP): 2.36KG	
PULP WEIGHT:	1.78 KG
PEELS WEIGHT:	0.58 KG ≈ 33%
FINAL WEIGHT:	0.285 KG
INITIAL M/C:	75-81%
FINAL M/C:	16%
DRYING TIME:	11HRS

DATE: 05/03/2019

TOTAL WEIGHT (PEEL &PULP): 1.137KG	
PULP WEIGHT:	0.856 KG
PEELS WEIGHT:	0.28 KG ≈ 29%
FINAL WEIGHT:	0.137 KG
INITIAL M/C:	75-81%
FINAL M/C:	16%
DRYING TIME:	9HRS

DATE: 27/02/2019

TOTAL WEIGHT (PEEL &PULP): 2.09KG	
PULP WEIGHT:	1.56 KG
PEELS WEIGHT:	0.53 KG ≈ 34%
FINAL WEIGHT:	0.235 KG
INITIAL M/C:	75-81%
FINAL M/C:	15%
DRYING TIME:	9HRS

DATE: 03/03/2019

TOTAL WEIGHT (PEEL &PULP): 1.73KG	
PULP WEIGHT:	1.32 KG
PEELS WEIGHT:	0.41 KG ≈ 31%
FINAL WEIGHT:	0.192 KG
INITIAL M/C:	75-81%
FINAL M/C:	14.5%
DRYING TIME:	9HRS

DATE: 26/02/2019

TOTAL WEIGHT (PEEL &PULP): 1.134 KG	
PULP WEIGHT:	0.84 KG
PEELS WEIGHT:	0.29 KG ≈ 35%
FINAL WEIGHT:	0.114 KG
INITIAL M/C:	75-81%
FINAL M/C:	13%
DRYING TIME:	8HRS

****** Average weight of one unpeeled banana ranges (0.254-0.274kg), pulp ranges (0.147-0.182kg)

Appendix IX. Costs and Materials used for manufacturing the solar dryer

S/n	Material	Unit Specifications	Cost per Unit (P/Unit)	Number of units/Quantity	Total Cost (Pula)
1	Aluminum sheet	2.5x1.25x1.6m	930	1	930
2	Square tube	32x32x1.6x6m	105.95	4	423.80
3	Square tube	25x25x1.6x6m	88.50	1	88.50
4	Plywood	2 x 4 x 0.02m	450/sheet	2	900
5	Glass	1.7x0.8x0.05mm	284.50	2	569
6	Angle iron	0.060x0.060x6m	165.90	1	165.90
7	Screws	-	30/pack	3	90
8	Flexible hose pipe	ϕ86mm, 1m	255	1	255
9	Solar Panel	45 x 30mm, 15W	199	1	199
10	Fan	120x120x20mm	95	1	95
11	Switch	2ways	35.9	1	35.9
12	Netting Material	3m x 1m	45/meter	3	135
13	Polyethylene foam	-			
14	Aluminum foil	I roller	225	1	225
15	Welding rod	2.5mm, 5KG	85	1	85
16	Castor Wheel	Medium	89.50	4	358
17	Matt black paint	125 ml	75	4	300
18	Bolt & Nuts (M6, M8, M12)	-	-	-	165
19	Silicon Sealant/wood binder	250ml	75	3	225
	Extension wire	5m	175	1	175
Total					**5420.10**

Appendix X: An estimate of Banana losses reduction for different volume sizes of dryers

Size of the dryer (Volume m^3)	Carrying capacity (kg)	Days in a Month	Possible Drying Runs in a Month	PHL's Reduction (kg)
0.21	**3.69**	**30**	**15**	**55.35**
0.42	7.38	30	15	110.7
0.84	14.76	30	15	221.4
1.68	29.52	30	15	442.8
3.36	59.04	30	15	885.6
6.72	118.08	30	15	1771.2
13.44	236.16	30	15	3542.4

Appendix XI: Assembly Drawings of the Developed Solar Dryer.

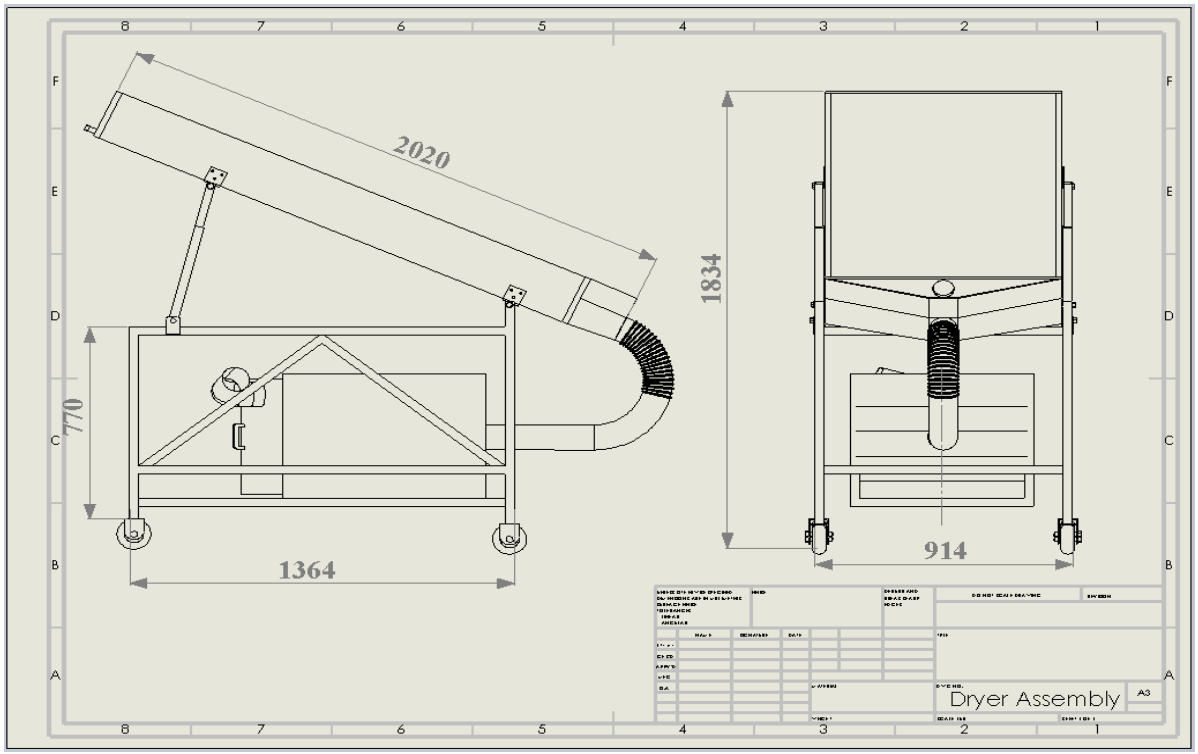

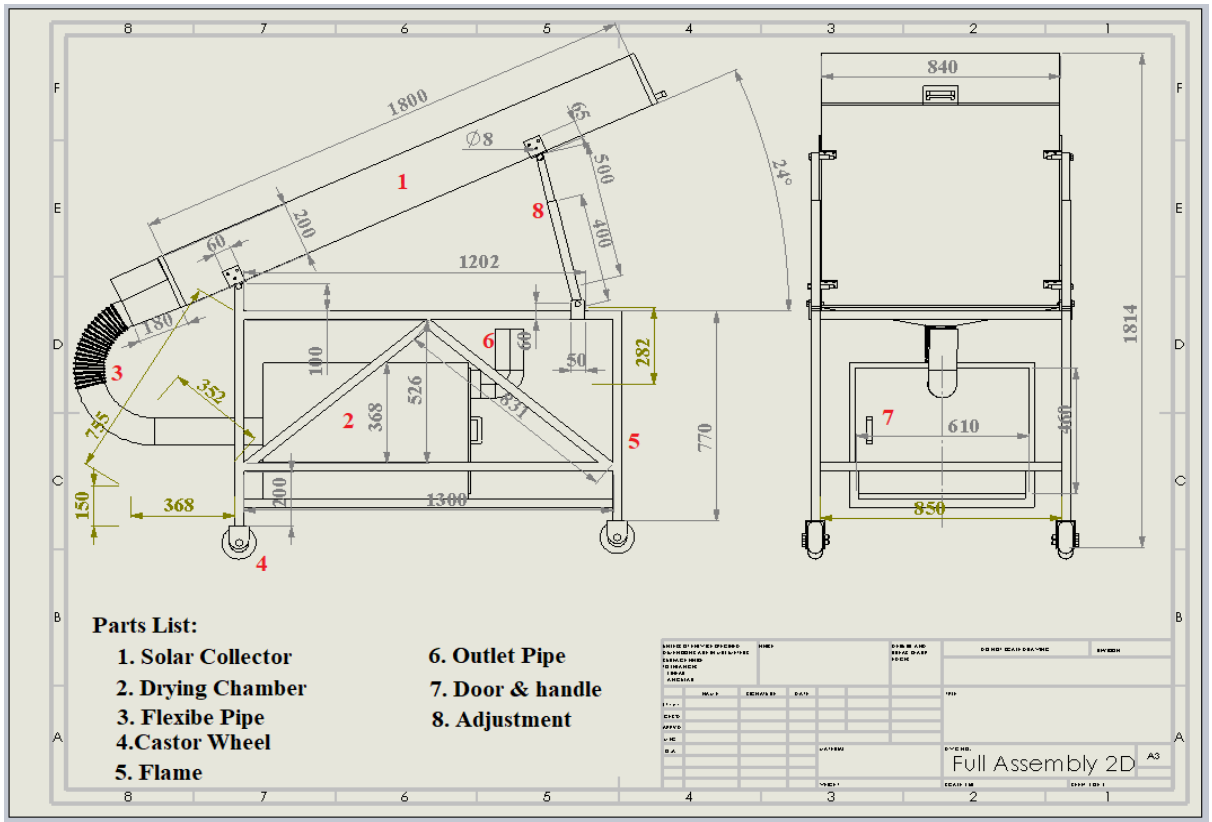

Appendix XII: Other useful parameters calculated from the experimental data.

Time	Solar Radiation	Heat Transfer coefficient (h)	Heat loss on top glass (Ut)[Eq. 5.4]	Radiative Heat transfer coefficient (hr) btw glasses[Eq. 5.6b]	Radiative Heat transfer coefficient (hr) btw glass/plate[Eq. 5.6c]	Convective heat tranfer coefficient(hc) btw glasses[Eq. 5.7]	Viscousity (u), [Eq. 5.11a]	Density, [Eq. 5.11b]	Specific Heat Capacity, [Eq. 5.11c]	Reynolds No in Lower Channel [Eq. 5.9]	Nusselt No in Lower Channel, [Eq. 5.9a]	Fliction Factor, f_s [Eq. 4.8b]	Pressure Drop in the Collector, Δp [Eq. 4.8a]	Prandtl number, [Eq. 5.9d]
Hrs	W/m2	W/m2K	W/m2K	W/m2K	W/m2K	W/m2K	m^2/s (*10^-5)	kg/m^3	J/kg.K				N/m^2 or Pa	
08:40AM	511	5.40	1.19	0.048	0.365	2.17	1.964	1.141	1.0064	18001	23.64	0.00598	2.16	0.0098
09:00AM	584	6.87	1.25	0.062	0.381	2.30	1.955	1.122	1.0067	18498	30.52	0.00593	2.35	0.0097
10:00AM	787	8.42	1.30	0.097	0.427	2.55	1.949	1.111	1.0069	23955	37.80	0.00546	3.73	0.0097
11:00AM	907	9.64	1.34	0.121	0.467	2.66	1.939	1.092	1.0073	24599	44.00	0.00541	4.07	0.0096
12:00PM	983	10.64	1.39	0.143	0.504	2.73	1.926	1.067	1.0077	24446	49.62	0.00543	4.25	0.0096
13:00PM	965	10.54	1.40	0.192	0.520	2.93	1.923	1.061	1.0078	23731	49.40	0.00548	4.10	0.0096
14:00PM	842	9.44	1.34	0.167	0.498	2.84	1.929	1.073	1.0076	20517	43.79	0.00574	3.12	0.0096
15:00PM	860	11.37	1.33	0.125	0.488	2.67	1.931	1.076	1.0076	24345	52.61	0.00543	4.14	0.0096
16:00PM	701	11.16	1.29	0.118	0.462	2.62	1.936	1.086	1.0074	22819	51.18	0.00555	3.63	0.0096
16:40PM	529	11.58	1.22	0.104	0.426	2.57	1.946	1.105	1.0070	23356	52.22	0.00550	3.62	0.0097